Electrocardiographic Techniques and Methods in the Detection of Ischaemic Heart Disease

Michael Jennings

Faculty of Computing, Engineering, and the Built Environment of Ulster University

This thesis has been submitted for the degree of *Doctor of Philosophy*

December 2022

I confirm that the word count of this thesis is less than 100,000 words.

supervised by

Prof. Dewar Finlay, Prof. James McLaughlin, & Prof. Colin Turner

Note on Access to Contents

Acknowledgements

I would like to thank my supervisors Professor Dewar Finlay, Professor Jim McLaughlin, and Professor Colin Turner, for their support and guidance throughout this studentship. Their patience and mentoring ability is admirable. I would like to extend this thanks to the many support staff and technicians in the School of Engineering within Ulster University who made my time worthwhile. In particular, Mr Stuart Christy, who has been a continuous source of inspiration for the past five years.

I would like to thank Prof. Dewar Finlay and the Eastern Corridor Medical Engineering Centre (ECME) team for providing the financial support necessary to make this research possible.

Finally, I would like to thank my family for putting up with my many stressful moments during this thesis, especially as a result of the isolation caused by the SARS-CoV-2 pandemic.

The work carried out as part of this thesis has been funded by the Special European Union Programmes Body (SEUPB) as part of the INTERREG VA scheme. Additionally, the SEUPB have funded the creation of the Eastern Corridor Medical Engineering centre (ECME) with 24 Ph.D and 5 post-doctoral researchers.

Abstract

Electrocardiographic analysis has the capability to diagnose and locate abnormalities relating to the heart. There are several lead systems, such as the 12-lead ECG, that are commonly used in clinical settings. One aspect of this thesis is to derive additional posterior and right-sided chest leads from the 12-lead ECG, and to evaluate the performance of the derived leads in the detection of ECG changes associated with myocardial ischaemia.

The 12-lead ECG is also not practicable for long term ambulatory monitoring, especially in the detection of paroxysmal cardiac abnormalities such as unstable angina. Therefore, the second study of this thesis introduces a novel patch-based short-spaced lead system sensitive to ST-segment changes associated with ischaemia.

With the increasing numbers of electronically-stored patient data, it is imperative that clinicians can develop their own algorithms. In the third study, a framework for biomedical algorithm development is introduced, with a focus on its use by non-coders to pass data through multi-lingual scripts.

Derived posterior (V7-V12) and right-sided chest leads (V3R-V6R) from the 12-lead ECG were closely correlated to those recorded. Myocardial infarction detection was improved as additional leads were added to the 12-lead ECG, however, this was not statistically significant.

A patch-based short spaced lead system that was sensitive to ST-segment changes associated with ischaemia was suggested. It consisted of two bipolar leads. Coefficients were generated to derive this short spaced lead system from the 12-lead ECG. ST-segment changes associated with ischaemia were detected with the highest F1 score (86.7%).

A web-based framework was introduced to reduce the barrier to entry in biomedical digital signal processing for non-coders. A Python framework was used with

the MATLAB Engine to allow users to create algorithms consisting of multi-lingual scripts capable of processing patient data, without the need to write code. The framework was reproducable and scalable.

Contents

List of Figures

List of Tables

Abbreviations

ACS Acute Coronary Syndrome. x, 19, 20, 23, 24, 33, 46, 47

AI Artificial Intelligence. 1, 2, 55, 59

AMI Acute Myocardial Infarction. x, xiii, 18, 20, 30, 34, 36, 37, 41, 42, 44–50, 52, 54, 55, 88–90, 105–107, 115, 122, 123, 142, 170

ANN Artificial Neural Network. 33, 50, 55, 57, 58

API Application Peripheral Interface. xii, 59, 156, 157, 160–162, 164

AUC Area Under the Curve. 47

AV Atrio-Ventricular. 39, 41

BSPM Body Surface Potential Map. x, 1, 2, 21–24, 26, 27, 29, 42, 52, 53, 56, 87, 88, 101, 104, 122, 125, 126, 128, 130, 170

CC Correlation Coefficient. 33, 55, 57, 58, 105, 109, 112–114, 116, 123, 128, 132, 140, 171

CHD Coronary Heart Disease. 29, 52, 60, 61

CNN Convolutional Neural Network. 61

CSV Comma Separated Variable. 153, 162

CVD Cardiovascular Disease. 41

DSP Digital Signal Processing. 1, 4, 62, 148, 150, 151, 162, 164

DWT Discrete Wavelet Transform. 170

ECG Electrocardiogram. 1

FDA US Food and Drug Administration. 26, 38

FFT Fast Fourier Transform. 32

FMC First Medical Contact. 20

GAN Generative Adversarial Network. 57

GUI Graphical User Interface. 61, 63

GVM General Vector Machine. 57

IaaS Infrastructure as a Service. 59

IEGM Intra-cardiac Electrogram. 32

JSON Javascript Object Notation. 59

KNN K-Nearest Neighbour. 50

LAD Left Anterior Descending. xi, xiii, xiv, 20, 32, 44, 52, 85, 87, 89, 115, 117, 129–132, 134, 139

LBBB Left Bundle Branch Block. 15, 17, 25, 46, 88

LCX Left Circumflex. xi, xiii, xiv, 20, 23, 32, 44, 52, 85, 87, 89, 115–118, 129, 131, 135, 139

LM Left Main. 52, 89

LSTM Long Short-Term Memory. 58

LVEF Left Ventricular Ejection Fraction. 32

LVRR Left Ventricular Reverse Remodelling. 31, 32

MCL Modified Chest Leads. ix, 40, 41

ML Mason-Likar. 16, 22, 25–27, 40, 42, 52, 56

MLP Multi-Layer Perceptron. 48, 50, 129

MLR Multiple Linear Regression. 55, 57

MRI Magnetic Resonance Imaging. 42, 52

NPV Negative Predictive Value. 114, 115, 135

NSTEMI Non ST-elevation Myocardial Infarction. 18, 19

PBI Peak Balloon Inflation. xi, 34, 52, 86, 87, 107, 125, 128–130, 132, 141, 142, 170

PCA Principal Component Analysis. 50, 56

PPV Positive Predictive Value. 115, 134

PTB Physikalisch-Technische Bundesanstalt. 49, 51, 53, 57

QRS Q, R, and S waves of the ECG. 24, 32, 41–43, 48, 50, 52, 58, 86, 90–96

QT Q to T segment of the ECG. 43, 94

RBBB Right Bundle Branch Block. 25, 41, 88

RCA Right Coronary Artery. xi, xiii, xiv, 20, 32, 44, 52, 85, 87, 89, 115–118, 129, 131, 132, 136, 139, 142, 170

RMSE Root Mean Square Error. 26, 29, 33, 104, 109, 112, 113, 116, 117, 123, 128, 132, 140, 171

ROC Receiver Operating Characteristic. 47, 133

RVH Right Ventricular Hypertrophy. 48

SA Spatial QRS-T Angle. 25–27

SaaS Software as a Service. 59

SSL Short-Spaced Lead. 3

ST Segment of the ECG between S and T waves. x, xi, 4, 13, 19, 20, 27, 28, 30–32, 34, 37, 42–46, 48–53, 55, 58, 63, 86, 94, 106, 110, 111, 117, 118, 122–125, 127–130, 132, 134, 135, 137, 140–143, 169–171

STEMI ST-elevation Myocardial Infarction. 18

SVG Spatial Velocity Gradient. 90–94

SVM Support Vector Machine. 49, 62

VSL Vessel-Specific Leads. 44, 124, 131, 132

Chapter 1

Introduction

1.1 Research Background and Motivation

Heart diseases cause more than a quarter of all deaths in the UK. One patient is admitted every five minutes with a heart attack [1]. The 12-lead Electrocardiogram (ECG) remains the most popular method to triage cardiac events [2], however, the sensitivity of 12-lead ECG for Myocardial Infarction (MI) detection remains low at 66% for an expert cardiologist [3]. Other lead systems have been introduced to detect MI, but the current diagnostic criteria and clinicians rely heavily on the 12-lead ECG to provide a diagnosis [4]. Moreover, electrode misplacement by clinicians can affect the diagnosis of cardiac abnormalities and decrease the specificity of the ECG for certain conditions [5]. Using computational techniques such as Digital Signal Processing (DSP) and Artificial Intelligence (AI), the sensitivity of MI detection can be improved [6].

In particular, the introduction of novel lead systems such as the BSPM has allowed a torso-wide view of the electrical activity surrounding the heart [7]. Previous studies have investigated the optimal leads to detect MI [8, 9], however, these are inconvenient for ambulatory use and long term monitoring. It is possible to expand the diagnostic capability of the 12-lead ECG by means of deriving additional leads [10]. There are two major challenges associated with the derivation of additional leads, however. The first is selecting the optimal lead system to derive. Previous studies have introduced novel lead systems [11, 12], but their clinical use is not famil-

iar or well understood by clinicians [13]. Furthermore, there are limited diagnostic criteria available for these novel lead systems. The second challenge associated with deriving additional leads is the introduction of amplitude errors during the interpolation process [14]. These amplitude errors are introduced due to the differences in body composition, heart structure, and skin conduction that vary between individuals. It is impossible to correct this without personalised models of each patient, however, using a highly varied dataset with a realistic study population can assist with reducing these amplitude errors. There are also multiple ways of interpolating expanded lead systems, such as linear interpolation, multiple linear regression, cubic interpolation, and deep learning methods [15].

The number of ambulatory ECG devices in use have increase dramatically in recent years [16, 17, 18]. These devices allow long-term recording of the ECG using a mobile patch or vest-based design, with captured data either transmitted or stored for later analysis. Many of these patch devices focus on paroxysmal conditions such as Atrial Fibrillation (AF) [19, 20, 21], however, few focus on MI or other ischaemic conditions such as unstable angina. Additionally, there are no open source patch-specific datasets that allow the evaluation of this lead system. However, just like the additional leads discussed previously, the leads in a patch device can be evaluated via the derivation of existing lead systems such as the 12-lead ECG [22]. Furthermore, existing datasets such as those containing BSPM data possess torso-wide electrode coverage to assist with the evaluation of novel patch devices by comparing the derived leads with those recorded on the BSPM [9, 23]. An additional challenge in the presentation of a patch-based diagnostic lead system is the lack of criteria relating to MI diagnosis. The use of AI techniques has enabled the introduction of both the automated diagnosis of cardiac conditions, and the suggestion of novel diagnostic criteria [24, 20, 25].

The processing of biomedical data is increasingly occurring using cloud computing architectures [26, 27, 28]. These architectures provide multiple frameworks and tools for developers, however, they are not useful for those who cannot code but have access to patient data, such as clinicians or administration staff. With patient data being increasingly stored electronically, this presents challenges to clinicians who seek to identify patterns in the data, or who seek to develop their own algorithms.

Many existing frameworks for cloud-based processing of biomedical data focus on a propriety solution whereby data is sent to a server, processed, and returned with a diagnosis [29, 30, 31]. For specific scenarios, such as MI diagnosis, this is sufficient, however this does not allow the clinician to experiment with the detection algorithm, or change how the data is handled. A web-based and code-free algorithm development environment is necessary to fulfill this requirement.

1.2 Aims and Objectives of this Project

The aim of this thesis is to investigate different processing techniques and methods to improve upon MI detection techniques from the ECG. The aim has been met by the following objectives:

1. Studying the current state-of-the-art in ECG processing techniques, with a focus on those relating to MI detection, to discover current gaps in the literature.

2. Identifying suitable datasets suitable to investigate how ischaemia affects the ECG.

3. Investigating how the spatial resolution of the 12-lead can be expanded using additional derived leads.

4. Introducing a patch-based Short-Spaced Lead (SSL) system suitable for ambulatory monitoring and the detection of ischaemic-type ECG changes associated with MI.

5. Developing a framework to assist non-developers to create their own ECG processing algorithms with an open-source web-based tool.

1.3 Structure of this Project

This thesis has been presented in seven chapters. Chapter one, this chapter, is an introduction to the thesis. It highlights the motivation and areas this thesis aims to investigate. Chapter two gives a description of the history of the ECG

with a thorough review of the literature surrounding ECG processing, lead systems used to record the ECG, the current detection methods for MI, datasets containing ischaemic ECG information, the derivation of leads, and how cloud computing can be used in the processing of the ECG. Chapter three presents the datasets used during this work, accompanied by the pre-processing methods necessary for the recordings to be used within the experimental chapters. Chapter four presents work aimed to derive additional leads from the 12-lead ECG. In particular, posterior and right-sided precordial chest leads to give an increased spatial resolution across the torso. This chapter aims to investigate whether these derived leads can improve on the diagnostic performance of the 12-lead ECG towards MI detection. Chapter five introduces a patch-based short spaced lead system that is sensitive to ST-segment changes associated with MI. This chapter includes the selection and derivation of the patch, with a study into the diagnostic ability of the patch using machine learning techniques. Chapter six covers the development of a web-based framework to assist with the rapid creation of algorithms to process biomedical data. A python-based solution is presented to handle multi-lingual scripts and user information, allowing a non-coder to develop their own DSP algorithms without the need for prior coding experience. Chapter seven, the conclusion, presents a summary of the findings introduced in this work with the future possibilities stemming from this thesis.

References

[1] British Heart Foundation, "Facts and figures - Information for journalists - BHF," 2018.

[2] J. Francis, "ECG monitoring leads and special leads," *Indian Pacing and Electrophysiology Journal*, vol. 16, pp. 92–95, 5 2016.

[3] J. L. Garvey, J. Zegre-Hemsey, R. Gregg, and J. R. Studnek, "Electrocardiographic diagnosis of ST segment elevation myocardial infarction: An evaluation of three automated interpretation algorithms," *Journal of Electrocardiology*, vol. 49, no. 5, pp. 728–732, 2016.

[4] K. Thygesen, J. S. Alpert, A. S. Jaffe, B. R. Chaitman, J. J. Bax, D. A. Morrow, and H. D. White, "Fourth universal definition of myocardial infarction (2018)," *European Heart Journal*, vol. 24, pp. 107–138, 8 2019.

[5] R. R. Bond, D. D. Finlay, C. D. Nugent, C. Breen, D. Guldenring, and M. J. Daly, "The effects of electrode misplacement on clinicians' interpretation of the

standard 12-lead electrocardiogram," *European Journal of Internal Medicine*, vol. 23, pp. 610–615, 10 2012.

[6] S. W. Smith, B. Walsh, K. Grauer, K. Wang, J. Rapin, J. Li, W. Fennell, and P. Taboulet, "A deep neural network learning algorithm outperforms a conventional algorithm for emergency department electrocardiogram interpretation," *Journal of Electrocardiology*, vol. 52, pp. 88–95, 1 2019.

[7] T. J. Montague, E. R. Smith, D. A. Cameron, P. M. Rautaharju, G. A. Klassen, C. S. Felmington, and B. M. Horacek, "Isointegral analysis of body surface maps: Surface distribution and temporal variability in normal subjects," *Circulation*, vol. 63, no. 5, pp. 1166–1172, 1981.

[8] F. Kornreich, "Identification of best electrocardiographic leads for diagnosing acute myocardial ischemia," *Journal of Electrocardiology*, vol. 31, pp. 157–163, 1 1998.

[9] B. Horacek, J. W. Warren, C. J. Penney, R. S. MacLeod, L. M. Title, M. J. Gardner, C. L. Feldman, B. M. Horacek, J. W. Warren, C. J. Penney, R. S. MacLeod, L. M. Title, M. J. Gardner, and C. L. Feldman, "Optimal electrocardiographic leads for detecting acute myocardial ischemia," *Journal of Electrocardiology*, vol. 34, pp. 97–111, 10 2001.

[10] P. M. Rautaharju, S. H. Zhou, E. Hancock, B. Hor[aacute][ccaron]ek, D. Q. Feild, J. M. Lindauer, G. S. Wagner, O. Pahlm, and C. L. Feldman, "Comparability of 12-lead ECGs derived from EASI leads with standard 12-lead ECGS in the classification of acute myocardial ischemia and old myocardial infarction," *Journal of Electrocardiology*, vol. 35, no. 4, pp. 35–39, 2002.

[11] D. Schreck, M. Viscito, and C. Brotea, "The derived N-Lead electrocardiogram," *Annals of Emergency Medicine*, vol. 44, pp. S73–S74, 10 2004.

[12] D. D. Finlay, C. D. Nugent, M. P. Donnelly, P. J. McCullagh, and N. D. Black, "Optimal electrocardiographic lead systems: Practical scenarios in smart clothing and wearable health systems," *IEEE Transactions on Information Technology in Biomedicine*, vol. 12, pp. 433–441, 7 2008.

[13] M. A. Serhani, H. T. El Kassabi, H. Ismail, and A. N. Navaz, "ECG monitoring systems: Review, architecture, processes, and key challenges," *Sensors (Switzerland)*, vol. 20, p. 1796, 3 2020.

[14] R. E. Gregg, S. H. Zhou, J. M. Lindauer, D. Q. Feild, and E. D. Helfenbein, "Where do derived precordial leads fail?," *Journal of Electrocardiology*, vol. 41, pp. 546–552, 11 2008.

[15] B. J. Schijvenaars, J. A. Kors, G. van Herpen, F. Kornreich, and J. van Bemmel, "Interpolation of body surface potential maps," *Journal of Electrocardiology*, vol. 28, pp. 104–109, 1 1995.

[16] D. Duncker, W. Y. Ding, S. Etheridge, P. A. Noseworthy, C. Veltmann, X. Yao, T. J. Bunch, and D. Gupta, "Smart Wearables for Cardiac Monitoring—Real-World Use beyond Atrial Fibrillation," *Sensors 2021, Vol. 21, Page 2539*, vol. 21, p. 2539, 4 2021.

[17] M. Zulqarnain, S. Stanzione, G. Rathinavel, S. Smout, M. Willegems, K. Myny, and E. Cantatore, "A flexible ECG patch compatible with NFC RF communication," *npj Flexible Electronics*, vol. 4, pp. 1–8, 7 2020.

[18] P. Guzik and M. Malik, "ECG by mobile technologies," *Journal of Electrocardiology*, vol. 49, pp. 894–901, 11 2016.

[19] M. A. Rosenberg, M. Samuel, A. Thosani, and P. J. Zimetbaum, "Use of a noninvasive continuous monitoring device in the management of atrial fibrillation: A pilot study," *PACE - Pacing and Clinical Electrophysiology*, vol. 36, pp. 328–333, 3 2013.

[20] D. Lai, Y. Bu, Y. Su, X. Zhang, and C. S. Ma, "Non-Standardized Patch-Based ECG Lead Together with Deep Learning Based Algorithm for Automatic Screening of Atrial Fibrillation," *IEEE Journal of Biomedical and Health Informatics*, vol. 24, pp. 1569–1578, 6 2020.

[21] N. E. Wineinger, P. M. Barrett, Y. Zhang, I. Irfanullah, E. D. Muse, S. R. Steinhubl, and E. J. Topol, "Identification of paroxysmal atrial fibrillation subtypes in over 13,000 individuals," *Heart Rhythm*, vol. 16, pp. 26–30, 1 2019.

[22] T. Stamkopoulos, M. Strintzis, C. Pappas, and N. Maglaveras, "One-lead ischemia detection using a new backpropagation algorithm and the European ST-T database," in *Proceedings Computers in Cardiology*, pp. 663–666, IEEE Comput. Soc. Press, 2003.

[23] F. Kornreich, T. J. Montague, and P. M. Rautaharju, "Body surface potential mapping of ST segment changes in acute myocardial infarction: Implications for ECG enrollment criteria for thrombolytic therapy," *Circulation*, vol. 87, no. 3, pp. 773–782, 1993.

[24] H. Atoui, J. Fayn, and P. Rubel, "A neural network approach for patient-specific 12-lead ECG synthesis in patient monitoring environments," in *Computers in Cardiology, 2004*, pp. 161–164, IEEE, 2005.

[25] J. Sohn, S. Yang, J. Lee, Y. Ku, and H. C. Kim, "Reconstruction of 12-lead electrocardiogram from a three-lead patch-type device using a LSTM network," *Sensors (Switzerland)*, vol. 20, pp. 1–13, 6 2020.

[26] B. P. Rimal and I. Lumb, "The Rise of Cloud Computing in the Era of Emerging Networked Society," pp. 3–25, Springer, Cham, 2017.

[27] R. R. Bond, D. D. Finlay, C. D. Nugent, and G. Moore, "A review of ECG storage formats," *International Journal of Medical Informatics*, vol. 80, pp. 681–697, 10 2011.

[28] R. Ranchal, P. Bastide, X. Wang, A. Gkoulalas-Divanis, M. Mehra, S. Bakthavachalam, H. Lei, and A. Mohindra, "Disrupting healthcare silos: Addressing data volume, velocity and variety with a cloud-native healthcare data ingestion service," *IEEE Journal of Biomedical and Health Informatics*, vol. 24, pp. 3182–3188, 11 2020.

[29] Z. Zhang, H. Li, Z. Gong, R. Jin, and T. S. Chung, "A Compatible ECG Diagnosis Cloud Computing Framework and Prototype Application," in *PervasiveHealth: Pervasive Computing Technologies for Healthcare*, pp. 135–139, 2020.

[30] O. Cheikhrouhou, R. Mahmud, R. Zouari, M. Ibrahim, A. Zaguia, and T. N. Gia, "One-Dimensional CNN Approach for ECG Arrhythmia Analysis in Fog-Cloud Environments," *IEEE Access*, vol. 9, pp. 103513–103523, 2021.

[31] C. Venkatesan, P. Karthigaikumar, and S. Satheeskumaran, "Mobile cloud computing for ECG telemonitoring and real-time coronary heart disease risk detection," *Biomedical Signal Processing and Control*, vol. 44, pp. 138–145, 7 2018.

Chapter 2

Literature Review

2.1 Physiology

This chapter aims to investigate the state-of-the-art research related to the work carried out as part of this thesis. It is important to understand the basic principles and physiology that create the ECG.

2.1.1 Circulatory System

The circulatory system is the network of arteries and veins throughout the body. This system centres around the heart and consists of three main circuits: pulmonary, systemic, and coronary. The following sections will provide an overview of this system.

2.1.1.1 Circulation

The primary role of the circulatory system is to enable respiration via the transportation of nutrients and oxygen to the tissues [1]. With blood as the transportation media, the heart provides the mechanical force to deliver these materiel around the body. To facilitate the delivery of nutrients to the tissues, blood will become enriched by passing through the gut and liver. To provide oxygen, blood will pass via the lungs where the infusion of oxygen and effusion of carbon dioxide occurs.

Starting at the lungs, oxygenated blood will return to the heart through the pulmonary artery. The heart will pump this oxygenated blood around the body

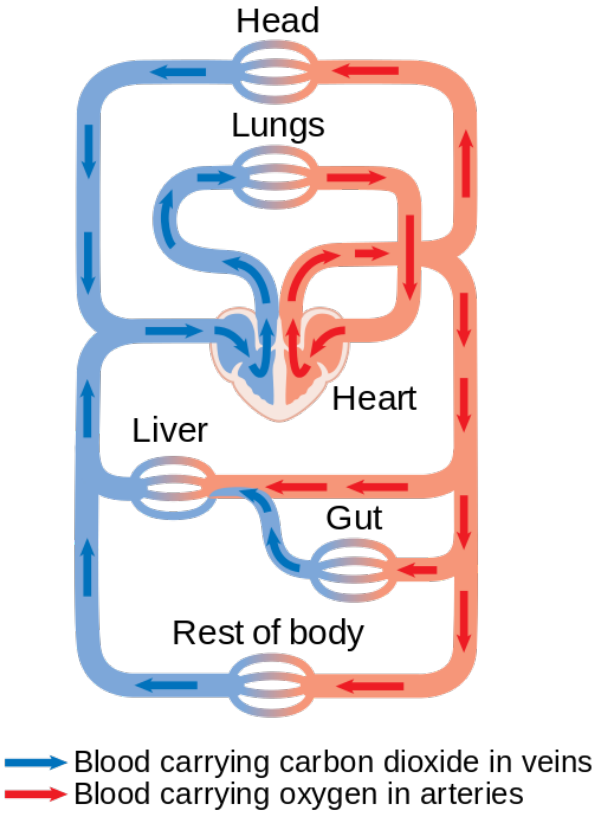

Figure 2.1: The human circulatory system [2]

via the aorta and branching arteries, where it will diffuse to the tissues through capillaries. Following diffusion, the subsequently deoxygenated blood will return to the heart through the veins and venae cavae. The heart will pump the blood through the lungs, where it is oxygenated and the cycle can repeat. A diagrammatic representation of the circulatory system is shown in Figure 2.1.

Within the circulatory system, the pressure of blood can vary. Arteries, in particular the aorta, are associated with higher pressure. This higher pressure is required to pump the oxygenated blood around the majority of the body. In contrast, the veins have a lower pressure due to perfusion to the tissues. Arterial blood pressure is the primary measure of blood pressure in the body. Two values are used in clinical practice: systolic, referring to the pressure under contraction of the heart and; diastolic, referring to the relaxed period in between heart beats.

The pulmonary circuit carries blood between the heart and lungs for oxygenation and waste gas release. The systemic circuit carries blood from the heart to the rest of the body for diffusion of nutrients into the tissues. There is a third circuit of

the circulatory system: the coronary circuit. This is the circuit responsible for the delivery of nutrients and oxygen to the heart itself. It is the smallest of the three circuits, but important to the function of the heart. Dysfunction of the coronary circuit may induce ischaemia of cardiac muscle. Its causes and effects will be analysed later.

2.1.1.2 Anatomy of the Heart

The primary role of the heart is a pump. The mechanical pumping action of the heart is possible using muscle cells, known as cardiac myocytes. These myocytes comprise most of mass of the heart, leading to many referring to the heart as as muscle. However, the heart also consists of tissues, chambers, vessels, and valves that allow it to pump blood around the body.

The diagram in Figure 2.2 show the heart to have four chambers: two atria and two ventricles. The heart is split into right and left halves. The right half supplies the pulmonary circuit and is supplied by the systemic circuit described in Section 2.1.1.1. The left half supplies the systemic and coronary circuits and is supplied by the pulmonary circuit. The right heart is a low pressure circuit, since the pressure required to perfuse the lungs is lower, and the return of blood from the body is under lower pressure. The left heart is a high pressure circuit because it is responsible for supplying blood to the rest of the body.

The heart is also split into atria and ventricles. The atria pump blood from the low pressure return from the systemic and pulmonary circuits into the ventricles. The ventricles then pump blood from the heart to the entire body.

The thickness of muscle is different for the four chambers. For example, the ventricles are the thickest since they pump blood through the lungs (right) and the rest of the body (left). The left ventricle is thicker than the right ventricle due to the systemic circuit requiring higher cardiac output to perfuse the tissues than the pulmonary circuit.

The heart also contains nerve tissue to initiate and execute contractions. The sinoatrial (SA) node is the “pacemaker” of the heart. Located in the right atrium, it initiates the contraction of the heart using specialised pacemaker cells. The contraction pulse is carried to the atrioventricular (AV) node where it is delayed. This

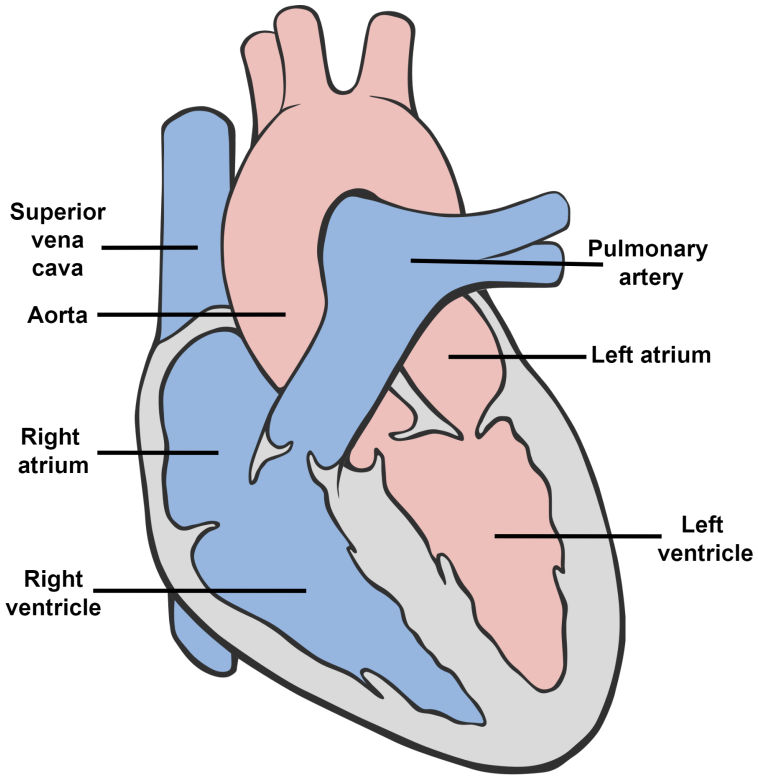

Figure 2.2: Structure of the heart. Areas containing deoxygenated blood shown in blue, and oxygenated areas in red. Modified from[3].

delay allows the atria to contract before the ventricles to deliver blood into the lower chambers. Following the delay, the Bundle of His carries the contraction pulse to the ventricles, where it expands via the Purkinje fibres. The ventricle myocytes contract during this contraction pulse, pumping blood out of the heart to supply the circulatory system.

The coronary system is the supply of blood to the heart itself. The blood travels from the left ventricle to one of three main coronary arteries: the RCA, left anterior descending, and left circumflex. Shown in Figure 2.3, the left anterior descending and circumflex arteries primarily supply the left ventricle, whereas the right coronary artery supplies the right ventricle. Later sections will discuss how restriction of these arteries can cause cardiac ischaemia.

2.1.2 Electrophysiology of Cardiac Cells

To initiate a contraction of the heart, the myocytes must be stimulated. There are three primary ions involved in a contraction: sodium (Na^+), potassium (K^+), and calcium (Ca^{2+}) [1]. This begins in in the sinoatrial node where the resting potential

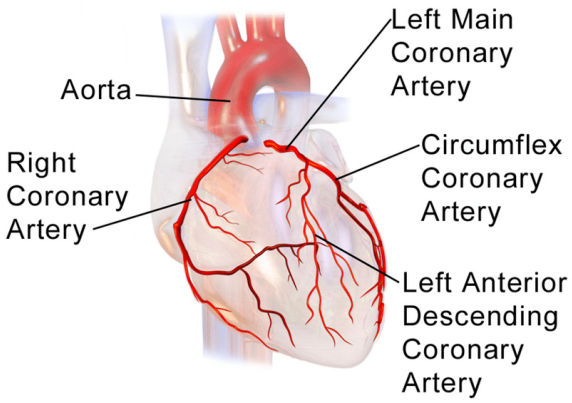

Figure 2.3: The heart the primary coronary arteries annotated [4]

is −60 mV. The slow intake of Na^+ ions decays this potential, until a threshold of −40 mV is reached. This triggers the intake of voltage-gated Ca^{2+}, which rapidly increases the potential until the cell is depolarised (0 mV). Channels in the cell membrane open to effuse K^+ ions. This repolarises the cell to its resting potential, where the cycle repeats. This process is visualised in 2.4a.

Cardiac myocytes differ to sinoatrial cells by the addition of voltage-gated Na^+ channels. Once a threshold of −65 mV is reached, these Na^+ channels allow a rapid intake and depolarisation of the cell, until +30 mV, where voltage-gated Ca^{2+} channels cause an influx that prevents the cell from repolarising. This causes a plateau effect shown in phase two of Figure 2.4b. The plateau lasts for approximately 250 ms until the channels close, allowing K^+ to flow out of the cell. This repolarises the cell, where the potassium channels close. Differing to sinoatrial cells, cardiac myocytes do not effuse Na^+, so they remain at a more stable and lower resting potential of −90 mV.

The activation and subsequent contraction of a single myocyte is spread to other cells in the vicinity via gap junctions. The increased potential caused by Ka^+ flowing to the next cell through a gap junction triggers to voltage-gated Na^+ channels, where the cycle repeats for the next cell.

2.1.3 Genesis of the Electrocardiogram

The flow of ions through the myocytes, Bundle of His, and Purkinje fibres cause a potential difference across the torso. The summation of the action potentials across the heart gives rise to the ECG, as seen in Figure 2.5[5].

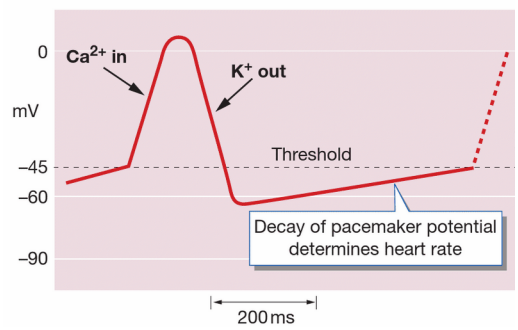

(a) Sinoatrial node action potential for one cardiac cycle.

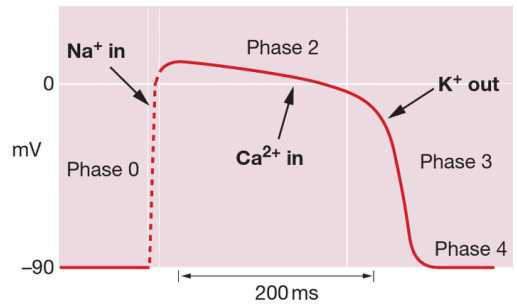

(b) Cardiac myocyte action potential for one cardiac cycle.

Figure 2.4: Cardiac action potentials for two different cardiac cells: sinoatrial node cells, and cardiac myocytes. Adapted from [1]

Atrial activity, including activation of the sinoatrial node, is associated with the P-wave. Rapid intake of Na^+ ions through the voltage-gated channels and the rapid transmission of this through the Bundle of His creates the QRS-complex. Repolarisation of the myocytes is seen as the T-wave. [6]

2.1.4 Cardiac Abnormalities

2.1.4.1 Myocardial Infarction

An infarction is the death of tissue following a blockage of blood supply. The lack of blood, or ischaemia, starves the cardiac myocytes of oxygen and nutrients, causing them to die. The primary cause of an MI is a coronary embolism. The death of cardiac myocytes can lead to reduced cardiac output, heart failure, and subsequent death due to arrhythmia or cardiogenic shock.

The position of an infarct within the heart can be detected using multiple ECG leads recorded simultaneously. The primary method of detecting an infarction is the presence of ST-elevation, the normally isoelectric segment between the S and T-waves. Ischaemic myocytes are surrounded by an increased concentration of K^+ ions [8]. Additionally, the plateau duration is also decreased. During repolarisation of the ventricles, an injury vector towards the centre of the heart is introduced, caused by a greater depression of epicardial action potentials. This causes the ST-segment to appear elevated [9]. An example of an ECG recording during MI can be seen in Appendix C.

Depression of the ST-segment can occur too. Ischaemia of the endocardium,

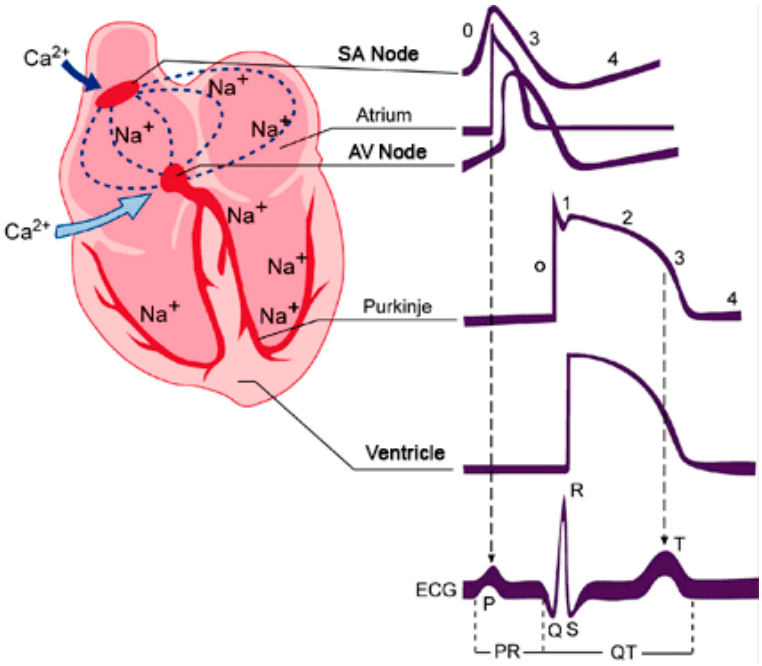

Figure 2.5: Representation of cardiac action potentials in the formation of the electrocardiogram signal [7]

the inner walls of myocytes, can cause an injury vector during repolarisation of the ventricles. This injury vector will radiate towards the epicardium, appearing as a depression.

2.1.4.2 Hypertrophy

Increased stress on the heart through high blood pressure or heart failure can cause a thickening of the cardiac muscle. This is known as hypertrophy [10]. This compensatory process ironically causes a reduction in cardiac output due to the restricted motion of the heart. The heart cannot contract as freely, decreasing the ejection fraction, the ratio of systolic to diastolic volume. Additionally, hypertrophy can restrict the conduction of action potentials across the heart. This may manifest as prolonged depolarisation on the ECG, leading to a wide-QRS. More likely is an increased R-wave amplitude, with a potential ST-depression. This effect on the ST-segment may cause confusion with MI. Hypertrophy is subsequently confirmed using an echocardiogram, and can occur in either

2.1.4.3 Bundle Branch Block

An altering or dysfunction of the His-Purkinje system can be referred to as Bundle Branch Block (BBB) [11]. The interruption of this system may cause one ventricle to contract before the other. The lack of His-Purkinje conduction on one ventricle means gap junctions are used to transmit the contraction across that side of the heart. This is a slow process and can block the next electrical stimuli causing further dysfunction of the ventricle.

Hypertrophy is also confused with MI, since the delayed depolarisation of the ventricle can cause ST-depression. Additionally the prescence of BBB, specifically Left Bundle Branch Block (LBBB) can mask a true MI. Therefore, modified criteria to detect infarcts are required which can complicate autonomous detection algorithms [12].

2.2 Electrocardiogram Information

The ECG is a term given to the measurement of electrical activity associated with the heart. There are a variety of methods, lead systems, and uses of this technology. The following section will provide an overview of these topics.

2.2.1 Measurement

The first record of electrical activity associated with an animal heart was made by Carlo Matteucci in 1842. [13]. Augustus Waller used a mercury capillary tube and two electrodes on the anterior and posterior torso to record the electrical activity of a human heart in 1887 [14]. Einthoven later used the term EKG (ECG) for the first time in 1893 [15] and improved previous designs of the electrometer capable of annotating the P, Q, R, S, and T waves in 1895 [16]. Each wave of the ECG denotes a difference phase of the cardiac cycle. The P-wave represents the depolarisation (contraction) of the atria, to pump blood into the ventricles of the heart. The QRS complex represents the depolarisation of the ventricles. The T-waves denote the repolarisation of the ventricles. The QRS complex is much larger than the P-wave, owing to the relative size of the ventricular muscle compared to the atria. Figure 2.6 shows an example of a single heart beat, with PQRST waves annotated.

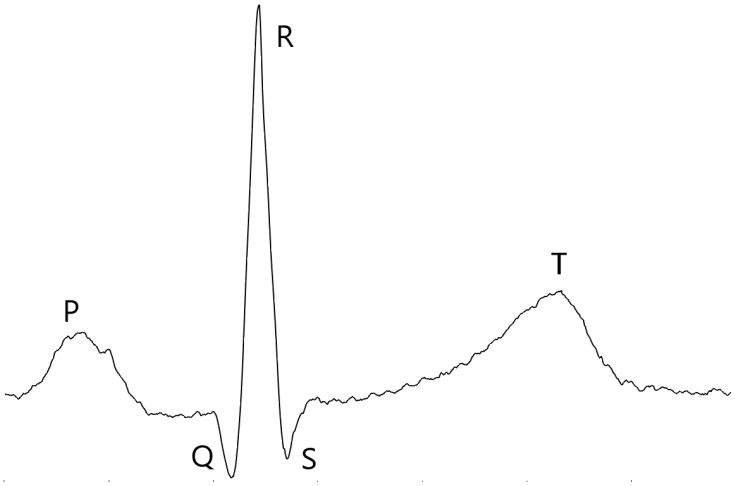

Figure 2.6: ECG lead II with annotated PQRST segments.

2.2.1.1 Bipolar Leads

Bipolar refers to a two-electrode measurement. The negative electrode potential is subtracted from the positive to give a lead. The orientation of each lead allows physicians to view the electrical activity of the heart from different angles. On a 12-lead ECG, leads I, II and III are real bipolar leads (Figure 2.7a). Three electrodes are used: right arm (RA), left arm (LA) and left leg (LL). These are referred to as the limb leads and are attached to the wrists and leg [17]. Figure 2.7b shows a modified version of the limb leads, called the Mason-Likar (ML) system [18]. The ML system is often referred to as 'exercise leads', since it allows a more ambulatory measurement than the 12-lead ECG.

The sum of these three leads form the Einthoven Triangle [19]. In the centre of the triangle, the signal is considered negligible and is referred to as the Wilson Central Terminal (WCT) [20].

2.2.1.2 Unipolar Leads

The WCT described in Section 2.2.1.1 is used as a reference for a series of unipolar leads. These comprise of six leads: V1-V6. The augmented leads (aVR, aVL, aVF) are oriented between the limb leads and can be calculated from their potentials as follows:

$$aVR = RA - 0.5(LA + LL) \tag{2.1}$$

$$aVL = LA - 0.5(RA + LL) \tag{2.2}$$

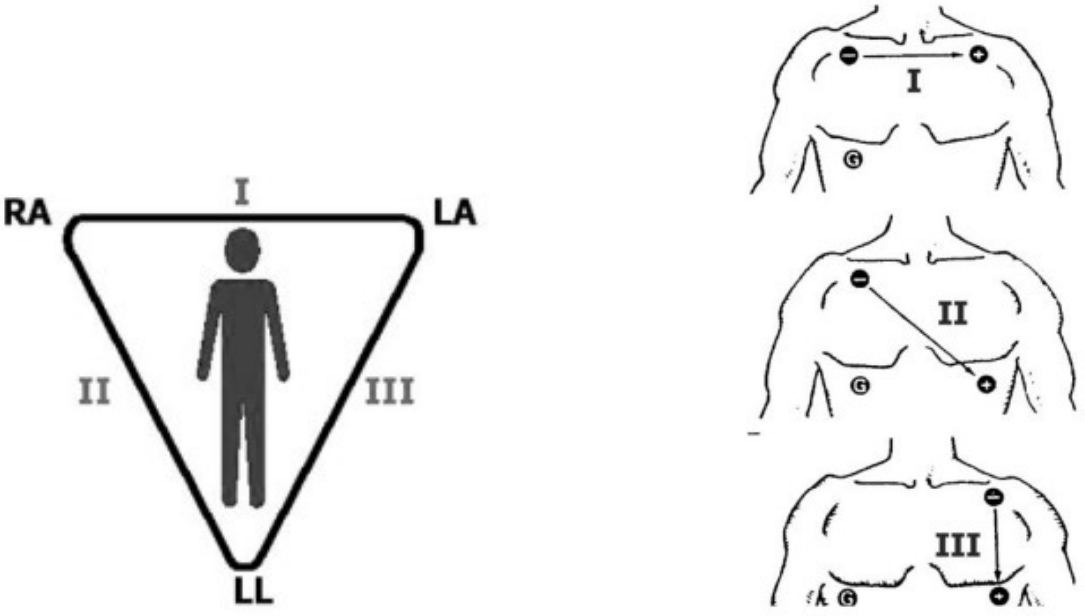

(a) Einthoven's triangle with leads I, II and III (b) ML limb leads I, II, and III

Figure 2.7: Bipolar leads of the 12-lead ECG [21]

$$aVF = LL - 0.5(LA + RA) \tag{2.3}$$

Using leads I-aVF, a physician can estimate the orientation of the heart, also known as the heart vector. Figure 2.8 shows the hexaxial reference system. This uses 30° sections rotating clockwise from the anterior view with lead I denoting the 0° point. Electrical activity travelling in the direction of a lead will produce a positive signal on the ECG. Therefore, some leads can be assumed to measure specific aspects of the heart's cycle. For example, aVF views the inferior wall of the ventrical [22]. Additionally, gaps in the hexaxial system can be filled by inverting one lead's signal. One example is the 30° point can be represented by -aVR.

The precordial leads give additional information along the ventricles of the heart and are used in the diagnosis or location-specific defects e.g. MI or LBBB. The leads are categorised based on their view of the heart: V1-V2 are septal leads, V3-V4 are anterior leads and V5-V6 are lateral leads. Figure 2.9 shows the location of these electrodes:

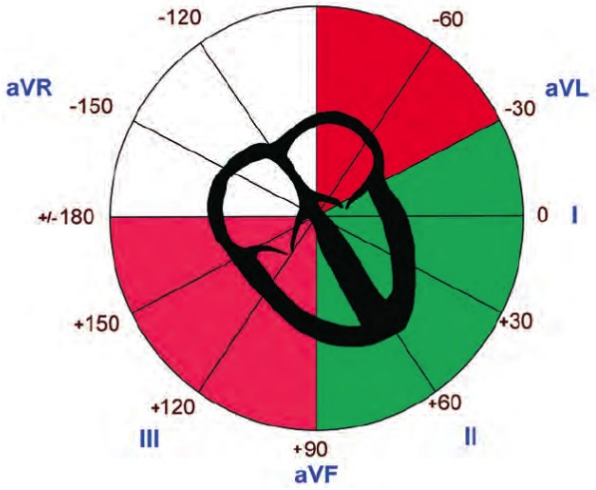

Figure 2.8: The hexaxial reference system with bipolar leads annotated [23]

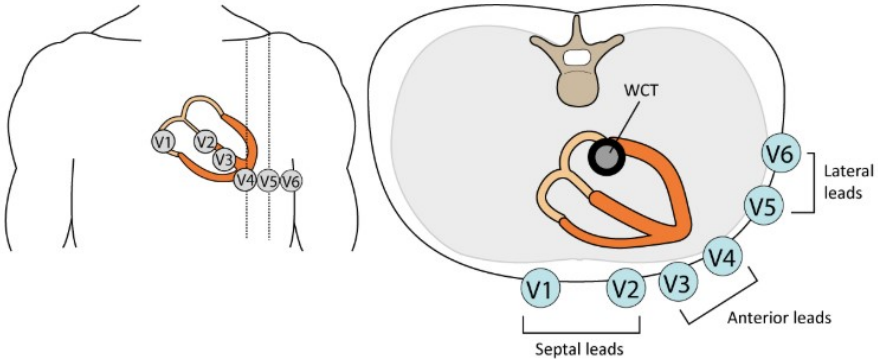

Figure 2.9: The precordial lead system - 12-lead ECG [22]

2.2.2 Short Term Recording

In many clinical settings, short duration recordings of 30 seconds or less are used to provide a snapshot of the electrical activity of the heart. Acute cardiac conditions that manifest on the ECG may be diagnosed quickly using some of the methods discussed below.

2.2.2.1 12-lead Electrocardiogram

The 12-lead ECG is captured on suspicion of AMI, and often transmitted from paramedics to the receiving hospital for expert diagnosis. To confirm MI, following diagnostic criteria are used as shown in Table 2.1.

Note, the confirmation of MI where elevation is present in the ST-segment is referred to as a ST-elevation Myocardial Infarction (STEMI). A Non ST-elevation

Table 2.1: STEMI detection criteria using the 12-lead ECG

Leads	**Criteria**
All, except V2-V3	ST-elevation $\geq 100\mu V$ at the J-point in two contiguous leads OR
V2-V3	$\geq 200\mu V$ in men ≥ 40 years; $\geq 250\mu V$ in men < 40 years; or $\geq 150\mu V$ in women OR
All leads	New horizontal or down-sloping ST depression $\geq 50\mu V$ in two contiguous leads OR
All leads	T-inversion $> 1mm$ AND prominent R wave or R/S ratio > 1

Myocardial Infarction (NSTEMI) is where a STEMI has not been confirmed using the ECG, but is later confirmed by other means. These make up roughly 40% of all diagnoses.

With the maturity of this lead platform and the standardisation of many diagnostic criteria, health informaticians have turned their focus into investigating how the lead system can improve patient outcome. A study from Sejersten et al. [24] aimed to investigate whether the transmission of the 12-lead ECG by paramedics could reduce the door-to-balloon time. The study found call to balloon time was reduced in those with a 12-lead ECG transmitted directly to a cardiologist compared to a control group (74 vs 127 minutes). This highlights how important multiple-lead short term recording systems can be in the triage of Acute Coronary Syndrome (ACS).

Van't Hof et al. [25] suggested the 12-lead ECG was capable of predicting cardiac risk factor following coronary artery reperfusion. A study of 403 patients who received successful reperfusion therapy had 12-lead ECGs recorded before and one hour after primary Percutaneous Coronary Intervention (PCI). A risk-factor was calculated using the relative thrombus size, biomarker activity and ventricular activity. The ST-segment deviation following reperfusion was compared to each patient's risk factor. Fifty-one percent of patients had complete ST-segment resolution, 34% partial and 15% no resolution. The mean total ischaemic time for patients with full ST-restoration was 226 minutes compared to those with no restoration at 338 minutes. The mortality rate was four percent for total resolution and 29% for those with no resolution after three years and one month. This study provides positive

evidence towards increased mortality for longer door-to-balloon times. Additionally, a connection between ST-segment restoration after an ischaemic event and predicted mortality has been established. Forty-four percent of the patients were not followed up after the study with no reason stated. The reasons may have affected the overall results.

Moye at al. [26] suggested the 12-lead ECG is insensitive to right coronary artery occlusion. A case study of the ECG traces from two patients presenting with confirmed RCA occlusion was conducted. Both patients met the STEMI criteria introduced in Table 2.1, however, the location of the infarct was more easily identified when using additional precordial leads. This was a small study, so additional leads will be discussed in more detail in Section 2.2.2.6.

2.2.2.2 Electrode Placement

During ACS, it is important to locate the position of the coronary lesion. The 12-lead ECG is the most commonly used method of determining the infarct location using the STEMI criteria previously mentioned. The performance of the 12-lead ECG has been evaluated for specific coronary arteries including the LAD, LCX and RCA by Zalenski et al. [27]. The patient cohort (n = 418) undergoing primary PCI would have ECG recordings analysed against the standard 12-lead ECG criteria in Table 2.1. The results concluded that ST-elevation using the standard 12-lead is marginally less sensitive without the addition of posterior and right-precordial leads. An improvement in sensitivity of 2%-8% from 85%/45%/85% (LAD/LCX/RCA) was noted with the patient cohort using additional leads (n = 102). These results fail to differentiate STEMI diagnosis for age and sex as discussed in the fourth universal definition of MI [28]. Furthermore, the 12-lead sensitivity is abnormally high compared to First Medical Contact (FMC) figures of 55.4% and 57% for AMI in related studies by Fesmire et al. [29] and Welch et al. [30], respectively. This is possibly because the ECG recordings were taken during Percutaneous Transluminal Coronary Angioplasty (PTCA); this would only be undertaken after the previous confirmation of AMI including angiography blood biomarker tests as discussed in a more recent study by Miranda et al. [31].

The effect of electrode misplacement in clinical settings can have significant im-

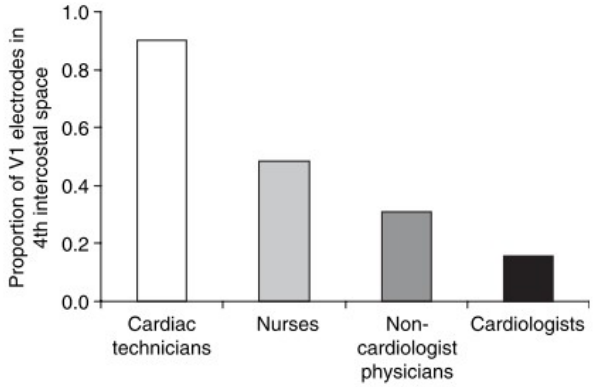

Figure 2.10: The proportion (100% = 1) of test subjects who placed precordial lead V1 in the correct location [33]

pact on the diagnostic quality of the ECG signal in computerised diagnosis. A study by Schijvenaars et al. [32] interpreted ECG changes on a BSPM with simulated electrode placement errors in a subset of 80 patients with cardiac abnormalities (n = 40 MI, n = 40 Left Ventricular Hypertrophy (LVH)). The precordial leads were shifted by up to ± 5 cm in four configurations including longitudinal, transverse and rotational movement. The computer algorithm recommended position changes in half (n = 20) of the STEMI subset, however, an expert cardiologist only agreed with four of these changes. This is an old study, dated 1997, with significant advances in algorithm development since then.

Further studies such as Rajaganeshan et al. [33] note the human-error aspect of electrode misplacement. A group of 120 professionals from cardiac technicians, nurses, physicians and cardiologists were asked to mark precordial leads (V1-V6) on a picture of the anterior torso. The results found a significant number of cardiologists misplaced the electrodes, with only 16% of cardiologists placing V1 correctly. The highest success rate was among the cardiac technicians at 90%. As previously discussed, electrode misplacement can affect the diagnosis for STEMI [32]. Figure 2.10 shows these results. Additionally, a recent study from Bickerton et al. [34] found a lack of refresher training and confidence in ECG electrode placement increased the number of diagnostic errors.

The use of machine learning has led to studies such as Kalkstein et al. [35] where errors in electrode placement of 12-lead ECG recordings can be classified. An accuracy of 91.2% was noted for the test set (n = 500 samples), with 93% accuracy on training data (n = 1000 samples). An ensemble of k-nearest neighbour (KNN),

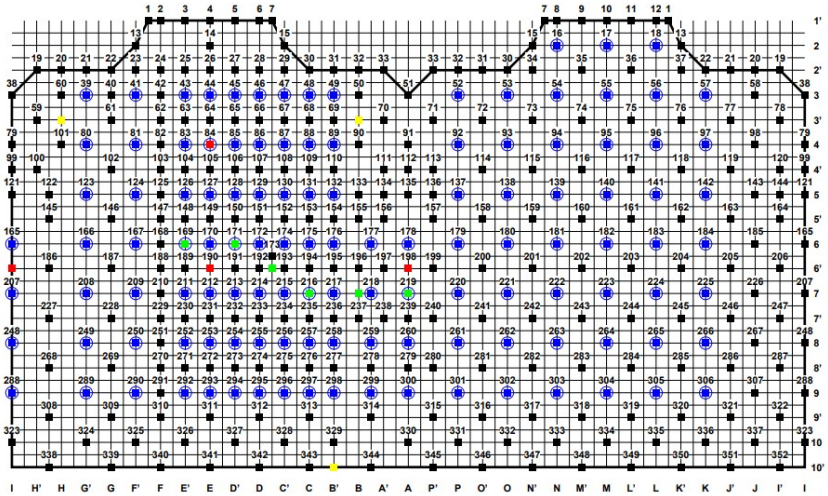

Figure 2.11: Locations of 352 nodes (black) and 120 leads of the Dalhousie torso [38]

random forest and quasi-linear classifiers were used to train the model. The ECG data was annotated by 3 to 18 examiners as part of the PhysioNet Computing in Cardiology challenge 2011 [36].

2.2.2.3 Body Surface Potential Maps

BSPMs were introduced with the goal of improving the sensitivity of heart abnormality detection by gaining a broader perspective of cardiac electrical activity. All BSPMs are recorded over the thorax, both anterior and posterior. The BSPM has not been standardised. In fact, there are multiple variations of recording, ranging from 32 leads (Lux-anterior) to 219 leads (Parma) [37]. Each map consists of unipolar leads referenced to the WCT. One such example of a mapping system is the Dalhousie torso, consisting of 120 recording sites. These sites have been expanded to 352 nodes through Laplacian interpolation. Figure 2.11 shows this BSPM with leads (blue) and nodes (black). EASI (red), ML (yellow) and precordial (green) are also annotated:

BSPMs are primarily used in two ways:

1. Clinical diagnosis

2. Experimental research

2.2.2.3.1 Clinical Diagnosis BSPMs have been proposed to improve diagnostic yield through increased spatial sampling. One of the early uses for this technology

was in the diagnosis of ischaemic heart disease. Kornreich et al. [39] aimed to find the most effective leads for diagnosing anterior and inferior myocardial infarction. There was significant work conducted at the Royal Victoria Hospital, Belfast, in these areas throughout the 1990s up to recently [40, 41, 42, 43]. These studies focused on the use of commercially available cable harnesses in a clinical setting (Heartscape, NI). Early work from this group reported the sensitivity of MI detection could be improved by increasing the number of available leads with respect to the 12-lead ECG [40, 41]. The work also focused on areas of MI detection with low sensitivity using the 12-lead ECG, specifically LCX occlusion. Later work from this group continued the investigation of improved performance in ACS. This included the investigation of performance gains that could be achieved through the addition of novel cardiac biomarkers [42] and the calculation of epicardial potentials from the BSPMs of patients presenting with chest pain [43]. Both agreed BSPMs were more valuable in MI detection than the conventional 12-lead ECG. Most recently this group have investigated the performance gain achieved when customised torso geometries were used in the calculation of epicardial potentials [44]. Other groups such as Hoekstra et al. [45] have reported large increases (27.5%) in STEMI detection using BSPMs in comparison to the 12-lead ECG. Currently there are a number of commercially available solutions toward BSPM capture [46, 47]. These are designed for both diagnostic purposes and epicardial potential mapping important to investigate arrhythmia-inducing abnormalities.

2.2.2.3.2 Experimental Research Finlay et al. [48] investigated the selection of optimum recording sites in BSPMs. This study sought to reduce the number of recording sites used in BSPMs, while retaining reconstruction integrity. BSPMs have proved valuable in experimental research relating to the development of electrocardiographic lead systems. Given that all potential lead combinations are effectively recorded simultaneously the opportunity arises to select lead subsets that are valuable for a particular purpose. Kornreich conducted a number of studies that used 117 lead BSPMs to find the best lead subjects for discriminating between a number of abnormalities which included MI and LVH [39, 49, 50, 51]. Barr [52] and Lux [53] sought to find the best subset of BSPM leads that would allow for the most accurate reconstruction of BSPMs. This is based on the assumption that leads that can most

accurate reconstruct the entire surface distribution are those which capture the most information. More recently the analysis of BSPMs by Horacek et al. [54] has been used to detect bipolar leads specific to vessel lesion location. Kennedy et al. [55] used BSPMs to select a lead specific to P-wave analysis.

As outlined above BSPMs have been used across a number of clinical and experimental application areas. The use of BSPMs in detection of acute coronary syndromes is less widespread for a number of reasons. BSPMs in the acute clinical environment have always been challenging due to the complexity of the recording process e.g. the high number of leads, difficulty in using the recording device and patient stability. In addition, the mechanisms for rapid treatment of ACS in the form of coronary artery lesions are much better established and come at a greatly reduced risk to the patient than was the case decades ago. The main change here has been in the introduction of Primary PCI. Whilst new treatment mechanisms have reduced the need to perform complex BSPM measurement procedures in the acute setting this does not negate the need for convenient ECG detection methods for acute coronary occlusion. For example, the triage of patients with chest pain and no STEMI diagnosis using the 12-lead ECG currently uses blood biomarker analysis. This could be improved by BSPM recording and subsequent diagnosis for a number of patients.

2.2.2.4 Vectorcardiogram

In 1954, Ernest Frank developed a VCG lead system for clinical use [56]. Eight electrodes were used denoting three leads: X±, Y± and Z±. Figure 2.12 shows the lead placement:

The time domain signal for one P–T complex from leads X, Y and Z are compared in three dimensions. When plotted against each other, the Q, R, and S waves of the ECG (QRS) complex forms a loop. The loop can be viewed from three planes: frontal (F), right sagittal (R) and transverse (T). This can show conduction changes in the heart including the flow of current for each contraction. Figure 2.13a shows the XYZ signals respectively. These are transformed in Figure 2.13b:

A study by Howitt & Lawrie [58] aimed to investigate the use of the Frank VCG in MI detection. The recordings from 100 patients were plotted and compared against

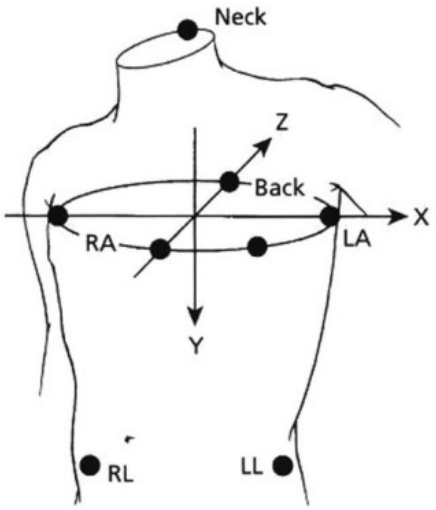

Figure 2.12: Frank lead system (VCG) placement - anterior torso [57]

each other. The population consisted of antero-septal infarction (n = 26), posterior infarction (n = 11), lateral infarction (n = 4) and posterior/septal infarctions (n = 9). The remaining patients were normal controls (n = 50). The authors witnessed distinct differences in the VCG for each condition. They noted the loops were abnormal or distorted in 78% of MI subjects. Spatial QRS-T Angle (SA) were also distorted from $-63°$ – $83°$ for normal subjects to $-175°$ – $153°$ for antero-septal infarcts. This study provided an insight into VCG for MI classification, however a small dataset and lack of information against conditions imitating MI (LVH, LBBB/Right Bundle Branch Block (RBBB)) on conventional ECGs lowers the specificity of the conclusions.

Starr et al. [59] used a larger dataset of 226 patients with the aim of developing criteria in MI detection for VCG. The algorithm was tested on another subset of 222 patients with >95% sensitivity and specificity respectively. Patients with BBB were excluded from this study, which may limit the specificity toward MI. Additionally, a single centre was used in the study, limiting the diversity of conditions present. The suggested criteria were compared against existing symptoms from Hugenholtz et al. [60].

Güldenring et al. [61] suggested the VCG was seldom recorded in clinical practice, but noted the SA was a useful tool for abnormality detection. A transformation matrix was derived to convert a ML 12-lead ECG into the Frank VCG in a single step via linear regression. BSPMs from 726 subjects consist of 120-leads of ECG

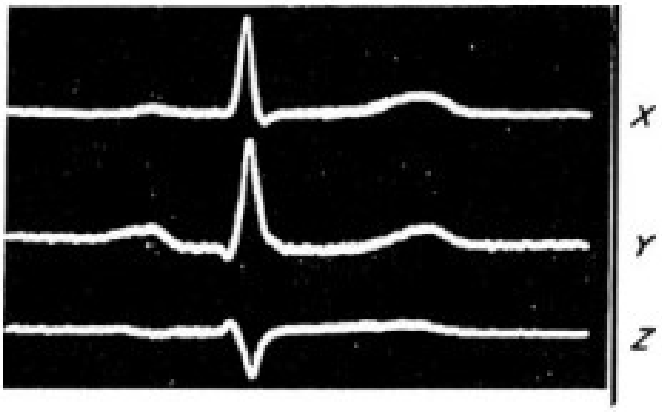

(a) Frank lead system signal in the time domain [5]

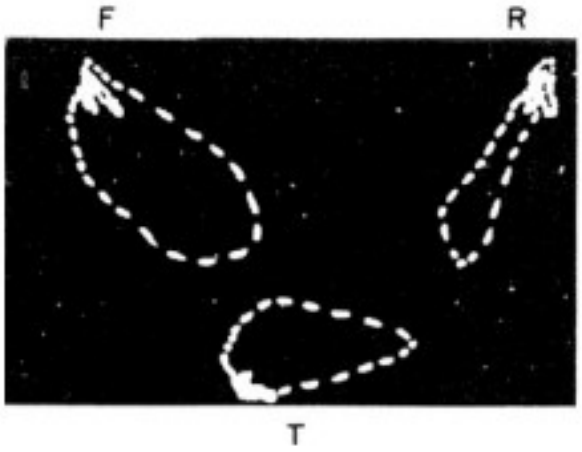

(b) Transformed XYZ signals (F = front, R = right sagittal, T = transverse) [5]

Figure 2.13: Vectorcardiogram derivation from the Frank lead system

recordings across the thorax of each patient. The recordings were split by patient condition. One third of subjects were normal, one third with MI and one third with LVH. The derived transformation matrix was compared against an existing two-step method. The authors found the Root Mean Square Error (RMSE) was lower for the single-transformation in comparison to a 2-step method. The use of BSPM assumes patient anatomy is identical across the study group. This may not be as reliable as placing the Frank VCG electrodes manually and comparing it with the ML 12-lead as a test data set. However, this method has been accepted by the US Food and Drug Administration (FDA) as the standard for computing VCG leads from a 12-lead ECG to evaluate drug effects on the heart (in vitro Proarrhythmia Assay (CiPA)). Vicente refers to this method as the "Güldenring matrix" [62].

Güldenring et al. [63] recognised the SA and spatial ventricular gradient have

clinical value. Using the Güldenring matrix discussed previously [61], the VCG of 181 subjects was computed from their respective ML 12-lead ECG recordings. In comparison to an existing 2-step method from Kors et al. [64], the SA and spatial ventricular gradient error was lower using the Güldenring matrix. This study was performed to compare two transformation methods directly using BSPMs. These assume all subjects have the same torso shape and may not reflect a true VCG recording to compare against.

2.2.2.5 Reduced Lead Sets

2.2.2.5.1 Lead Transformation A reduced lead set is often more convenient in a clinical setting than bulkier recording platforms such as the 12-lead ECG. However, many cardiac diagnostic criteria rely on the 12-lead ECG. Therefore, it is important that reconstruction of the 12-lead ECG ensures a high coefficient of correlation between recorded and derived leads. Wei [65] investigated a method of using leads I, II, V1 and V6 to reconstruct leads V2–V5. A lead vector algorithm based on the Frank torso least squares method [56] produced coefficients to reconstruct V2–V5 as a function of the recorded leads. They concluded their system was more convenient than conventional 12-lead systems for ambulatory monitoring, however, their results only provide 12-lead traces with no statistical analysis.

Drew et al. [66] aimed to prove the clinical effectiveness of derived 12-lead systems from reduced lead sets. A set of 250 patients presenting with transient MI were monitored using a reduced lead system using lead II and V1. The 12-lead ECG was derived from the reduced lead set. The derived ECG detected ischaemic ST-changes in 55 patients, whereas the more convenient reduced lead set failed to detect 64% of these. Of the five patients with reocclusion following PTCA, 100% were detected by derivation and only 40% where detected via routing monitoring. This is a relatively small study size to prove effectiveness towards ischaemia, however, constant monitoring via an ambulatory system will be more sensitive to acute changes in the ST-segment.

Drew et al. [67] continued by investigating the use of derived 12-lead ECGs further. They measured ST-segment changes during PTCA-induced ischaemia in a cohort of 207 patients who had a derived 12-lead ECG recording. Of these, 151

had a concurrent conventional 12-lead recording. The derived ECG detected 82.1% of ischaemic episodes, compared to 82.8% of episodes detected by the conventional 12-lead ECG (99% similarity). The study concluded a reduced lead system can be used to detect episodes of ischaemia with a comparable performance to current systems. During the study, the derived ECG collection method changed. Although the results are similar, this has introduced a variable which may have skewed the results.

Kors et al. [68] reviewed the principle in reconstructing missing leads that were not recorded as a practical application in clinical settings. A study from Nelwan et al. [69] was cited where noisy or poorly connected leads could be negated by removal and reconstruction. A dataset of 234 twenty-four hour continuous 12-lead ECG recordings was used. All patients were presenting with ischaemic chest pain and had previously recorded ST-segment changes. Five precordial leads were removed in differing orders, with the missing leads being calculated by linear regression. There was a 94.5–100% agreement between baseline samples for both the derived and recorded 12-lead signals. ST+60 ms amplitude differences ranged from a median of 9 μV with one lead removed to 43 μV with five leads removed.

Feild et al. [57] agreed that reconstruction of the 12-lead ECG from a subset produces an error which is too large for the reliable detection of abnormalities. For example, the MI predictor leads V2 and V3 showed up to 150μV of error where a STEMI diagnosis might be missed.

Other studies have investigated the use of reduced lead sets [70, 71, 65, 72], as reviewed by Finlay et al. [73]. All of these studies expanded signals to a 12-lead ECG. Drew et al. [71] uses six electrodes to focus on diagnosing cardiac abnormalities and ischaemia. A dataset of 649 patients, 120 of which were ischaemic through MI or balloon catheter inflation, was used to verify the interpolated leads. A similarity of 82–97% was reported during ischaemic events. This does not necessarily represent a diagnosis of MI, although it is credible since the original 12-lead ECG is available where the original diagnosis was given.

2.2.2.5.2 EASI The EASI lead system was introduced by Dower et al. [74] as replacement of the 12-lead ECG with fewer electrodes. The system uses five electrodes on the anterior torso. Four of these are bipolar (EASI), with one as a

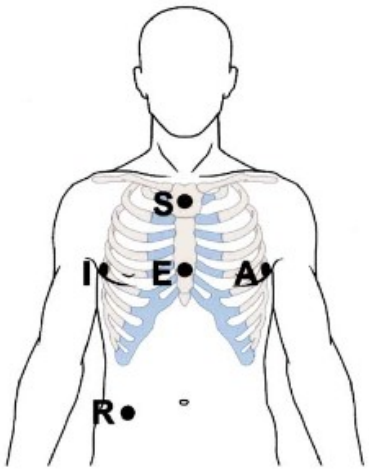

Figure 2.14: The EASI lead system electrode positions [75]

reference electrode (R). A series of coefficients based on the Frank lead system (XYZ) expand the recorded signal to a 12-lead ECG. Figure 2.14 shows their position on the torso:

Nelwan et al. [72] tested the EASI lead system as a method of detecting ischaemic events using the algorithm described by Dower et al. [74]. This study derived the 12-lead ECG from the EASI recordings. The median correlation for each lead between derived leads of the 12-lead and those physically recorded were 0.886–0.987. The standard summated 12-lead ST-deviation (SUMST) was the highest (113 μV) compared to generic population linear regression coefficients (104 μV) and patient specific coefficients (62 μV).

Horacek et al. [76] used a series of BSPM from 892 subjects with various conditions to derive an 18-lead ECG from the EASI lead system. Two methods were used: a set of transformation coefficients based on the recorded data alone; a linear regression method based on the location of the electrodes in 3D space. The large dataset used in this study contained healthy controls (n = 290), previous MI (n = 497) and Ventricular Tachycardia (VT) patients (n = 105). Ninety-one patients with single-vessel Coronary Heart Disease (CHD) undergoing PTCA were used to simulate ischaemic changes on the ECG. Correlation for transformation by recorded data was between 0.725 (III) and 0.979 (V2). Correlation by torso model transformation was between 0.597 (III) and 0.971 (V2). V2 is a predictor lead for MI detection [28], therefore a strong correlation between the EASI lead system and the 12-lead ECG is positive. The mean RMSE was 95 μV and 122 μV respectively.

A study from Drew et al. [77] aimed to compare the EASI lead system with the conventional 12-lead ECG for diagnosing cardiac abnormalities. A cohort of 540 subjects had an EASI recording taken. Included were 426 subjects whom a continuous 12-lead ECG was taken concurrently. Of this, 238 ST-events were recorded (26 AMI; 62 PTCA-induced ischaemia; 150 transient ischaemia). They found a 100% agreement between the two systems in recognising AMI, 90% for PTCA-induced ischaemia and 89% for transient ischaemia. The study provides strong evidence in favour of the EASI lead system, however serial ECGs were not recorded. Furthermore, the criteria for ischaemic events was ST-changes only which does not reflect a true diagnosis of cardiac ischaemia.

Although studies show strong correlation between EASI-derived and conventional 12-lead ECG recordings, cardiologists are sceptical toward replacing the latter. A recommendation was made by Kligfield et al. [78] to use EASI systems for rhythm analysis and labelling the recording as a derived 12-lead ECG. Additionally, these recordings must not be used routinely in cardiac abnormality diagnosis.

2.2.2.6 Additional Lead Sets

The 12-lead ECG, particularly the precordial leads, has limited sensitivity in detecting abnormalities associated with the right and inferior sides of the heart [79]. Additional leads to complement the 12-lead ECG have been introduced. These include posterior leads V7–V9 and right precordial leads V3R–V5R, known as the 18-lead ECG. During an 18-lead ECG recording, V1R and V2R are the same as V2 and V1 respectively. Figure 2.15a shows the added precordial leads (V7–V9) and Figure 2.15b shows additional right precordial leads (V1R–V6R).

Schmitt et al. [82] investigated the sensitivity of STEMI diagnosis in comparison with extended precordial leads (V7–V9, V3R–V6R) for right ventricular MI diagnosis. An occluded vessel was identified during coronary angioplasty to ensure all patients were experiencing AMI. Of the two patients observed, both showed larger ST-segment deviation in the extended precordial leads, especially right chest leads.

Hebbal et al. [83] aimed to investigate the role of aVR with additional precordial leads V7–V9. A study of 209 patients presenting with anterior and inferior wall STEMI were used. All patients were followed-up one month after revascularisation.

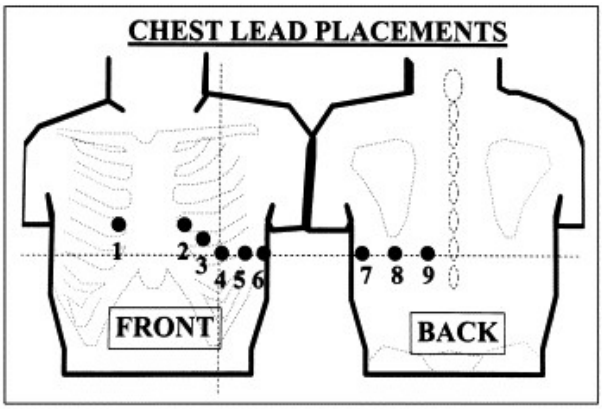

(a) Extended precordial lead placement (V1–V9) [80]

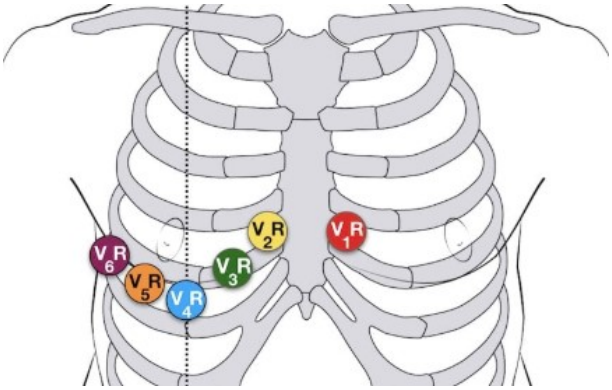

(b) Right precordial leads (V1R–V6R) [81]

Figure 2.15: Extended ECG electrode placement (V1–V9, V1R–V6R)

They found a more pronounced ST deviation in V7 was prognostic of high-risk patients. All patients who died in hospital (11.9% mortality total population) had V7 and aVR deviation. Sixty-five percent of these had aVR depression and 88% had V8–V9 depression. Different levels of ST-elevation and the prognosis of mortality were not evaluated, neither was a healthy control population used. There is limited information in the 1-month follow up to further evaluate the additional leads.

Wong [84] reviewed the usefulness of ST-elevation in leads V7–V9 to diagnose posterior MI. They confirmed a posterior MI will masquerade as an Non-ST Elevation Myocardial Infarction (MI) on the standard 12-lead ECG. Six studies were reviewed on detecting MI with the 15-lead ECG. There was a wide range of results between 3.7%–22.4% regarding the additional diagnostic value of using V7-V9. One study by Brady et al. [85] found no additional diagnostic value, however, there were only 13 STEMI patients.

Konishi et al. [86] studied the effectiveness of synthesising an 18-lead ECG from the 12-lead to detect Left Ventricular Reverse Remodelling (LVRR). A cohort of

216 patients hospitalised with a Left Ventricular Ejection Fraction (LVEF) $\leq$35% were confirmed to have non-ischaemic cardiomyopathy previously. On the 12-lead ECG, the study introduced three indicators of LVRR as a result: QRS amplitude in aVR $\geq$675 μV; QRS duration <106 ms without fragmentation; and QRS axis <67°. Their results confirmed the 18-lead ECG is useful, however the information can be synthesised from an existing 12-lead configuration. The study was conducted in an institute specialising in heart transplantation. Given it is not a community hospital and a single centre study, there may have been referral filter bias.

Ashida et al. [87] conducted a retrospective study on the sensitivity of a synthesised 18-lead ECG. A cohort of 33 patients presenting with STEMI had a 12-lead ECG recording taken within 10 minutes after first medical contact. An angiogram further confirmed the diagnosis of STEMI during PTCA, including the infarct location. They found ST-elevation in the synthesised leads was higher in patients in whom the RCA or the LCX was the occluded artery (15/22 (68.2%)) than in those in whom the LAD was the occluded artery (3/11 (27.3%)). They also claim the 12-lead ECG could only locate the area of infarction in 45.5% of patients, with the synthesised 18-lead ECG diagnosing the remaining 54.5%. The study size was small (n = 33) and conducted in a single centre. It is unclear how the 18-lead ECG was synthesised as there is no description in the article.

Additional precordial leads have been shown to detect more than ST-deviation. A study from Sasaki et al. [88] used leads V7–V9 to analyse the dominant frequencies associated with AF-induced atrial remodelling. In total, 48 patients with AF had a 15-lead ECG and Intra-cardiac Electrogram (IEGM) recorded before AF ablation. The QRS-T complex was removed to analyse the AF wave. A Fast Fourier Transform (FFT) revealed the dominant frequency for each subject. The results found a strong correlation (R) between the dominant frequencies in V8–V9 and the left-atrial floor (R = 0.55, p = 0.0061; R = 0.68, p<0.0001 respectively). This study compares both IEGM and ECG to give a more specific insight into atrial activity. However, the algorithm used to remove the QRS-T complex was by a third-party source (Cuoretech Pty Ltd) and have not been described. It is possible this system has introduced harmonics, decreasing the specificity in locating the source of fibrillation.

The addition of right precordial leads has been shown to increase the sensitivity

of right ventricular MI in a review by Nagam et al. [79]. Using the criteria V4R ≥ 1 mm, the sensitivity of right ventricular MI was 100%, specificity 87%. However, their reference later states the sensitivity was 80%–100% [89]. This makes the accuracy of the review questionable. The article also referenced Andersen et al. [90] who claimed there is a significant correlation between right ventrical ejection fraction and ST-depression in lead V4R. This was a case-study of five patients, which is too small a cohort.

2.2.3 Long Term Recording

Where short-term recordings can provide rapid diagnoses of ACS, long term recording can extend this capability. Additionally, many of these systems record for several hours to days. Such systems are discussed in the following sections.

2.2.3.1 Single-lead Systems

At present, at least two contiguous leads are required to diagnose MI [28]. However, there are several patch-based devices available that aim to detect cardiac abnormalities using short spaced leads. Additionally, a wearable device may assist physicians by extending the duration of ECG records and catch events happening outside the surgery. In this section, we will discuss the studies leading to patch development and their uses.

Studies such as Stamkopoulos et al. [91] investigated the use of a single lead in MI detection. Records from the European ST-T dataset [92] (n = 90) were used to construct a back-propagated neural network able to classify MI with 84.4% sensitivity. This is not useful in a clinical setting, but studies such as Atoui et al. [93] have synthesised the 12-lead ECG from a reduced lead set. Using a 12-lead dataset [94] (n = 300), three leads were selected (I, II, V2) to reconstruct the remaining precordial leads. An Artificial Neural Network (ANN) was trained and compared to a linear regression-based model. The RMSE ranged between 64–127 μV with an ANN approach being more accurate. Despite the high RMSE, the Correlation Coefficient (CC) was high between 0.91–0.98.

Drew et al. [95] aimed to determine whether all 12-leads in a conventional ECG are required to detect ischaemia. A total of 422 patients had continuous

Figure 2.16: Vital Connect® disposable patch (left) and wireless activity tracker (right) [96].

12-lead ECG recordings taken while experiencing AMI or during PTCA at Peak Balloon Inflation (PBI). An algorithm determined which lead showed the largest ST-segment deviation. In the refractory period, 28% of patients experienced an ischaemic episode. Using the single lead system, 80% of these were undetected. The article concluded the 12-lead ECG is necessary to detect ischaemia, however more recent studies have contradicted these findings.

A single-lead and short-spaced lead wireless patch introduced by Vital Connect® measures ECG, respiration and kinetic activity. The patch is disposable, with a removable activity monitor and transmission device. A study by Chan et al. [96] investigated the patch performance by comparing it to existing pedometers Fitbit®, Omron® and a nasal canula. Three patch orientations were tested. They found the patch location with the least number for beat errors was diagonally oriented on the left side of the upper torso. This gave the lowest median heart rate error and highest fall detection sensitivity (95.7%). Figure 2.16 shows the patch and wireless activity tracker below:

Breteler et al. [97] used the Vital Connect Health Patch® in a study of 25 high-risk surgical patients admitted to a step-down unit. They concluded the patch was accurate for heart rate detection (-8.8 to $+6.5$ bpm), however, respiration rate was inaccurate (-15.8 to $+11.2$ breaths per minute). The authors admitted the technology is useful for monitoring potential patient decline post-discharge from a high-risk procedure.

The CardioSTAT® is a single-lead patch which can detect and report AF [98]. The patch is placed laterally in the upper centre of the chest, similar to the lead I

configuration. A study by Nault et al. [99] compared the patch with a 24h Holter monitor. Seven patients with suspected AF were recruited for a 24-hour recording from both devices. They found a strong correlation between the CardioSTAT and Holter monitors, with 100% detection similarity for AF beats.

iRhythm's Zio XT® monitor is a single lead patch designed to compete with the Holter monitor [100]. The XT has been reviewed by many articles [101, 102, 103, 104, 105, 106, 107]. Rosemberg et al. [104] attached the patch and a Holter monitor to 74 patients with diagnosed paroxysmal AF for a mean of 10.8 days. There was no difference in AF burden estimated between the two. The patch changed the diagnosis and further treatment of 28.4% of patients in the study, an improvement over the existing technology. Additionally, it was noted the patch allowed a significantly longer recording period up to 14 days.

The BardyDX Carnation Ambulatory Monitor (CAM)® [108] is a single lead patch which adheres vertically along the sternum. It is primarily for detecting P-wave abnormalities toward AF diagnosis. Rho et al. [102] compared the Zio XT® to the CAM® in a study of 30 patients. The CAM® performed more favourably, with a 40% higher detection rate of abnormalities than the competitor. A study from Smith et al. [109] found 96% of patients preferred to wear a patch device than a Holter monitor.

The RootiCare® is a single lead patch mounting laterally across the upper chest, much like lead I [110]. It can record for seven days continually and has a patient event button. The supplied software suggest a diagnosis for abnormal beats. Karaoguz et al. [111] held a study with 33 healthy subjects and 67 patients referred from an arrthythmia clinic. They found a strong (98%) correlation in beats to the Holter monitor. Detectable abnormalities included AF, VT, paroxysmal supraventricular VT and abnormal R–R pause.

2.2.3.2 Holter Monitors

A Holter monitor is an ambulatory lead system designed to be worn for 24–48 hours, similar to that shown in Figure 2.17. The Holter is primarily designed to monitor arrhythmia, however studies from Vukajlovic et al. have investigated the use of the device for 12-lead reconstruction and subsequent abnormality diagnosis [112, 113].

Table 2.2: Current patch-based ECG recorders

Ref.	Manufacturer	Electrodes (#)	Description
[96]	Vital Connect	2 (1-lead)	A single-lead disposable patch with activity, fall and respiration tracking
[98]	CardioSTAT	2 (1-lead)	Primarily for AF and paroxysmal AF detection
[100]	iRhythm Zio XT	2 (1-lead)	Primarily for AF and paroxysmal AF detection, up to 14 days recording
[108]	BardyDX CAM	2 (1-lead)	Primarily for detecting P-wave abnormalities, including AF.
[110]	BeyondCare EPM/RootiCare	2 (1-lead)	Lead I configuration

This work particularly focused on AF detection. Stern & Tzivoni [114] identified the use of Holter monitoring for ischaemic heart disease. A 12-lead was recorded in situ, with transient ischaemic attacks identified in all patients by both systems.

Jernberg et al. [115] found patients who had continuous 12-lead ECG recordings gave clinicians a clearer understanding of their cardiac risk. Kuchar et al. [116] showed the monitor can improve the prognosis of patients discharged after MI. Treatment can be delivered for paroxysmal or transient arrhythmia after analysis of the ECG traces.

A study from Brodsky et al. [117] highlighted the importance of cardiac monitoring in the absence of symptoms. A cohort of 50 apparently healthy male volunteers were fitted with Holter monitors for 24 hours. Fifty percent of subjects experienced sinus arrhythmia without symptoms. Using the monitor, the authors concluded frequent atrial and ventricular premature beats are unusual in a young adult male population, with bradyarrhythmia being common.

The use of ambulatory monitors has allowed correlation between arrhytmia and life-threatening illnesses. Ventricular ectopic beats were found to correlate cardiac death after AMI by Moss et al. [118]. Analysis of the frequency domain of Holter recordings post-MI showed signals relating to malignant arrhythmia lack power at higher frequencies (0.15 to 0.50 Hz) [119]. Holter monitoring has use in cardiac performance under strain. Langer et al. [120] investigated the effects of exercise

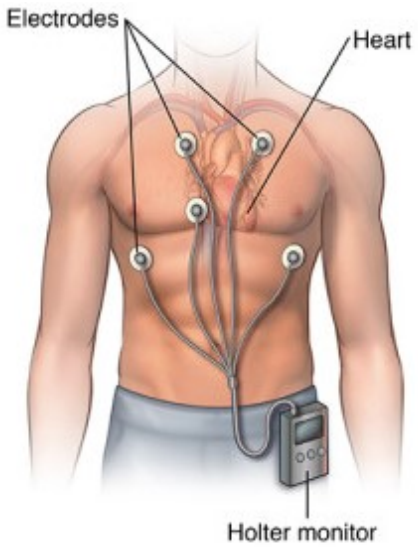

Figure 2.17: Holter monitor with electrodes fitted [122]

after AMI. Thirty-three percent of patients developed ST-depression, with the same group having a higher mortality rate (27% vs 6%). They concluded the utility of Holter monitoring for prognosis post-MI.

More recently, Mäkikallio et al. [121] aimed to evaluate the risk of Sudden Cardiac Death (SCD) following AMI using a Holter monitor. Two thousand, one hundred and thirty subjects who had suffered MI were fitted with monitors and followed up after a median of 1012 days. The study concluded the Holter monitor was sensitive in the detection of SCD with an ejection fraction >35%, but insensitive ≤35% Ejection Fraction (EF).

2.2.3.3 Ambulatory Multiple-lead Systems

Mason et al. [123] highlighted the need for long term ambulatory ECG systems, particularly to monitor arrhythmia during exercise. Roelandt et al. [124] recognised the need by investigating 20 instances of monitored cardiac death. The study found no warning arrhythmia or predictors of SCD, but highlighted the need for further research and large-scale ambulatory monitoring of high-risk patients.

Deanfield et al. [125] monitored 20 patients with stable angina for four days about their daily lives. Downsloping ST-depression was an indicator of angina in 24% of cases in the absence of symptoms. This study allows clinicians to better understand how out-of-hospital behaviours affect the heart, particularly in managing the risk of a future MI.

To further understand the mechanisms of SCD, Bayés de Luna et al. [126] used ambulatory monitoring to investigate the fatal arrhythmia of 157 patients. The most common arrhythmia as the cause of death was ventricular tachyarrhythmia (84%). The study theorised spontaneous VT was the cause of death, but there is little evidence on the root cause in the article. Subsequent studies have used more portable monitors to detect SCD, such as Simpson et al. [105] who used a single lead patch.

Martinez et al. [127] found continuous ECG monitoring increases the sensitivity of myocardial ischaemia detection. During the study, 149 patients undergoing elective infrainguinal or aortic vascular surgery who were admitted to the intensive care unit post-operatively were used. The results showed the current intensive care 5-lead monitor is not sensitive in detecting prolonged MI (12%). The study urged caution in the use of reduced-lead systems in critical-care environments. This is a small study, with advances being made toward MI detection since then.

Finlay et al. [128] reviewed practical scenarios for wearable ECG monitors. Although the study investigated optimal lead placement, the focus was to develop a shirt-based lead system for smart clothing/smart textiles. BSPM data was used to select multiple areas of the thorax to capture the most electrocardiograhic information. Ten recording sites were proposed, with the number of electrodes ranging from 10 to 32. Since then, numerous studies have investigated the use of wearable shirt-based devices to capture ECG data [129, 130, 131, 132].

Having recently been granted FDA approval, the LifeSignals Patch is available for clinical trials, ambulatory monitoring and consumer use [133]. It has six electrodes and a software package to further analyse signals. The device is disposable and communicates via Wi-Fi for up to five days. LifeSignals has designed the device to work on their CardiacApp and Receiver platforms. There are currently no studies validating the patch accuracy. The ScottCare Novi® patch is a 3-lead device with 14-days recording time. It is compatible with existing Holter monitor software and is offered as a replacement monitor. No publications were found for this device.

2.2.3.4 Cardiac Event Recorders

A cardiac event recorder is a wearable ECG-based device which allows patients to record when they experience symptoms. The monitor is worn for days or weeks. A clinician will review the recorded events before recommending further treatment or medication. They are typically sorted into two categories:

1. **Loop recorders -** a pager-sized device with electrodes attached to the chest with an event button. The patient will press the button upon symptom onset to begin the recording

2. **Symptom event monitors -** a handheld or wrist-worn device designed to be placed on the chest when the patient experiences symptoms

Roche et al. [134] aimed to test the accuracy of a device called the R-Test Evolution in arrhythmia detection. A small study of 35 patients were fitted with the device and a Holter monitor. The device performed with 100% agreement in bradyarrhythmia, but 86% for tachyarrthyhmia. The single-lead system was able to capture Atrio-Ventricular (AV)-block and AF upon further analysis from a clinician.

The value of event recorders was investigated by Caires et al. [135] with the conclusion that symptom outcome from advanced treatment was more favourable in those who had worn a device (97% vs 55%). This is particularly true in the case of sporadic symptoms. Kinlay et al [136] suggested event recorders were more cost effective than 48-hour Holter monitors in monitoring patients experiencing palpitations. A small study of 43 patients with previously uninvestigated palpitations were referred for Holter monitoring. The event recorders detected arrhythmia in 19% of patients, with the Holter monitors detecting none. The study concluded Holter monitoring is $213 more expensive for each diagnostic rhythm strip and less sensitive. Each patient had either a Holter or an event recorded fitted, not both. These findings are confirmed by Asmundis et al. [137] using the OMRON HeartScan®. A larger study of 577 patients with palpitations (92.3%) and dizziness in 48 (7.7%) found the Holter was only sensitive to 1.8% of arrhythmia. Conversely, the Heartscan detected 89% of arrhythmia. Rothman et al. [138] compared the two-lead MCOT monitor to a single-lead loop recorder in the detection of arrhythmia. 300 patients were recruited who had presented to a clinician with previous symptoms. The MCOT

device was found to be more sensitive (89% vs 69%) in providing the clinician with sufficient information for diagnosis.

Numerous studies have investigated the use of event recorders in diagnosing patients experiencing syncopal (fainting) episodes [139, 140, 141, 142]. Sarasin et al. [140] used a population of 611 patients experiencing syncope. Of these, 69% had the cause identified, however the remaining patients underwent further testing including event recorder fitting. A further 25% of arrhythmatic causes were identified, with this group showing the highest mortality rate (9%). This highlights the need for ambulatory monitoring. More recently, Brandt et al. [143] investigated the link between syncopal hallucinations and out-of-body experiences using an event recorder. Multiple events of arrhythmia were noted, with subsequent treatment involving a pacemaker implant. Syncopal episodes and hallucinations stopped following surgery. This is a single case study so a larger dataset is needed before drawing conclusions.

Multiple studies have used cardiac event recorders in the detection of paroxysmal AF [144, 145, 146]. In these studies, there is particular interest in the area of transient ischaemic attacks and their connection with AF.

Early intervention in cardiac abnormalities is essential. A study by Park et al. [147] emphasised the use of monitors for all ages. A study of 30 children between 9–14 years experiencing syncopal episodes led to the subsequent diagnosis of superventricular tachycardia in four patients. All were treated with cardiac ablation therapy and showed no further symptoms.

2.2.3.5 Modified Chest Leads

MCL are adaptations of standard bipolar leads worn on the anterior torso. They offer the advantage of maximising P-waves for dysrhythmia monitoring and increase sensitivity of three electrode system for anterior wall ischaemia monitoring [148]. Most variations range from the 3-electrode MCL_1 to the 5-electrode MCL_5 with the precordial lead V1 recorded. The ML 12-lead ECG described previously in Section 2.2.1.1 is also an example of a MCL, with distal limb leads moved proximally to the shoulders. Figure 2.18 shows a limited number of MCL configurations:

The use of MCLs was investigated by Marriott [149] who suggested MCL_1 was a suitable variation for detecting arrhythmia and conduction defects. From a practical

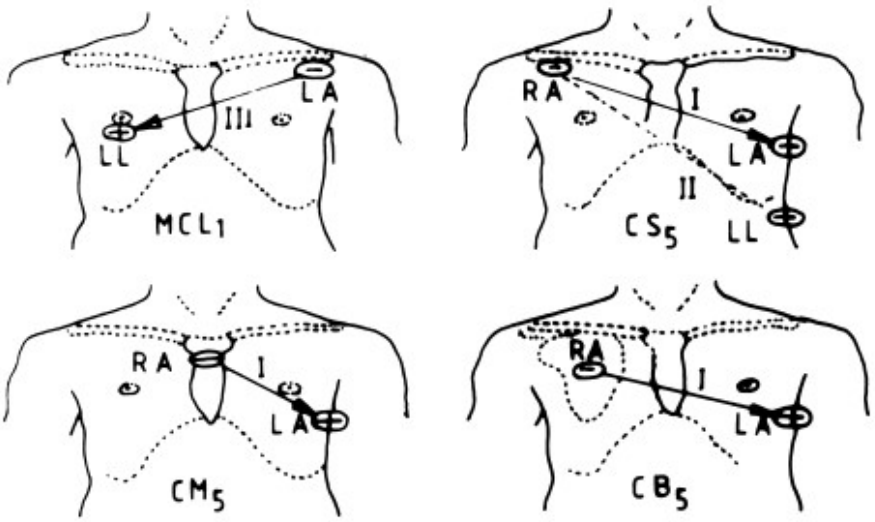

Figure 2.18: MCL positions on the anterior torso [148]

view, Desanctis et al. [150] agreed MCL_1 was convenient and commented it removed electrodes from areas frequently examined by clinicians. At the time (1972), recording ECGs was done by memory loops. A single lead setup like this also reduced the need for large recording systems. Additional early work from Gay & Brown [151] saw the use of MCLs toward the detection of RBBB after AMI.

Marriott later confirms the use of MCLs as a detector for AV block. Specifically, it was noted the use of a right chest lead for continuous monitoring is sensitive for AV block and BBB detection [152]. Campbell et al. [153] compared an MCL lead variation for Holter monitoring, noting 56% of subjects developing arrhythmia during anaesthesia who had a history of MI or Cardiovascular Disease (CVD).

Drew et al. [154] conducted a study into the value of MCL_1 and MCL_6 in the diagnosis of wide QRS complex tachycardia. They found a single MCL was more valuable than a single bipolar lead II. The combination of MCL_1 and MCL_6 was also more sensitive than the routinely monitored V1 with lead II.

2.2.4 Other Lead Systems

2.2.4.1 Condition-specific leads

A condition-specific lead system is designed with high sensitivity in detecting a small number of abnormalities. Early work from Aldric et al. focused on selecting the optimal leads toward AMI [155]. This work aimed to find ST-deviations during ischaemia using existing 12-lead ECG. Specifically, ST-elevation was used as the predictor. Lead III saw the highest frequency of ST-elevation for inferior MI (94%) and lead V2 for anterior MI (99%). All patients were previously triaged as STEMI and no BBB or LVH was noted. This may not be accurate for the additional conditions mentioned.

Work from Lux et al. [156] studied the use of optimal leads for ST-T elevation in a large-scale study of 1,000 patients. Leads chosen from earlier work [157] were tested against Mortara H12 Holter monitors (leads I, II, V2, V6). Initial findings found 17% of MI diagnoses (troponin positive) could be detected as STEMI using MI-specific leads. More recent work from Loewe et al. [158] has attempted to localise the position of infarct to 17 areas using Magnetic Resonance Imaging (MRI) and ECG data. The specific lead detected 60% of AMI. Of those, the location was detected correctly between 50–75% of the time in the left ventrical. The authors admit only two patients MRI models were used, but personalised medicine could improve the sensitivity of STEMI classification.

Numerous studies have investigated optimum leads of measuring atrial activity, with the focus towards AF [159, 160, 161, 162, 163, 164, 165]. The P-wave is an indicator of atrial activity, so work by Waktare et al. [160] aimed to subtract QRS-T complexes from each beat, leaving only atrial information. Gerstenfeld et al. [159] used BSPMs to find seven optimum leads in detecting pulmonary ectopic beats. The seven-electrode setup was more sensitive than the nine-electrode ML 12-lead ECG (97% vs 95.7%). Ihara et al. [161] sought to modify the precordial lead positions of the 12-lead ECG to focus on atrial activity. A simulation moved the six leads to a closely-spaced grid on the anterior torso, however there is limited information of the diagnostic significance of this. Ihara et al. [163] improved the study by using a larger dataset of 25 patients, suggesting modified precordial leads offer a five-fold

increase in AF detection rates compared to the 12-lead ECG. Igual et al. [162] noted the practicality of a reduced lead set towards AF detection. BSPMs were used to extract the areas with significant potential differences during AF episodes. Only five patients were used in this study, so further investigation is required. Petrénas et al. [164] used a modified Lewis lead system [166] in comparison with the ES lead of the EASI system for ambulatory monitoring. The study concluded that strenuous activity such as heavy lifting can trigger AF.

Patch-based devices are often designed for single-condition diagnosis. For example, a study from Alcaraz et al. [165] aimed to cancel ventricular activity from a single-lead system to ease AF detection. Invasive methods such as the esophageal ECG have been used in monitoring atrial activity, including a study from Haeberlin et al. [167] which aimed to investigate the optimum depth insertion for electrodes.

Electrocardiograms also capture noise. A study from Finlay et al. [48] identified three bipolar leads, called Eigenleads, to capture the maximum signal amplitude and reconstruct the total body surface potential while minimising signal to noise ratio (SNR). The chosen leads were shown to increase signal strength (RMS) by 27.9%, 39.0%, and 20.3% for P-waves, QRS, and ST-T segments. These leads were primarily in the precordial region of the anterior torso.

Ito et al. [168] highlighted the need for specific leads during ablation therapy. Analysis of 12-lead ECG suggested an algorithm correlating to the ablation, however the authors admitted a limitation could have been the choice of recording site. This has been more thoroughly investigated by Hachiya et al. [169].

For drug dose validation, Sadanaga et al [170] suggested limb leads are more sensitive to Q to T segment of the ECG (QT) prolongation, however concluded the use of leads V3 and V4 together would differentiate between QT interval and prolongation more accurately. The use of VCG has more recently been used to validate drug dosages with the introduction of the Güldenring matrix [61], as discussed in Section 2.2.2.4.

2.2.4.2 Vessel-specific Leads

Early work from Feldman et al [171] aimed to find the optimum recording sites for use during PTCA. The priority was the detection of ST-segment deviation during

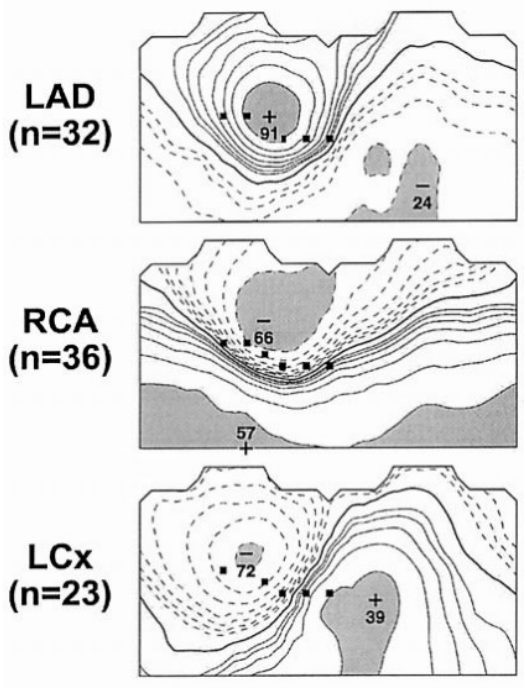

Figure 2.19: Optimal electrode locations (+,-) to detect myocardial ischaemia for each coronary artery with precordial leads shown (V1–V6) [54]

balloon inflation and subsequent deflation. The study highlighted the need for a complete 12-lead ECG to be recorded, as different coronary vessel occlusions will show elevation in different leads. Since then, other studies have highlighted the importance of locating the coronary lesion [172, 173].

Horacek et al. [54] investigates the use of vessel-specific leads towards a more sensitive detection of STEMI. Patients undergoing elective PTCA have ECG recordings taken before and during balloon inflation in LAD, LCX and RCA vessels. The difference in ST-segment amplitudes are recorded (ΔST) for each possible lead. The leads with the highest ΔST for each coronary artery were found. These can be seen in Figure 2.19. The use of Vessel-Specific Leads (VSL)s for STEMI detection is not described in the definition of MI, therefore, it is difficult for a physician to diagnose AMI with certainty. Horacek et al. [174] built upon the previous study by extrapolating the VSL from a 12-lead ECG. Linear regression developed a series of coefficients to estimate each VSL. The results improved upon the 12-lead ECG sensitivity, from 60% to 76%. A ΔST of 125 μV is set as the threshold for STEMI detection. This also contradicts the universal definition of MI [28] and does not take sex-specific changes into account. They note the sample size (n = 99) is too small to take individual differences into account.

2.3 Myocardial Infarction Detection

2.3.1 Clinical Definitions

The first agreed clinical classification of ischaemic heart disease (IHD) between the World Health Organisation and Joint International Society and Federation of Cardiology defined ECG changes as a classifier of MI [175]. Specifically, T-wave inversion, new Q-waves and conduction changes are symptoms of AMI. This definition has evolved to a first universal definition of MI from the joint ESC/ACCF/AHA/WHF task force [176]. The fourth universal definition of MI is the current edition at the time of writing [28]. Based off this, MI can be sorted into five categories, with only relevant ECG changes described below:

1. Atherothrombotic occlusion: new ischaemic ECG changes and the development of pathological Q-waves

2. Mismatch between oxygen supply and demand: new ischaemic ECG changes and the development of pathological Q-waves

3. Deceased patients with presumed MI: ECG changes leading to Ventricular Fibrillation (VF) and subsequent death

4. Medically-induced MI: split into three categories encompassing type 4a to 4c. Percutaneous Coronary Intervention thrombosis, stent/scaffold thrombosis and restenosis following PCI

5. Thrombosis during coronary artery bypass grafting

The ECG is measured using a 12-lead ECG or equivalent. An elevated ST-segment in at least two contiguous leads is an indicator of MI, designated as an STEMI. Specifically, >1 mm (100 μV) ST-elevation in all leads other than V2/V3. Men over 40 require ≥ 2 mm (200 μV) ST-elevation in leads V2/V3 and ≥ 2.5 mm (250 μV) in men below 40 years old. Women require ≥ 1.5 mm (150 μV) ST-elevation regardless of age. ST-depression of ≥ 0.5 mm (50 μV) in two contiguous leads or >1 mm of T-wave inversion with an R/S ratio of >1 also indicate AMI. If a previous ECG recording of the same patient is available, this can be compared with a current

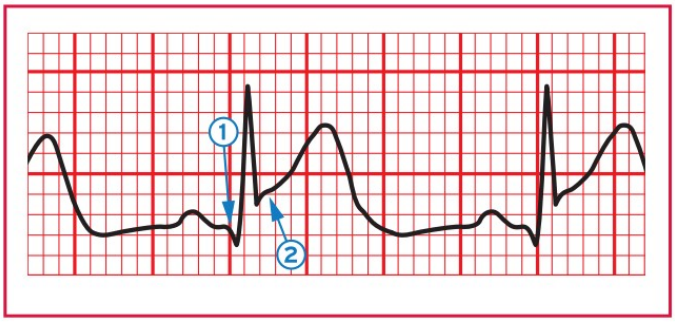

Figure 2.20: Electrocardiogram trace during AMI. (1) new pathological Q-wave. (2) ST-elevation at the J-point [28]

recording with new J-point (ST) elevation of >1 mm as an ischaemic response. The aforementioned criteria are absent of LBBB and LVH. Figure 2.20 shows the effect of a STEMI on the ECG. New pathological Q-waves are visible with 2 mm (200 μV) of ST-elevation at the J-point.

Patients may delay visiting a hospital after AMI. A prior MI can be detected as a Q-wave in leads V2/V3 >0.02 s (0.5 mm) or >0.03 s (0.75 mm) in leads of contiguous grouping. Any contiguous lead grouping with a QS complex indicates prior MI. A wide R-wave >0.04 ms (1 mm) in V2/V3 and an R/S ratio of >1 with a positive T-wave is also indicative of a prior MI.

Upon presenting to paramedics with chest pain, an ECG is recorded and interpreted by a trained professional. A STEMI diagnosis will be treated with primary PCI. The affected coronary artery will undergo reperfusion within 120 minutes of symptom onset. Patients not fulfilling the STEMI criteria require further testing including serial ECGs every 15–30 minutes and blood tests. A MI may be diagnosed, where primary PCI or fibrinolysis will treat the lesion [177]. Figure 2.21 shows the Minnesota Chest Pain/ACS tool-kit guidelines of ACS treatment. The focus of this review is on ECG changes during MI, so we will focus on STEMI diagnosis and treatment.

2.3.2 Rule-based Diagnosis

Although universal definitions of MI exist, many institutions develop rule-based diagnostic methods which claim higher sensitivities toward MI detection.

Mair et al. [178] investigated existing methods of MI detection at the time including creatine-kinase, troponin, and myoglobin biomarkers. They noted that

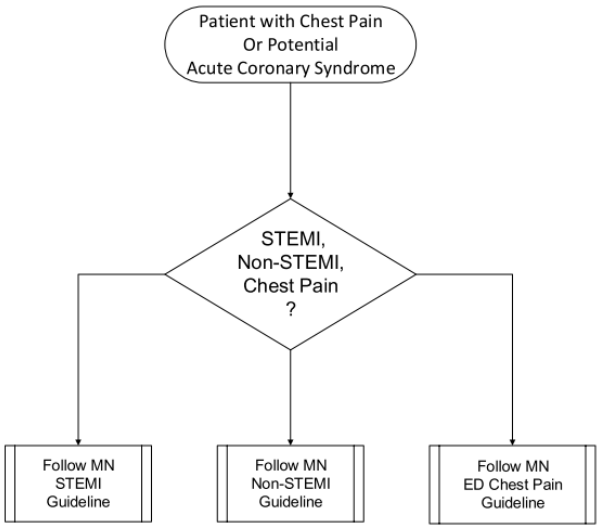

Figure 2.21: Minnesota Chest Pain/ACS diagnosis toolkit guidelines showing three steams of ACS treatment [177]

ECG had the highest Area Under the Curve (AUC) in the Receiver Operating Characteristic (ROC) curve. Grijseels et al. [179] suggested a pre-hospital rule matrix to more efficiently triage patients with chest pain. The study focused on the use of five predictors to qualify further treatment. The more predictors were present, the more likely the patient would be admitted. For inferior MI, Pahlm et al. [180] developed a decision rule approach focused on Q-wave amplitude with 75% sensitivity and 97% specificity. Cayley [181] developed a broader decision tree to triage chest pain into MI, heart failure, pulmonary embolism and asthma. The aim was to improve the current triage of chest pain so more serious conditions like MI are correctly treated. Following this trend, Christenson et al. [182] developed prediction rules to expedite the discharge of less critical patients based on ECG, pain levels and blood biomarkers. More recently, Hess et al. [183] used a wider number of variables from patient history, demographics and physical characteristics to triage emergency department patients with chest pain. Glickman et al. [184] used numerous features from emergency department visits and subsequent STEMI diagnoses to develop a simplified flowchart for further treatment. Conditions such as dyspnea, altered mental status and syncope were identified for immediate triage. A rule-in, rule-out strategy towards high sensitivity cardiac troponin (hs-cTn) was developed by Reichlin et al. [185]. This was designed to reduce the complexity in AMI triage, noting further treatment will rule-out AMI if the test was not specific.

2.3.3 Automated Diagnosis

The use of automated tools assists physicians in the detection of AMI. Many devices exist with embedded algorithms which monitor the ECG and alert medical staff in the presence of abnormalities [186][187][188]. In this section we will investigate the scope of current MI detection methods.

The fourth universal definition of MI notes ST-segment changes and T wave deviations as indicators of AMI for clinicians [28]. Research by Prescedo et al. [189] discussed the use of fuzzy logic to detect deviations in the ST-segment of ECG recordings. Using the European ST-T dataset [92], five subjects were selected who were previously diagnosed with MI. Deviations in the ST-segment were weighted and increased linearly from 50 μV to 100 μV. The duration of ST-deviation was also weighted linearly between 20–30 seconds. The combination of fuzzy logic variables yielded a sensitivity of 98.00% and specificity of 91%. With the low number of participants (n = 5), these values were calculated based on the total number of ischaemic beats.

Bozzola et al. [190] built upon this with the introduction of a neuro-fuzzy hybrid classifier. A larger dataset from the Catholic University of Louvain [191] was used with 539 subjects: 300 subjects with diagnosed MI, 139 with LVH/Right Ventricular Hypertrophy (RVH) and 100 healthy controls. Linguistic description (fuzzifier) weights the extracted features where a Multi-Layer Perceptron (MLP) outputs the certainty of MI. The linguistic justifier determines whether the MLP certainty is $\geq$75% for diagnosis. Both MLP and hybrid fuzzy-MLP methods were used. Fuzzy-MLP performed marginally better than the former. The sensitivity was between 60.00–72.00% depending on the ischaemic location with a specificity between 92.73–95.45%.

Vectorcardiograms have been used by Correa et al. [192] to identify key features between healthy and ischaemic subjects. A cohort of 132 subjects were chosen: 80 of these were recorded before PTCA with 52 healthy controls. The VCGs were calculated from X, Y and Z electrodes, with the QRS loop selected for further analysis. The differences between QRS loops of normal vs ischaemic subjects were clustered. A classifier was used to suggest MI, exhibiting 85.50% sensitivity and 92.10% specificity. A follow-up study from Correa et al. [193] identified four VCG

features they deemed most suitable for MI detection using the same dataset. This improved the sensitivity and specificity to 90.50% and 92.60% respectively.

Similar to VCG studies, Dhawan et al. [194] suggested transforming an ECG into three dimensions. A total of 201 subjects presenting to an emergency department (n = 113) or cath lab (n = 88) were selected, with 52 STEMI, 60 MI and 89 subjects with no AMI. The three-dimensional ECGs were clustered based on the differences between STEMI, MI and control. A Support Vector Machine (SVM) was able to classify MI for both STEMI and MI, with a sensitivity of 86.82% and specificity of 91.05%.

A study from Wang et al. [195] used the 12-lead ECG to propose the cardiodynamicsgram (CDG). A learning algorithm extracts ST-T features from the Physikalisch-Technische Bundesanstalt (PTB) database [196] and compares ischaemic responses with normal ECG. Three hundred and eighty five subjects of which 234 suffering MI and 151 healthy subjects were used. A sensitivity of 90.30% and specificity of 87.80% was achieved.

The diagnostic performance of ECG recording devices in clinical settings varies significantly. A retrospective study by Garvey et al. [197] analysed three algorithms on a subset of 500 patients. Of these, 151 of the subjects were presenting to an emergency department with confirmed STEMI, 349 were controls. The three algorithms had a sensitivity of 67–79% and specificity of 95–98%. There was a larger number of males in the STEMI group compared to females (104 vs 47). The control group, in contrast, had more females (180 vs 169). The authors admit this may have affected the results. Additionally, there was no follow-up with patients after visiting the catheterisation lab, so there may have been more patients in the MI group.

Table 2.3 compares the sensitivity and specificity of various algorithms discussed:

Table 2.3: Comparison of existing algorithms toward the detection of AMI

Author	Method	Sample size	Sensitivity	Specificity	Notes
Pueyo et al. (2008) [198]	QRS slope detection	800 ECG recordings, 83 patients	N/A	N/A	Accuracy not measured
Lahiri et al. (2009) [199]	Phase space fractal dimension analysis with an ANN	302 (177 MI, 125 non-MI)	96.55%	95.24%	Non-MI cohort consisted of BBB, cardiomyopathy and healthy control (n = 77) subjects
Orrego et al. (2009) [200]	Quick reduct algorithm for feature extraction, Bayes classifier and K-Nearest Neighbour (KNN) for classification	79 subjects with MI	99.00%	98.5%	No non-MI patients used, the priority is to detect ischaemic beats
Bozzola et al. (2002) [190]	Hybrid neuro-fuzzy logic (MLP classifier)	539 subjects (100 normal, 139 ventricular hypertrophy, 300 MI)	72.00%	92.73%	FMLP outperformed the classic MLP
Presedo et al. (1996) [189]	Fuzzy logic to determine T-deviation and ST-deviation	Five subjects from the European ST-T database [201]	98.00%	91.00%	Start and end of ischaemic episodes are not included, only beats around peak inflation
Stamkopoulos et al. (2003) [91]	Back-propagation learning on a neural network	60 subjects (selected out of 90) using the European ST-T database [201]	84.40%	78.80%	Single-lead used to detect MI based on annotated data
Correa et al. (2006) [202]	Combination of ECG and vectorcardiography with a linear discriminant classifier	95 MI, 52 healthy	95.80%	94.20%	N/A
Dhawan et al. (2012) [194]	SVM and MLP network	201 subjects (52 STEMI, 60 MI, 89 normal)	86.82%	91.05%	Heart-vectors based on heart geometry weight each lead
Kan & Yang (2012) [203]	3-lead VCG warping between healthy and AMI patients using a self-organising map	388 subjects (309 MI, 79 healthy)	88.10–97.00%	90.70–98.70%	Different number of neuron levels were used (1–4)
Wang et al. (2016) [195]	Correlation between cardiodynamicsgrams of healthy vs AMI subjects	385 subjects (234 MI, 151 healthy)	90.30%	87.80%	VCG-based
Correa et al. (2013) [192]	Vectorcardiogram estimation and QRS alignment with clustering to detect abnormalities	132 subjects (80 PTCA, 52 healthy)	88.50%	92.10%	N/A
Correa et al. (2014) [193]	Proposing four VCG parameters for ST and T waves	132 subjects (80 PTCA, 52 healthy)	90.50%	92.60%	Improving upon the previous study
Arif et. al. (2010) [204]	Back-propagation neural network extracting T, Q and ST information	294 subjects (148 MI, 146 healthy)	97.50%	99.10%	Principal Component Analysis (PCA) was attempted, but yielded a lower sensitivity (93.7%)

2.4 Ischaemic Electrocardiogram Datasets

Norman et al. [205] discussed the use of public ECG databases toward a less-biased diagnosis of cardiac abnormalities. The use of clinical data which would have been previously discarded could promote better informed algorithm development and a better understanding of the "grey-areas" in cardiology. A selection of currently available public databases relevant to ischaemia are described below:

PhysioNet [36] contains a large selection of datasets from various sources. There are over 30 ECG-specific datasets, including six ischaemic ECG sets. The site also hosts data for the annual Computing in Cardiology challenge [206]. All datasets discussed below are taken from PhysioNet.

The European ST-T dataset [92] contains 91 recordings from 79 subjects with suspected myocardial ischaemia. Each recording is two hours long and is annotated with ST-segment and T-wave changes. Header files give additional information such as medications, electrolyte imbalance and technical information which may be useful to modern deep learning algorithms.

The PTB dataset [196] contains 549 records from 290 subjects. A 12-lead ECG recording is included with three Frank leads for VCG. The subjects have the following conditions: MI (148), cardiomyopathy/heart failure (18),BBB (15), dysrhythmia (14), myocardial hypertrophy (7), valvular heart disease (6), myocarditis (4), misc (4), healthy control (52) and 22 not annotated. A header file is also provided with patient details.

Data from the Catholic University of Louvain [191] records 12-lead ECG and 3-lead Frank signals across an enormous cohort of 2810 subjects. Of these, 1042 were normal, 279 had anterior MI, 589 interior MI, 203 dual location infarct and 95 LVH with MI. Other records included ventricular hypertrophy and BBB. The data was collected over five years from patients presenting to the emergency room with chest pain with the original purpose of reconstructing a VCG from 12-lead ECGs for improved MI detection sensitivity. The data is not publicly available. This may be due to ethical concerns, or the authors are not willing to release it.

The Long-Term ST Database [207] contains 86 recordings from 80 subjects lasting between 21 to 24 hours each. Each subject had known ST-segment changes, in-

cluding ischaemia, axis-related ST episodes, and non-ischaemic ST deviation. Each record contains detailed patient information. The dataset was originally intended to support the development of algorithms to differentiate ischaemic from non-ischaemic episodes using ST-segment deviation.

The PhysioNet/Computing in Cardiology (CinC) challenge 2007 dataset [208] contains BSPM recordings of four subjects (labelled case 1–4). Each recording was taken using a 120-lead device, expanded to 352 nodes using Laplacian extrapolation. This is known as the Dalhousie torso, described by Horacek, Warren & Penney [54]. The subjects were undergoing elective PTCA where baseline (normal) and PBI (ischaemic) recordings were sampled. One subject (case 3) has a detailed heart geometry and thorax models taken from MRI. An expanded version of this dataset from Dalhousie university contains 99 subjects with balloon inflation in three coronary arteries: LAD, LCX and RCA.

The St.-Petersburg Institute of Cardiological Technics 12-lead Arrhythmia Database [209] contains 75 annotated recordings from 32 subjects. Each recording lasts 30 minutes and contains 12-lead ECGs. The data was recorded from patients presenting with suspected CHD. Included in the dataset are two AMI, five transient ischaemic attack, four prior MI and seven CHD samples. Header files are available for all patients and all beats are marked using an automated QRS detection algorithm.

The STAFF III database [210] contains 152 recordings of PTCA-based occlusion of the main coronary arteries (3 Left Main (LM), 58 LAD, 59 RCA, 32 LCX) including 35 patients with prior MI. 12-lead ECGs were recorded five minutes before catheter insertion. Mean balloon-inflation time was 4 min 23 seconds with annotations available in the dataset. Post-inflation ECG was recorded for five minutes after balloon deflation. Precordial leads were standard to the 12-lead format, however, limb leads were modified to the ML (exercise lead) configuration to reduce skeletal noise.

A summary of the datasets discussed in this section is included in Table 2.4.

Table 2.4: Ischaemic ECG datasets

Ref.	Source	Participants	Description
[36]	PhysioNet	Various	PhysioNet contains multiple studies mentioned below. It is a database for distribution of data and challenges
[92]	European ST-T	79 subjects (all suspected of MI)	367 episodes of ST segment change, 401 episodes of T-wave change. Samples lasting 30 s to several minutes
[196]	PTB	290 subjects (148 MI)	12-lead ECG with 3 Frank leads (XYZ) for each subject.
[191]	Catholic University of Louvain	2810 patients (1042 normal, 279 anterior MI, 589 interior MI, 203 dual location infarct, 95 LVH with MI)	12-lead ECG with 3-lead Frank recordings for each patient. Data is not publicly available
[207]	Long-Term ST	86 recordings of 80 subjects with known ST-segment changes	Recordings are between 21 to 24 hours in duration. The dataset was intended to support development of algorithms differentiating ischaemic and non-ischaemic waveforms
[208]	CinC Challenge 2007 Data (BSPM)	Four subjects with 352-node BSPM recordings	3D geometry is provided with the electrode positions and information on 12-lead, EASI and Frank extrapolation
[209]	St.-Petersburg ICT Arrhythmia	32 subjects (11 ischaemic), 75 annotated recordings	12-lead ECG recordings lasting 30 minutes for each patient
[210]	STAFF III	152 recordings (3 LM, 58 LAD, 59 RCA, 32 LCX, 35 prior MI)	ECG recordings prior and post PTCA balloon inflation

2.5 Derivation of Lead Systems

2.5.1 Background

Studies such as that from Pahlm et al. [211] have shown additional leads such as the 24-lead ECG to be more capable of detecting AMI than the 12-lead ECG. Many additional lead systems with a larger number of leads, such as the 18-lead ECG are inconvenient when used in a clinical setting. This is due to both the large number of electrodes needing placed on the chest, and the requirement to move a patient to apply electrodes to the posterior torso. Additionally, the requirement for more electrodes to be placed may increase the number of placement errors introduced. This has been highlighted in a review from Lynch [212]. This review identified the confusion by clinical staff that may arise when placing chest electrodes, even when the instrument provides colour-coded labels. It may be more convenient to derive non-standard lead systems from that of leads already recorded. For example, deriving additional chest leads from the 12-lead ECG. This means one standard ECG can be used, with other leads systems derived from it, potentially reducing the effects of electrode misplacement from unfamiliar lead systems.

Due to the prevalence of the 12-lead ECG, many datasets have focused on this lead system during their respective studies, as shown in Table 2.4. When attempting to evaluate a novel lead system, this requires the researcher to prove the capability of their introduced lead system with the well established gold standard of the 12-lead ECG. For example, a pilot study by Ashida et al. [213] and later by Wada et al. [214], investigated the use of a synthesised 18-lead ECG in the detection of AMI when compared with the 12-lead ECG. This 18-lead system used six derived leads: the right-sided chest leads V3R–V5R, and the posterior chest leads V7–V9. A small improvement in diagnostic sensitivity was observed between the 12 and 18 lead ECGs, with 94.7% and 95.2% respectively. This study only considered those who had been diagnosed with either STEMI or MI via ECG or blood biomarkers. This means the specificity of these synthesised leads could not be accurately determined.

With derived leads, there is always the danger that the derived lead is dissimilar to a lead physically recorded. A study from Li et al. [215] showed a 100% agree-

ment between derived and recorded leads of the 18-lead ECG in the diagnosis of ST-elevation and ST-depression among AMI patients. However, the derived leads had 95% sensitivity in identifying T-wave inversions. Although this dataset had a large number of participants, with 295 enrolled, only 45% of the study population underwent cardiac catheterisation as a result of either a STEMI or blood biomarker diagnosis. This may not be enough data to be conclusive. Additionally, the data were recorded in a single centre with non-standard lead locations compared to the clinical standard of the 12-lead ECG. Confusion with lead placement may have introduced subtle errors when recording the data.

Derivation of lead systems is not just limited to expanding the 12-lead ECG. It can also be used to derive the 12-lead ECG from a more limited lead set. This may be required where the limited lead-set is difficult to interpret using existing diagnostic criteria. In the context of AMI, the 12-lead is the current diagnostic standard, so a patch-based lead system or ambulatory monitor is required to generate a 12-lead ECG plot before a diagnosis can be made. Obviously, with the introduction of AI-based approaches, MI can still be diagnosed, however, this "black box" approach is often not trusted by clinicians [216].

A study from Lee et al. [217] investigated the derivation of the 12-lead ECG from reduced lead sets. The study used ANN and Multiple Linear Regression (MLR) methods to derive the 12-lead ECG from several different combinations of leads across the anterior torso. The CC across all combinations of leads was at least 0.92, but the reconstruction performance was lower in leads III and aVL. The bottom-centre of the chest was found to have the most favourable 12-lead ECG derivation performance. A small number of recordings were used, with only 14 participants. To produce coefficients suitable for a population, a wider variety of participants would be required.

2.5.2 Reconstruction

It is often required to reconstruct an ECG lead where misplacement, disconnection, or noise occurs. Additionally, a lead may require reconstruction in instances where it is deliberately not recorded due to injury or simplistic sample-capture equipment. A study by Schijvenaars et al. [218] investigated four methods of reconstructing

leads via interpolation. The leads were selected from a 117-electrode BSPM in a dataset containing 746 recordings. The study extracted a subset of leads from the BSPM, interpolated to form a reference signal, then resampled based on the number of leads to be evaluated. The four interpolation methods used were linear, fourier transform, Chebyshev, and cubic spline interpolation. The results suggested cubic spline interpolation to have the best overall performance. This was determined by interpolating leads in both horizontal and vertical directions, while measuring the mean absolute error between interpolated leads and those physically recorded.

Rababah et al. [219] employed a similar method using the same dataset, which aimed to derive leads that may have been disconnected in a clinical setting due to poor electrode contact or noise. However, Laplacian interpolation and PCA was used instead of the aforementioned interpolation methods. Additionally, a hybrid method using both Laplacian interpolation and PCA were also used. Seven problem-areas where leads may be disconnected were chosen to be derived from the BSPM data. Laplacian interpolation was found to have the lowest relative error of the two methods. The hybrid method improved upon this relative error further.

Reconstruction of lead systems can also be used to make them more convenient in a clinical setting. For example, a study from Drew et al. [220] aimed to evaluate the ischaemic diagnostic performance of derived precordial chest leads (V2–V4; V6) from a modified 12-lead ECG, with only ML limb leads, V1 and V5 recorded. The recordings were acquired from patients experiencing myocardial ischaemia with continuous 12-lead ECG monitoring (n=120). The standard 12-lead ECG and interpolated ECGs were compared against each other using a blinded test from a cardiologist. Ischaemic-type ECG changes were detectable by the interpolated ECG in 97% of those deemed ischaemic by the 12-lead ECG. This shows a strong clinical impact for the interpolation of missing leads in a clinical setting, however, these results do not include healthy controls. Therefore, the more popular criteria to determine performance, such as sensitivity or specificity cannot be reliably calculated from this study.

It is also possible to derive other lead systems from the well-established 12-lead ECG. Kusayama et al. [221] performed a study which aimed to determine how the derived right-sided chest leads were characterised in patients with pulmonary

embolism. Fifty six patients with the condition had 12-lead ECG recordings taken at rest. The right-sided chest leads V3R–V5R were derived using the least-squares method. The study concluded that the derived V3R lead was useful in the detection of T-wave changes associated with pulmonary embolism, and derivation of this lead should be performed on suspicion of pulmonary embolism. However, there were no physically recorded right-sided chest leads during this study, so the derived leads cannot be properly evaluated.

2.5.3 Deep Learning

The majority of research into deep learning-based methods of lead derivation focus on the estimation of the 12-lead ECG from a reduced lead set. This is primarily due to the inconvenience of the 12-lead ECG for remote and long-term monitoring. For example, a study from Lee et al [222] aimed to synthesise the 12-lead ECG precordial chest leads (V leads) from the limb leads. Using the PTB dataset [196], summarised previously in Table 2.4, each ECG beat was extracted from the recordings of the 52 subjects. The R wave peaks were aligned using the Pan-Tompkins algorithm, before classification by a Generative Adversarial Network (GAN). The correlation for each synthesised lead was either 0.99 or 1.00, suggesting that a GAN-based architecture is highly accurate when estimating precordial leads.

Xu et al. [223] proposed a similar method using the PTB dataset, whereby the precordial chest leads were being derived from leads I, II, and the chest lead V2. A General Vector Machine (GVM) was employed in the estimation of chest leads. This network was compared with MLR, backpropagation and a genetic algorithm optimised backpropagation network. It was found that a GVM performed between 1.5–11% better than the other methods investigated. The mean CC of the derived leads was between 0.81 for V5, to 0.96 for V1. This study is limited by the inability of the chosen networks to fit the R wave peaks, which may have worsened the performance.

Lee et al. [224] were more ambitious in the synthesis of a 12-lead ECG from a reduced lead set. They presented a four-electrode patch-based device which used an ANN-based approach to estimate the 12-lead ECG. The electrode patch was selected from a matrix of 35 electrodes on the anterior torso, spaced five centimetres

apart in a grid. This was placed on 19 participants with the 12-lead ECG recorded simultaneously. The authors reported a CC of between 0.95 for aVL, and 0.99 for V3. This is promising for a patch with electrode distances of five centimetres apart, however, such a small number of subjects used in the study and a lack of information on the diversity of the cohort makes it difficult to determine whether this device would work for a wide variety of individuals.

A study by Sohn et al. [225] aimed to reconstruct the 12-lead ECG from a three-lead patch device using a Long Short-Term Memory (LSTM) approach. A population of 60 subjects, 30 of which were normal and 30 were patients with an ECG abnormality, were fitted with a four-electrode patch on the left-superior anterior torso. The patch transmitted ECG data from the device to a LabView equiped receiver, where an LSTM model would derive the 12-lead ECG. The mean CC was between 0.92 for lead I, and 0.96 for lead II, aVR, and V2–V5 respectively. Using the derived ECGs, the sensitivity and specificity were 100% in the affirmation of LVH, ST elevation, ST depression, and wide QRS respectively.

Grande-Fidalgo et al. [226] was a sponsored study from Analog Devices, which shows the application of commercial hardware to ECG capture and further processing. This study used an analogue frontend, coupled with an ANN-based backend to derive the 12-lead ECG. The signals were captured using the standard 12-lead ECG for reference, three electrodes on the anterior-central torso, and one on the posterior-left torso. These four extra electrodes for the basis of the custom three-lead system. The three leads were passed through an ANN to derive the 12-lead ECG. The CC between derived and recorded 12-lead ECG signals was 0.99, suggesting a pseudo perfect performance. This is promising, however, the lead system is non-standard and may be confusing for clinicians. The spacing between electrodes is also an issue. It is too large for a patch, and the posterior-attached electrode may be inconvenient in a clinical setting. Furthermore, only healthy subjects were used in this study, so there is no evidence to suggest its efficacy to detecting cardiac abnormalities.

2.6 Cloud Computing in ECG Processing

2.6.1 Background

Over recent years, there has been an increased use of cloud computing technologies related to healthcare [227]. Vendors such as Amazon Web Services (AWS), Microsoft Azure, and Google Cloud have popularised the use of Infrastructure as a Service (IaaS) [228]. This is where a consumer will rent hardware to run scripts, servers or algorithms. On example of this may be hosting a website in a distributed network. This frees the creator from the burden of hosting, load managing and hardware maintenance. An abstraction of IaaS is the use of platform or Software as a Service (SaaS). This is where the platform provider hosts their software, then allows users to access it remotely. For example, the use of an API to process requests sent from users or devices. The API receives a request, performs some computation and returns a rendered response via Javascript Object Notation (JSON) or similar format. Not all cloud computing is IaaS or SaaS based, however. It is possible to manage your own cloud platform by means of self-hosting. This may be more suitable for security-sensitive applications, but presents challenges in deployment and upkeep [229].

In relation to the processing of ECG information, progress is somewhat restricted due to several reasons. First, the concerns of passing confidential patient data to a third party provider provides a path for so-called bad actors to steal information. Second, many ECG capture methods are proprietary, where the manufacturer is not willing to share the data. Third, the need for server-side processing of ECGs has not been realised until AI-based processing methods have matured. Some of these methods are discussed in Table 2.3. While providing a diagnosis on the manufacturer's device is ideal, the AI model used is fixed. This would not allow retraining and reinforcement learning which is commonplace amongst AI-based algorithms. This necessitates the need for sending the ECG data to a server for further analysis. Electrocardiographic data, such as the 12-lead ECG is often sampled between 250–1000 Hz and captured over a ten second period in 12 channels of data. Given a sampling resolution of 12 bits per channel, one recording may only be up to 1.4

megabytes in size, not including patient metadata. This is a relatively small package size for cloud computing architectures that are capable of handling real-time voice and video applications.

With the rise of "big data" and cloud computing, open source software has also expanded rapidly. This is particularly true in the field of medicine, where the sharing of open datasets have been shown to produce innovations years after release, often not in the same area as the publisher originally intended [230]. Many companies are reluctant to release open source software, especially in the field of cloud computing, citing losses of revenue as a potential reason. However, open source software can encourage users to become more loyal towards a particular application [231]. Additionally, the switch from proprietary to open source evolves a project into a community-led ecosystem, furthering the technological progress of the original product. In the field of ECG processing, a platform for sharing open-source datasets such as Physionet has further progressed the development of beat-detection algorithms beyond the original study where the data were recorded [232].

The aim of this section is to evaluate the current application of cloud computing architectures in the processing of ECG signals. In particular, the use of cloud computing in telemedicine, ambulatory devices, the hosting of algorithms, and the development of novel algorithms.

2.6.2 Remote Monitoring

One of the main advantages of a cloud-based ECG service is the realisation of rapid diagnosis from ambulatory devices. The transmission of ECG data to the cloud presents several challenges, mainly from the architecture or framework of either the data formatting or handling. Hsieh & Hsu [233] aimed to provide a telemedicine approach to this issue. This service allows the processing of 12-lead ECG data that has been sent via the internet. The Microsoft Azure-based system receives ECG data and queues it via a scheduler called a 'fabric controller', where it is parsed and processed by the Azure kernel. The results of the process are stored in an SQL database after encryption.

Similarly, Venkatesan et al. [234] introduced a CHD detector suitable for the storage and processing of single-lead ECG data. The server backend hosts a heart

rate variability detector and CHD classifier to provide a diagnosis and waveform on a Graphical User Interface (GUI). However, there was no consideration given to allowing a user to store the diagnoses and view multiple at one time.

Shu et al. [235] provided a full-stack solution to the transmission and processing of ECG data in the cloud. An analogue frontend was designed with signal acquisition, filtering, and encoding performed by an android-based device. The recorded ECG data were then transmitted to a cloud platform to be decoded and linked to a patient-profile while being stored on the server. This data were then accessible via an android application on the transmitting device. For a physician, this may be convenient as it allows a tablet device to transmit ECG data to be stored and recalled at a later date. However, there is no consideration for further processing of the ECG on the cloud, for example, automated diagnosis of cardiac abnormalities.

2.6.3 Hosted Algorithms

The previous section discussed systems that focus on the transmission or storage of ECG data in the cloud, but a cloud-based system is also capable of hosting various algorithms to process the incoming ECG data and provide diagnoses.

A study from Mutlag et al. [236] investigated the role of fog computing, also known as edge computing, to process patient data from multiple sources. Their solution used a task scheduler to prioritise incoming data before being passed into the dedicated processing algorithm on the cloud. This is inherently scalable as it can divert traffic away from a cloud server if it is perceived as being overloaded. This fog computing system was also used by Cheikhrouhou et al. [237] to produce a system capable of diagnosing ECG arrhythmia using a Convolutional Neural Network (CNN). Data were sent from multiple sources, where a fog system would queue and transmit the ECG data to the cloud for processing. The cloud server hosted the CNN that provided a diagnosis. The fog system provided a lower latency from transmission to the receipt of diagnosis, but it was unclear how the diagnosis would be shown to the clinician.

Zhang et al. [238] provided a full stack example to the processing of ECG data in the cloud. Data were collected using a sensor that would transmit the ECG data via Bluetooth to an Android device. A Python-based web socket would allow data to be

streamed from the device to the backend server. The server passes the collected data to a MATLAB engine that provides an SVM classifier to diagnose any abnormalities. The diagnostic results are then passed back to the Android application to be shown along with the ECG signal. The solution presented in this study shows how an established DSP software package such as MATLAB can be used in real-time with web-based applications. It also demonstrates how the classification algorithms can be changed using a single language, rather than converting it to C++, or hosting the algorithm on a dedicated platform such as AWS.

2.6.4 Algorithm Development Platforms

There has been a huge increase in the number of biomedical data collection platforms, primarily those in the consumer sector, such as Fitbit and the Apple Watch. Devices such as the Apple Watch are capable of providing basic diagnosis on a single lead ECG, that has led many consumers to seek medical advice. This has led to clinicians becoming overwhelmed with novel data platforms, and little means to sift through the information other than running additional tests. This has led to articles like that from Bose & Saxon [239] highlighting the need for new methods to break the inefficiency of emergency departments in dealing with this data. One such solution may be platforms designed to assist clinicians in the handling of patient data.

Kasthurirathne [240] discussed the development of an open source software platform to allow clinicians to process patient records, called OpenMRS. The platform is operable with no prior programming knowledge, a key requirement for systems for use by medical staff. A patient workflow can be created which facilitates report generation and efficient patient transfer.

Van Poucke et al. [241] highlighted the need for visual platforms to gain novel insights into data and correlate patterns. They created a system which allows users to extract information from a dataset, build a predictive model, and deploy it under different feature selection schemes. The platform focuses on the use of draggable blocks that can be connected together to form a data flow. This allows a code-free option for clinicians to evaluate new data, whether creating reports or providing a basic diagnosis.

Ghaderi [242] provided a meta-platform to allow clinicians to create an appli-

cation and dashboard-type GUI to assist with the automation of disease diagnosis. In their example, the platform was used to create a patient-facing breast cancer screening tool that can triage patients that have concerns about their own health. They can fill out a series of questionnaires to track their symptoms before alerting a clinician. This has the capability to decrease the time a clinician may spend in triaging false positives from overly-concerned individuals, however, care should be taken that the platform does not turn away those who genuinely need medical intervention.

Sanders et al [243] combined deep learning with a GUI to allow clinicians to train their own AI classification models on patient data. This code-free platform enables the user to load data, create a model architecture, then store the model for later use. The application also supports the use of existing models as part of a transfer learning approach. Whilst any clinician using this application will need some knowledge of deep learning architectures, the barrier to entry has been significantly reduced by removing the need to write code.

2.7 Conclusions

This chapter has investigated the current state of the art in ECG technologies, with a focus on the use of ECG toward MI detection. This review of the literature has shown gaps, specifically in the use of derived additional lead systems, other than the 12-lead ECG. Furthermore, the lack of ST-sensitive monitoring devices suited towards detecting ischaemic-type ECG changes has been identified. Many of the technologies reviewed in the processing of ECG, particularly the use of systems capable of designing novel ECG processing algorithms are complex and not suited for clinical use or experimentation by non-experts. The areas identified in this literature review will guide the work presented in upcoming chapters, while informing many of the methods employed during the work.

References

[1] J. P. T. Ward and R. W. A. Linden, *Physiology at a Glance*. Wiley Blackwell, fourth ed., 2013.

[2] Cancer Research UK, "Diagram showing the circulatory system of the body," 7 2014.

[3] P. J. Lynch, "Heart circulation diagram," 12 2006.

[4] C. M. Scannell, *Automated quantitative analysis of first-pass myocardial perfusion magnetic resonance imaging data*. PhD thesis, King's College, London, 5 2021.

[5] P. W. Macfarlane, A. van Oosterom, O. Pahlm, P. Kligfield, M. Janse, and J. Camm, eds., *Comprehensive Electrocardiology*. London: Springer London, 2010.

[6] B. G. Petty, *Basic Electrocardiography*. Switzerland: Springer Nature, second ed., 2020.

[7] ITACA, "Proyecto ITACA," 2020.

[8] R. M. Shaw and Y. Rudy, "Electrophysiologic effects of acute myocardial ischemia: A theoretical study of altered cell excitability and action potential duration," *Cardiovascular Research*, vol. 35, pp. 256–272, 8 1997.

[9] J. I. Okada, K. Fujiu, K. Yoneda, T. Iwamura, T. Washio, I. Komuro, T. Hisada, and S. Sugiura, "Ionic mechanisms of ST segment elevation in electrocardiogram during acute myocardial infarction," *Journal of Physiological Sciences*, vol. 70, pp. 1–14, 7 2020.

[10] N. Frey, H. A. Katus, E. N. Olson, and J. A. Hill, "Hypertrophy of the Heart: A New Therapeutic Target?," 4 2004.

[11] W. T. Harkness and M. Hicks, "Right Bundle Branch Block," *StatPearls*, 8 2022.

[12] S. W. Smith, K. W. Dodd, T. D. Henry, D. M. Dvorak, and L. A. Pearce, "Diagnosis of ST-elevation myocardial infarction in the presence of left bundle branch block with the ST-elevation to S-wave ratio in a modified sgarbossa rule," *Annals of Emergency Medicine*, vol. 60, pp. 766–776, 12 2012.

[13] M. C. Matteucci, "Sur un phénomène physiologique produit par les muscles en contraction," *Ann Chim Phys*, vol. 6, pp. 339–342, 1842.

[14] A. D. Waller, "A Demonstration on Man of Electromotive Changes accompanying the Heart's Beat," *The Journal of Physiology*, vol. 8, no. 5, pp. 229–234, 1887.

[15] W. Einthoven, "Nieuwe methoden voor clinisch onderzoek [New methods for clinical investigation].," *Ned T Geneesk*, vol. 29, no. II, pp. 263–286, 1893.

[16] W. Einthoven, "Ueber die Form des menschlichen Electrocardiogramms," *Pflüger, Archiv für die Gesammte Physiologie des Menschen und der Thiere*, vol. 60, pp. 101–123, 3 1895.

[17] P. Macfarlane and S. Update, "Resting 12-lead electrode placement," *Society*, 1995.

[18] R. E. Mason and I. Likar, "A new system of multiple-lead exercise electrocardiography," *American Heart Journal*, vol. 71, pp. 196–205, 2 1966.

[19] W. Einthoven, "Un nouveau galvanometre," *Soc. Holl. des Sciences*, 1901.

[20] F. N. Wilson, F. D. Johnston, F. F. Rosenbaum, and P. S. Barker, "On Einthoven's triangle, the theory of unipolar electrocardiographic leads, and the interpretation of the precordial electrocardiogram," *American Heart Journal*, vol. 32, pp. 277–310, 9 1946.

[21] D. E. Becker, "Fundamentals of electrocardiography interpretation.," *Anesthesia progress*, vol. 53, no. 2, pp. 53–63, 2006.

[22] Clinical ECG Interpretation, "The ECG leads: electrodes, limb leads, chest (precordial) leads, 12-Lead ECG (EKG)," 2017.

[23] A. Rowlands and A. Sargent, *The ECG workbook*. M&K Update Ltd, 2014.

[24] M. Sejersten, G. S. Wagner, O. Pahlm, J. W. Warren, C. L. Feldman, and B. M. Horáček, "Detection of acute ischemia from the EASI-derived 12-lead electrocardiogram and from the 12-lead electrocardiogram acquired in clinical practice," *Journal of Electrocardiology*, vol. 40, pp. 120–126, 3 2007.

[25] A. W. Van 'T Hof, A. Liem, M. J. De Boer, and F. Zijlstra, "Clinical value of 12-lead electrocardiogram after successful reperfusion therapy for acute myocardial infarction," *Lancet*, vol. 350, pp. 615–619, 8 1997.

[26] S. Moye, M. F. Carney, C. Holstege, A. Mattu, and W. J. Brady, "The electrocardiogram in right ventricular myocardial infarction," *American Journal of Emergency Medicine*, vol. 23, pp. 793–799, 10 2005.

[27] R. J. Zalenski, R. J. Rydman, E. P. Sloan, K. H. Hahn, D. Cooke, J. Fagan, D. J. Fligner, W. Hessions, D. Justis, L. M. Kampe, S. Shah, J. Tucker, and D. Zwicke, "Value of posterior and right ventricular leads in comparison to the standard 12-lead electrocardiogram in evaluation of ST-segment elevation in suspected acute myocardial infarction," *American Journal of Cardiology*, vol. 79, pp. 1579–1585, 6 1997.

[28] K. Thygesen, J. S. Alpert, A. S. Jaffe, B. R. Chaitman, J. J. Bax, D. A. Morrow, and H. D. White, "Fourth universal definition of myocardial infarction (2018)," *European Heart Journal*, vol. 24, pp. 107–138, 8 2019.

[29] F. M. Fesmire, R. F. Percy, J. B. Bardoner, D. R. Wharton, and F. B. Calhoun, "Usefulness of automated serial 12-lead ECG monitoring during the initial emergency department evaluation of patients with chest pain," *Annals of Emergency Medicine*, vol. 31, pp. 3–11, 1 1998.

[30] R. D. Welch, R. J. Zalenski, P. D. Frederick, J. A. Malmgren, S. Compton, M. Grzybowski, S. Thomas, T. Kowalenko, and N. R. Every, "Prognostic value of a normal or nonspecific initial electrocardiogram in acute myocardial infarction," *Journal of the American Medical Association*, vol. 286, pp. 1977–1984, 10 2001.

[31] D. F. Miranda, A. S. Lobo, B. Walsh, Y. Sandoval, and S. W. Smith, "New Insights Into the Use of the 12-Lead Electrocardiogram for Diagnosing Acute Myocardial Infarction in the Emergency Department," *Canadian Journal of Cardiology*, vol. 34, pp. 132–145, 2 2018.

[32] B. J. Schijvenaars, J. A. Kors, G. Van Herpen, F. Kornreich, and J. H. Van Bemmel, "Effect of electrode positioning on ECG interpretation by computer," *Journal of Electrocardiology*, vol. 30, pp. 247–256, 7 1997.

[33] R. Rajaganeshan, C. L. Ludlam, D. P. Francis, S. V. Parasramka, and R. Sutton, "Accuracy in ECG lead placement among technicians, nurses, general physicians and cardiologists," *International Journal of Clinical Practice*, vol. 62, pp. 65–70, 8 2007.

[34] M. Bickerton and A. Pooler, "Misplaced ECG electrodes and the need for continuing training," *British Journal of Cardiac Nursing*, vol. 14, pp. 123–132, 3 2019.

[35] N. Kalkstein, Y. Kinar, M. Na'aman, N. Neumark, and P. Akiva, "Using Machine Learning to Detect Problems in ECG Data Collection," in *Computing in Cardiology 2011*, vol. 38, (Hangzhou, China), pp. 437–440, [IEEE], 2011.

[36] A. L. Goldberger, L. A. N. Amaral, L. Glass, J. M. Hausdorff, P. C. Ivanov, R. G. Mark, J. E. Mietus, G. B. Moody, C.-K. Peng, and H. E. Stanley, "PhysioBank, PhysioToolkit, and PhysioNet," *Circulation*, vol. 101, pp. 215–220, 6 2003.

[37] R. Hoekema, G. J. Uijen, and A. Van Oosterom, "On selecting a body surface mapping procedure," *Journal of Electrocardiology*, vol. 32, pp. 93–101, 4 1999.

[38] E. Hedström, M. Ugander, and H. Arheden, "Multimodal Cardiovascular Imaging, Principles and Clinical Applications," in *Cardiac Magnetic Resonance Imaging in Ischemic Heart Disease*, pp. 104–127, The McGraw-Hill Companies, 2011.

[39] F. Kornreich, T. J. Montague, P. M. Rautaharju, P. Block, J. W. Warren, and M. B. Horacek, "Identification of best electrocardiographic leads for diagnosing anterior and inferior myocardial infarction by statistical analysis of body surface potential maps," *The American Journal of Cardiology*, vol. 58, pp. 863–871, 11 1986.

[40] I. B. Menown, R. S. Patterson, G. MacKenzie, and A. A. Adgey, "Body-surface map models for early diagnosis of acute myocardial infarction," in *Journal of Electrocardiology*, vol. 31, pp. 180–188, 1 1998.

[41] A. J. McClelland, C. G. Owens, I. B. Menown, M. Lown, and A. A. Adgey, "Comparison of the 80-lead body surface map to physician and to 12-lead electrocardiogram in detection of acute myocardial infarction," *American Journal of Cardiology*, vol. 92, pp. 252–257, 8 2003.

[42] M. J. Daly, C. J. McCann, C. G. Owens, M. T. Harbinson, and J. A. Adgey, "Heart fatty acid-binding protein in combination with the 80-lead body surface potential map improves early detection of acute myocardial infarction in patients who are cardiac troponin T-negative at presentation," in *Journal of Electrocardiology*, vol. 44, pp. 432–438, 7 2011.

[43] C. Owens, A. McClelland, S. Walsh, B. Smith, and J. Adgey, "Comparison of Value of Leads from Body Surface Maps to 12-Lead Electrocardiogram for Diagnosis of Acute Myocardial Infarction," *American Journal of Cardiology*, vol. 102, pp. 257–265, 8 2008.

[44] M. J. Daly, D. D. Finlay, D. Guldenring, R. R. Bond, A. J. McCann, P. J. Scott, J. A. Adgey, and M. T. Harbinson, "Epicardial potentials computed from the body surface potential map using inverse electrocardiography and an individualised torso model improve sensitivity for acute myocardial infarction diagnosis," *European heart journal. Acute cardiovascular care*, vol. 6, no. 8, pp. 728–735, 2017.

[45] J. W. Hoekstra, B. J. O'Neill, Y. B. Pride, C. Lefebvre, D. B. Diercks, W. F. Peacock, G. J. Fermann, C. M. Gibson, D. Pinto, J. Giglio, A. Chandra, C. B. Cairns, M. A. Konstam, J. Massaro, and M. Krucoff, "Acute Detection of ST-Elevation Myocardial Infarction Missed on Standard 12-Lead ECG With a Novel 80-Lead Real-Time Digital Body Surface Map: Primary Results From the Multicenter OCCULT MI Trial," *Annals of Emergency Medicine*, vol. 54, no. 6, pp. 779–788, 2009.

[46] EP Solutions, "Amycard 01C."

[47] Medtronic, "Cardioinsight Mapping Vest."

[48] D. D. Finlay, C. D. Nugent, M. P. Donnelly, R. L. Lux, P. J. McCullagh, and N. D. Black, "Selection of optimal recording sites for limited lead body surface potential mapping: A sequential selection based approach," *BMC Medical Informatics and Decision Making*, vol. 6, p. 9, 12 2006.

[49] F. Kornreich, T. J. Montague, P. M. Rautaharju, M. Kavadias, and M. B. Horacek, "Identification of best electrocardiographic leads for diagnosing left ventricular hypertrophy by statistical analysis of body surface potential maps," *The American Journal of Cardiology*, vol. 62, pp. 1285–1291, 12 1988.

[50] F. Kornreich, M. Kavadias, T. J. Montague, P. M. Rautaharju, and M. B. Horacek, "Selection of optimal electrocardiographic leads from body surface potential maps for the diagnosis of left ventricular hypertrophy," *Journal of Electrocardiology*, vol. 22, p. 269, 7 1989.

[51] F. Kornreich, "Identification of best electrocardiographic leads for diagnosing acute myocardial ischemia," *Journal of Electrocardiology*, vol. 31, pp. 157–163, 1 1998.

[52] R. C. Barr, M. S. Spach, and G. S. Herman-Giddens, "Selection of the Number and Positions of Measuring Locations for Electrocardiography," *IEEE Transactions on Biomedical Engineering*, vol. BME-18, pp. 125–138, 3 1971.

[53] R. L. Lux, C. R. Smith, R. F. Wyatt, and J. A. Abildskov, "Limited Lead Selection for Estimation of Body Surface Potential Maps in Electrocardiography," *IEEE Transactions on Biomedical Engineering*, vol. BME-25, pp. 270–276, 5 1978.

[54] B. Horacek, J. W. Warren, C. J. Penney, R. S. MacLeod, L. M. Title, M. J. Gardner, C. L. Feldman, B. M. Horacek, J. W. Warren, C. J. Penney, R. S. MacLeod, L. M. Title, M. J. Gardner, and C. L. Feldman, "Optimal electrocardiographic leads for detecting acute myocardial ischemia," *Journal of Electrocardiology*, vol. 34, pp. 97–111, 10 2001.

[55] A. Kennedy, D. D. Finlay, D. Guldenring, R. R. Bond, and J. McLaughlin, "Detecting the elusive P-wave: A new ECG lead to improve the recording of atrial activity," *IEEE Transactions on Biomedical Engineering*, vol. 63, pp. 243–249, 2 2016.

[56] E. Frank, "The image surface of a homogeneous torso," *American Heart Journal*, vol. 47, pp. 757–768, 5 1954.

[57] D. Q. Feild, S. H. Zhou, E. D. Helfenbein, R. E. Gregg, and J. M. Lindauer, "Technical challenges and future directions in lead reconstruction for reduced-lead systems," *Journal of Electrocardiology*, vol. 41, pp. 466–473, 11 2008.

[58] G. Howitt and T. D. V. Lawrie, "Vectorcardiography in Myocardial Infarction," *Heart*, vol. 22, no. 1, pp. 61–72, 1959.

[59] J. W. Starr, G. S. Wagner, R. M. Draffin, J. B. Reed, A. Walston IInd, and V. S. Behar, "Vectorcardiographic criteria for the diagnosis of anterior myocardial infarction," *Circulation*, vol. 53, no. 2, pp. 229–234, 1976.

[60] P. G. Hugenholtz, T. J. Ryan, T. Woerner, and H. D. Levine, "Recognition of anterior wall infarction in patients with left ventricular hypertrophy. A study by the Frank vector-cardiogram.," *Circulation*, vol. 27, pp. 386–96, 3 1963.

[61] D. Guldenring, D. D. Finlay, D. G. Strauss, L. Galeotti, C. D. Nugent, M. P. Donnelly, and R. R. Bond, "Transformation of the Mason-Likar 12-lead electrocardiogram to the Frank vectorcardiogram," in *Proceedings of the Annual International Conference of the IEEE Engineering in Medicine and Biology Society, EMBS*, pp. 677–680, IEEE, 8 2012.

[62] J. Vicente, "Update on the ECG component of the CiPA initiative," 11 2018.

[63] D. Guldenring, D. D. Finlay, R. R. Bond, A. Kennedy, J. McLaughlin, L. Galeotti, and D. G. Strauss, "The derivation of the spatial QRS-T angle and the spatial ventricular gradient using the Mason-Likar 12-lead electrocardiogram," in *Journal of Electrocardiology*, vol. 48, pp. 1045–1052, Churchill Livingstone, 11 2015.

[64] J. A. Kors, G. v. Herpen, A. C. Sittig, and J. H. v. Bemmel, "Reconstruction of the Frank vectorcardiogram from standard electrocardiographic leads: diagnostic comparison of different methods.," *European heart journal*, vol. 11, no. 12, pp. 1083–1092, 1990.

[65] D. Wei, "Deriving the 12-lead electrocardiogram from four standard leads based on the Frank Torso model," in *Annual Reports of the Research Reactor Institute, Kyoto University*, vol. 1, pp. 381–384, 2001.

[66] B. J. Drew, M. G. Adams, M. M. Pelter, and S. F. Wung, "ST segment monitoring with a derived 12-lead electrocardiogram is superior to routine cardiac care unit monitoring," *American Journal of Critical Care*, vol. 5, pp. 198–206, 5 1996.

[67] B. J. Drew, M. G. Adams, M. M. Pelter, S. F. Wung, and M. A. Caldwell, "Comparison of standard and derived 12-lead electrocardiograms for diagnosis of coronary angioplasty-induced myocardial ischemia," *American Journal of Cardiology*, vol. 79, pp. 639–644, 3 1997.

[68] J. A. Kors, "Lead transformations and the dipole approximation: Practical applications," in *Journal of Electrocardiology*, vol. 48, pp. 1040–1044, 11 2015.

[69] S. P. Nelwan, J. A. Kors, S. H. Meij, J. H. Van Bemmel, and M. L. Simoons, "Reconstruction of the 12-Lead Electrocardiogram from Reduced Lead Sets," *Journal of Electrocardiology*, vol. 37, pp. 11–18, 1 2004.

[70] A. Robertson and E. Clark, "ECG monitoring using a limited lead set," *International Journal ...*, vol. 4, no. 2, pp. 295–296, 2002.

[71] B. J. Drew, M. M. Pelter, D. E. Brodnick, A. V. Yadav, D. Dempel, and M. G. Adams, "Comparison of a new reduced lead set ECG with the standard ECG for diagnosing cardiac arrhythmias and myocardial ischemia," *Journal of Electrocardiology*, vol. 35, pp. 13–21, 10 2002.

[72] S. P. Nelwan, S. W. Crater, S. H. Meij, T. B. van Dam, J. A. Kors, M. L. Simoons, and M. W. Krucoff, "Simultaneous comparison of three derived 12-lead ECGs with standard ECG at rest and during percutaneous coronary occlusion," *Journal of Electrocardiology*, vol. 37, pp. 171–172, 10 2004.

[73] D. D. Finlay, C. D. Nugent, J. G. Kellett, M. P. Donnelly, P. J. McCullagh, and N. D. Black, "Synthesising the 12-lead electrocardiogram: Trends and challenges," *European Journal of Internal Medicine*, vol. 18, pp. 566–570, 12 2007.

[74] G. E. Dower, A. Yakush, S. B. Nazzal, R. V. Jutzy, and C. E. Ruiz, "Deriving the 12-lead electrocardiogram from four (EASI) electrodes," *Journal of Electrocardiology*, vol. 21, pp. 182–7, 1988.

[75] G. Wehr, R. J. Peters, K. Khalifé, A. P. Banning, V. Kuehlkamp, A. F. Rickards, and U. Sechtem, "A vector-based, 5-electrode, 12-lead monitoring ECG (EASI) is equivalent to conventional 12-lead ECG for diagnosis of acute coronary syndromes," *Journal of Electrocardiology*, vol. 39, pp. 22–28, 1 2006.

[76] B. M. Horacek, J. W. Warren, D. Q. Feild, C. L. Feldman, B. M. Horáček, J. W. Warren, D. Q. Feild, and C. L. Feldman, "Statistical and deterministic approaches to designing transformations of electrocardiographic leads," in *Journal of Electrocardiology*, vol. 35, pp. 41–52, 10 2002.

[77] B. J. Drew, M. M. Pelter, S. F. Wung, M. G. Adams, C. Taylor, G. T. Evans, and E. Foster, "Accuracy of the EASI 12-lead electrocardiogram compared to the standard 12-lead electrocardiogram for diagnosing multiple cardiac abnormalities.," *Journal of electrocardiology*, vol. 32 Suppl, pp. 38–47, 1999.

[78] P. Kligfield, L. S. Gettes, J. J. Bailey, R. Childers, B. J. Deal, . E. W. Hancock, F. . Gerard Van Herpen, J. A. Kors, . P. Macfarlane, D. M. Mirvis, O. Pahlm, P. Rautaharju, and G. S. Wagner, "Recommendations for the Standardization and Interpretation of the Electrocardiogram Part I: The Electrocardiogram and Its Technology A Scientific Statement From the American Heart Association Electrocardiography and Arrhythmias Committee, Council on Clini," *Circulation*, vol. 115, pp. 1306–1324, 2007.

[79] M. Nagam, D. Vinson, and J. Levis, "ECG Diagnosis: Right Ventricular Myocardial Infarction," *The Permanente Journal*, vol. 21, pp. 16–105, 2016.

[80] Manuel Celedon, "Posterior MI Recognition," 2015.

[81] Mike Cadogan, "ECG Lead positioning," 2019.

[82] C. Schmitt, G. Lehmann, S. Schmieder, M. Karch, F. J. Neumann, and A. Schömig, "Diagnosis of acute myocardial infarction in angiographically documented occluded infarct vessel: Limitations of ST-segment elevation in standard and extended ECG leads," *Chest*, vol. 120, pp. 1540–1546, 11 2001.

[83] V. Hebbal, H. N. Setty, C. Sathvik, V. Patil, S. Sahoo, and C. Manjunath, "Acute ST-segment elevation myocardial infarction: The prognostic importance of lead augmented vector right and leads V 7 –V 9," *Journal of Natural Science, Biology and Medicine*, vol. 8, no. 1, p. 104, 2017.

[84] C. K. Wong, "Usefulness of leads V7, V8, and V9 ST elevation to diagnose isolated posterior myocardial infarction," *International Journal of Cardiology*, vol. 146, pp. 467–469, 2 2011.

[85] W. J. Brady, V. Hwang, R. Sullivan, N. Chang, C. Beagle, C. T. Carter, M. L. Martin, and T. P. Aufderheide, "A comparison of 12- and 15-lead ECGs in ED chest pain patients: Impact on diagnosis, therapy, and disposition," *American Journal of Emergency Medicine*, vol. 18, pp. 239–243, 5 2000.

[86] S. Konishi, T. Ohtani, H. Mizuno, F. Sera, K. Nakamoto, M. Chimura, K. Sengoku, H. Miyawaki, R. Higuchi, M. Kanzaki, Y. Tsukamoto, S. Hikoso, and Y. Sakata, "Simple Electrocardiographic Score Can Predict Left Ventricular Reverse Remodeling in Patients With Non-Ischemic Cardiomyopathy," *Circulation Reports*, vol. 1, pp. 171–178, 4 2019.

[87] T. Ashida, S. Tani, K. Nagao, T. Yagi, N. Matsumoto, and A. Hirayama, "Usefulness of synthesized 18-lead electrocardiography in the diagnosis of STEMI," *American Journal of Emergency Medicine*, vol. 35, pp. 448–457, 3 2017.

[88] N. Sasaki, Y. Okumura, I. Watanabe, A. Madry, Y. Hamano, M. Nikaido, K. Nagashima, K. Sonoda, R. Kogawa, K. Takahashi, K. Iso, K. Ohkubo, T. Nakai, and A. Hirayama, "Frequency analysis of atrial fibrillation from the

specific ECG leads V7-V9: A lower DF in lead V9 is a marker of potential atrial remodeling," *Journal of Cardiology*, vol. 66, pp. 388–394, 11 2015.

[89] M. P. Somers, W. J. Brady, D. C. Bateman, A. Mattu, and A. D. Perron, "Additional Electrocardiographic Leads in the ED Chest Pain Patient: Right Ventricular and Posterior Leads," *American Journal of Emergency Medicine*, vol. 21, pp. 563–573, 11 2003.

[90] H. R. Andersen, D. Nielsen, O. Lund, and E. Falk, "Prognostic significance of right ventricular infarction diagnosed by ST elevation in right chest leads V3R to V7R," *International Journal of Cardiology*, vol. 23, pp. 349–356, 6 1989.

[91] T. Stamkopoulos, M. Strintzis, C. Pappas, and N. Maglaveras, "One-lead ischemia detection using a new backpropagation algorithm and the European ST-T database," in *Proceedings Computers in Cardiology*, pp. 663–666, IEEE Comput. Soc. Press, 2003.

[92] A. Taddei, G. Distante, M. Emdin, P. Pisani, G. B. Moody, C. Zeelenberg, and C. Marchesi, "The European ST-T Database: standard for evaluating systems for the analysis of ST-T changes in ambulatory electrocardiography," *European Heart Journal*, vol. 13, pp. 1164–1172, 1992.

[93] H. Atoui, J. Fayn, and P. Rubel, "A neural network approach for patient-specific 12-lead ECG synthesis in patient monitoring environments," in *Computers in Cardiology, 2004*, pp. 161–164, IEEE, 2005.

[94] M. Ohlsson, H. Öhlin, S. M. Wallerstedt, and L. Edenbrandt, "Usefulness of serial electrocardiograms for diagnosis of acute myocardial infarction," *American Journal of Cardiology*, vol. 88, pp. 478–481, 9 2001.

[95] B. J. Drew, M. M. Pelter, M. G. Adams, S. F. Wung, T. M. Chou, and C. L. Wolfe, "12-lead ST-segment monitoring vs single-lead maximum ST-segment monitoring for detecting ongoing ischemia in patients with unstable coronary syndromes.," *American journal of critical care : an official publication, American Association of Critical-Care Nurses*, vol. 7, pp. 355–363, 9 1998.

[96] A. M. Chan, N. Selvaraj, N. Ferdosi, and R. Narasimhan, "Wireless patch sensor for remote monitoring of heart rate, respiration, activity, and falls," in *2013 35th Annual International Conference of the IEEE Engineering in Medicine and Biology Society (EMBC)*, pp. 6115–6118, IEEE, 7 2013.

[97] M. J. Breteler, E. Huizinga, K. Van Loon, L. P. Leenen, D. A. Dohmen, C. J. Kalkman, and T. J. Blokhuis, "Reliability of wireless monitoring using a wearable patch sensor in high-risk surgical patients at a step-down unit in the Netherlands: A clinical validation study," *BMJ Open*, vol. 8, no. 2, p. 20162, 2018.

[98] "CardioSTAT Monitor," 2019.

[99] I. Nault, B. Plourde, J. Sarrazin, G. O'Hara, F. Philippon, L. Blier, F. Molin, and J. Champagne, "Validation of a Novel Single Lead Heart Rhythm Monitor," *Canadian Journal of Cardiology*, vol. 31, p. S236, 10 2015.

[100] iRhythm, "Zio XT," 2019.

[101] N. Ben-Dov, D. Gladstone, A. Micieli, E. Crystal, and D. Newman, "Single-lead patch recording systems: The expanding role for long-term ECG recording systems," *Journal of Electrocardiology*, vol. 55, pp. 54–58, 7 2019.

[102] R. Rho, M. Vossler, S. Blancher, and J. E. Poole, "Comparison of 2 ambulatory patch ECG monitors: The benefit of the P-wave and signal clarity," *American Heart Journal*, vol. 203, pp. 109–117, 9 2018.

[103] P. Guzik and M. Malik, "ECG by mobile technologies," *Journal of Electrocardiology*, vol. 49, pp. 894–901, 11 2016.

[104] M. A. Rosenberg, M. Samuel, A. Thosani, and P. J. Zimetbaum, "Use of a noninvasive continuous monitoring device in the management of atrial fibrillation: A pilot study," *PACE - Pacing and Clinical Electrophysiology*, vol. 36, no. 3, pp. 328–333, 2013.

[105] T. F. Simpson and N. Goldschlager, "Sudden cardiac death preceded by ST segment elevations during ECG patch monitoring," *Journal of Electrocardiology*, vol. 51, pp. 330–331, 3 2018.

[106] A. Bansal and R. Joshi, "Portable out-of-hospital electrocardiography: A review of current technologies," *Journal of Arrhythmia*, vol. 34, pp. 129–138, 4 2018.

[107] M. P. Turakhia, D. D. Hoang, P. Zimetbaum, J. D. Miller, V. F. Froelicher, U. N. Kumar, X. Xu, F. Yang, and P. A. Heidenreich, "Diagnostic utility of a novel leadless arrhythmia monitoring device," *American Journal of Cardiology*, vol. 112, pp. 520–524, 8 2013.

[108] BardyDX, "Carnation Ambulatory Monitor," 2019.

[109] W. M. Smith, F. Riddell, M. Madon, and M. J. Gleva, "Comparison of diagnostic value using a small, single channel, P-wave centric sternal ECG monitoring patch with a standard 3-lead Holter system over 24 hours," *American Heart Journal*, vol. 185, pp. 67–73, 3 2017.

[110] Rooti Medical, "RootiCare," 2019.

[111] M. R. Karaoğuz, E. Yurtseven, G. Aslan, B. G. Deliormanlı, O. Adıgüzel, M. Gönen, K. M. Li, and E. N. Yılmaz, "The quality of ECG data acquisition, and diagnostic performance of a novel adhesive patch for ambulatory cardiac rhythm monitoring in arrhythmia detection," *Journal of Electrocardiology*, vol. 54, pp. 28–35, 5 2019.

[112] D. Vukajlovic, B. Bojovic, L. Hadzievski, S. George, I. Gussak, and D. Panescu, "Wireless remote monitoring of atrial fibrillation using reconstructed 12-lead ECGs," in *2010 Annual International Conference of the IEEE Engineering in Medicine and Biology Society, EMBC'10*, pp. 1113–1118, IEEE, 8 2010.

[113] D. Vukajlovic, I. Gussak, S. George, G. Simic, B. Bojovic, L. Hadzievski, B. Stojanovic, L. Angelkov, and D. Panescu, "Wireless monitoring of reconstructed 12-lead ECG in atrial fibrillation patients enables differential diagnosis of recurrent arrhythmias," in *Proceedings of the Annual International Conference of the IEEE Engineering in Medicine and Biology Society, EMBS*, pp. 4741–4744, IEEE, 8 2011.

[114] S. Stern and D. Tzivoni, "Early detection of silent ischaemic heart disease by 24-hour electrocardiographic monitoring of active subjects.," *British heart journal*, vol. 36, no. 5, pp. 481–6, 1974.

[115] T. Jernberg, B. Lindahl, and L. Wallentin, "ST-segment monitoring with continuous 12-lead ECG improves early risk stratification in patients with chest pain and ECG nondiagnostic of acute myocardial infarction," *Journal of the American College of Cardiology*, vol. 34, pp. 1413–1419, 11 1999.

[116] D. L. Kuchar, C. W. Thorburn, and N. L. Sammel, "Prediction of serious arrhythmic events after myocardial infarction: Signal-averaged electrocardiogram, holter monitoring and radionuclide ventriculography," *Journal of the American College of Cardiology*, vol. 9, pp. 531–538, 3 1987.

[117] M. Brodsky, D. Wu, P. Denes, C. Kanakis, and K. M. Rosen, "Arrhythmias documented by 24 hour continuous electrocardiographic monitoring in 50 male medical students without apparent heart disease," *The American Journal of Cardiology*, vol. 39, pp. 390–395, 1 1977.

[118] A. J. Moss, H. T. Davis, J. DeCamilla, and L. W. Bayer, "Ventricular ectopic beats and their relation to sudden and nonsudden cardiac death after myocardial infarction," *Circulation*, vol. 60, pp. 998–1003, 11 1979.

[119] J. T. Bigger, P. Albrecht, R. C. Steinman, L. M. Rolnitzky, J. L. Fleiss, and R. J. Cohen, "Comparison of time- and frequency domain-based measures of cardiac parasympathetic activity in Holter recordings after myocardial infarction," *The American Journal of Cardiology*, vol. 64, pp. 536–538, 9 1989.

[120] A. Langer, J. Minkowitz, P. Dorian, L. Casella, L. Harris, C. D. Morgan, and P. W. Armstrong, "Pathophysiology and prognostic significance of holter-detected ST segment depression after myocardial infarction," *Journal of the American College of Cardiology*, vol. 20, pp. 1313–1317, 11 1992.

[121] T. H. Mäkikallio, P. Barthel, R. Schneider, A. Bauer, J. M. Tapanainen, M. P. Tulppo, G. Schmidt, and H. V. Huikuri, "Prediction of sudden cardiac death after acute myocardial infarction: Role of Holter monitoring in the modern treatment era," *European Heart Journal*, vol. 26, pp. 762–769, 4 2005.

[122] Bradenton Heart Center, "Holter and Event Monitoring."

[123] R. E. Mason, I. Likar, R. O. Biern, and R. S. Ross, "Multiple-lead exercise electrocardiography. Experience in 107 normal subjects and 67 patients with angina pectoris, and comparison with coronary cinearteriography in 84 patients.," *Circulation*, vol. 36, pp. 517–525, 10 1967.

[124] J. Roelandt, P. Klootwuk, J. Lubsen, and M. J. Janse, "Sudden death during longterm ambulatory monitoring," *European Heart Journal*, vol. 5, pp. 7–20, 1 1984.

[125] J. E. Deanfield, A. P. Selwyn, S. Chierchia, A. Maseri, P. Ribeiro, S. Krikler, and M. Morgan, "Myocardial Ischaemia During Daily Life in Patients with Stable Angina: Its Relation to Symptoms and Heart Rate Changes," *The Lancet*, vol. 322, pp. 753–758, 10 1983.

[126] A. B. de Luna, P. Coumel, and J. F. Leclercq, "Ambulatory sudden cardiac death: Mechanisms of production of fatal arrhythmia on the basis of data from 157 cases," *American Heart Journal*, vol. 117, pp. 151–159, 1 1989.

[127] E. A. Martinez, L. J. Kim, N. Faraday, B. Rosenfeld, E. B. Bass, B. A. Perler, G. M. Williams, T. Dorman, and P. J. Pronovost, "Sensitivity of routine intensive care unit surveillance for detecting myocardial ischemia," *Critical Care Medicine*, vol. 31, pp. 2302–2308, 9 2003.

[128] D. D. Finlay, C. D. Nugent, M. P. Donnelly, P. J. McCullagh, and N. D. Black, "Optimal electrocardiographic lead systems: Practical scenarios in smart clothing and wearable health systems," *IEEE Transactions on Information Technology in Biomedicine*, vol. 12, pp. 433–441, 7 2008.

[129] J. Yoo, L. Yan, S. Lee, H. Kim, and H. J. Yoo, "A wearable ECG acquisition system with compact planar-fashionable circuit board-based shirt," *IEEE Transactions on Information Technology in Biomedicine*, vol. 13, pp. 897–902, 11 2009.

[130] B. A. Dolezal, D. M. Boland, J. Carney, M. Abrazado, D. L. Smith, and C. B. Cooper, "Validation of heart rate derived from a physiological status monitor-embedded compression shirt against criterion ECG," *Journal of Occupational and Environmental Hygiene*, vol. 11, pp. 833–839, 12 2014.

[131] T. Morrison, J. Silver, and B. Otis, "A single-chip encrypted wireless 12-lead ECG smart shirt for continuous health monitoring," in *IEEE Symposium on VLSI Circuits, Digest of Technical Papers*, pp. 1–2, IEEE, 6 2014.

[132] A. Boehm, X. Yu, W. Neu, S. Leonhardt, and D. Teichmann, "A Novel 12-Lead ECG T-Shirt with Active Electrodes," *Electronics*, vol. 5, p. 75, 11 2016.

[133] LifeSignals, "Life Signal Patch," 2018.

[134] F. Roche, J. M. Gaspoz, V. Pichot, F. Costes, K. Isaaz, C. Ferron, C. Roche, A. Geyssant, J. R. Lacour, and J. C. Barthélémy, "Accuracy of an automatic and patient-triggered long-term solid memory ambulatory cardiac event recorder," *American Journal of Cardiology*, vol. 80, pp. 1095–1098, 10 1997.

[135] G. Caires, C. Aguiar, L. Parreira, P. Adragão, F. Morgado, D. Bonhorst, M. J. Grilo, F. Mesquita, and R. Seabra-Gomes, "Value of "cardiac event recorders" in the assessment of sporadic cardiac symptoms," *Revista portuguesa de cardiologia : orgão oficial da Sociedade Portuguesa de Cardiologia = Portuguese journal of cardiology : an official journal of the Portuguese Society of Cardiology*, vol. 16, pp. 863–71, 11 1997.

[136] S. Kinlay, J. W. Leitch, A. Neil, B. L. Chapman, D. B. Hardy, and P. J. Fletcher, "Cardiac event recorders yield more diagnoses and are more cost-effective than 48-hour Holter monitoring in patients with palpitations: A controlled clinical trial," *Annals of Internal Medicine*, vol. 124, pp. 16–20, 1 1996.

[137] C. De Asmundis, G. Conte, J. Sieira, G. B. Chierchia, M. Rodriguez-Manero, G. Di Giovanni, G. Ciconte, M. Levinstein, G. Baltogiannis, Y. Saitoh, R. Casado-Arroyo, and P. Brugada, "Comparison of the patient-activated event recording system vs. traditional 24 h Holter electrocardiography in individuals with paroxysmal palpitations or dizziness," *Europace*, vol. 16, pp. 1231–1235, 8 2014.

[138] S. A. Rothman, J. C. Laughlin, J. Seltzer, J. S. Walia, R. I. Baman, S. Y. Siouffi, R. M. Sangrigoli, and P. R. Kowey, "The diagnosis of cardiac arrhythmias: A prospective multi-center randomized study comparing mobile cardiac outpatient telemetry versus standard loop event monitoring," *Journal of Cardiovascular Electrophysiology*, vol. 18, pp. 241–247, 3 2007.

[139] C. J. Daniels and W. H. Franklin, "Common cardiac diseases in adolescents," *Pediatric Clinics of North America*, vol. 44, pp. 1591–1601, 12 1997.

[140] F. P. Sarasin, M. Louis-Simonet, D. Carballo, S. Slama, A. Rajeswaran, J. T. Metzger, C. Lovis, P. F. Unger, and A. F. Junod, "Prospective evaluation of patients with syncope: A population-based study," *American Journal of Medicine*, vol. 111, pp. 177–184, 8 2001.

[141] L. G. Futterman and L. Lemberg, "Ambulatory electrocardiographic monitoring: use of the implantable loop recorder in the evaluation of syncope.," *The Journal of cardiovascular nursing*, vol. 16, pp. 24–33, 4 2002.

[142] B. B. Pavri and R. T. Ho, "Syncope. Identifying cardiac causes in older patients," *Geriatrics*, vol. 58, no. 5, pp. 26–31, 2003.

[143] C. Brandt, C. Kramme, H. Storm, and B. Pohlmann-Eden, "Out-of-body experience and auditory and visual hallucinations in a patient with cardiogenic syncope: Crucial role of cardiac event recorder in establishing the diagnosis," *Epilepsy and Behavior*, vol. 15, pp. 254–255, 6 2009.

[144] J. C. Barthélémy, S. Féasson-Gérard, P. Garnier, J. M. Gaspoz, A. Da Costa, D. Michel, and F. Roche, "Automatic cardiac event recorders reveal paroxysmal atrial fibrillation after unexplained strokes or transient ischemic attacks," *Annals of Noninvasive Electrocardiology*, vol. 8, pp. 194–199, 7 2003.

[145] L. A. Sposato, L. E. Cipriano, G. Saposnik, E. R. Vargas, P. M. Riccio, and V. Hachinski, "Diagnosis of atrial fibrillation after stroke and transient ischaemic attack: A systematic review and meta-analysis," *The Lancet Neurology*, vol. 14, pp. 377–387, 4 2015.

[146] K. Yayehd, D. Irles, C. Akret, W. Vadot, G. Rodier, T. Berremili, S. Perenet, M. Chevallier-Grenot, L. Belle, and A. Dompnier, "Detection of paroxysmal atrial fibrillation by prolonged electrocardiographic recording after ischaemic

stroke in patients aged ¡ 60 years: A study with 21-day recording using the SpiderFlash® monitor," *Archives of Cardiovascular Diseases*, vol. 108, pp. 189–196, 3 2015.

[147] M. H. K. Park, C. De Asmundis, G. B. Chierchia, A. Sarkozy, A. Benatar, and P. Brugada, "First experience of monitoring with cardiac event recorder electrocardiography Omron system in childhood population for sporadic, potentially arrhythmia-related symptoms," *Europace*, vol. 13, pp. 1335–1339, 9 2011.

[148] P. K. Dash, "Electrocardiogram Monitoring," Tech. Rep. 4, Sree Chitra Tirunal Institute for Medical Sciences and Technology, 2002.

[149] H. L. Marriott, "Constant monitoring for cardiac dysrythmias and blocks.," *Modern concepts of cardiovascular disease*, vol. 39, pp. 103–8, 6 1970.

[150] M. J. Goldman, "Cardiac arrhythmias in myocardial infarction," *American Heart Journal*, vol. 39, pp. 884–886, 3 1950.

[151] R. Gay and D. F. Brown, "Bradycardia dependent bundle branch block in acute myocardial infarction," *CHEST*, vol. 64, pp. 114–116, 7 1973.

[152] H. J. L. Marriott and D. C. Thorne, "Dysrhythmic dilemmas in coronary care," *The American Journal of Cardiology*, vol. 27, pp. 327–330, 3 1971.

[153] R. L. Campbell, W. G. Langsten, and G. A. Ross, "A comparison of cardiac rate-pressure product and pressure-rate quotient with Holter monitoring in patients with hypertension and cardiovascular disease," *Oral Surgery, Oral Medicine, Oral Pathology, Oral Radiology, and Endodontics*, vol. 84, pp. 125–128, 8 1997.

[154] B. J. Drew and M. M. Scheinman, "Value of electrocardiographic leads MCL1, MCL6 and other selected leads in the diagnosis of wide QRS complex tachycardia," *Journal of the American College of Cardiology*, vol. 18, pp. 1025–1033, 10 1991.

[155] H. R. Aldrich, N. B. Hindman, T. Hinohara, M. G. Jones, J. Boswick, K. L. Lee, W. Bride, R. M. Califf, and G. S. Wagner, "Identification of the optimal electrocardiographic leads for detecting acute epicardial injury in acute myocardial infarction," *The American Journal of Cardiology*, vol. 59, pp. 20–23, 1 1987.

[156] R. Lux, M. Bilbao, M. Pelter, K. Fleischmann, J. Zegre, D. Schindler, and B. Drew, "Optimal leads, estimation, and continuous monitoring improve detection of acute MI and transient ischemia," *Journal of Electrocardiology*, vol. 37, pp. 240–243, 2004.

[157] R. L. Lux, M. J. Burgess, R. F. Wyatt, A. K. Evans, G. M. Vincent, and J. A. Abildskov, "Clinically practical lead systems for improved electrocardiography: Comparison with precordial grids and conventional lead systems," *Circulation*, vol. 59, pp. 356–363, 2 1979.

[158] A. Loewe, W. Schulze, Y. Jiang, M. Wilhelms, and O. Dössel, "Determination of Optimal Electrode Positions of a Wearable ECG Monitoring System for Detection of Myocardial Ischemia: A Simulation Study," *Computing in Cardiology, 2011*, pp. 741–744, 2011.

[159] E. P. Gerstenfeld, A. SippensGroenewegen, R. L. Lux, and M. D. Lesh, "Derivation of an optimal lead set for measuring ectopic atrial activation from the pulmonary veins by using body surface mapping," *Journal of Electrocardiology*, vol. 33, pp. 179–185, 1 2000.

[160] J. Waktare, K. Hnatkova, C. Meurling, H. Nagayoshi, T. Janota, A. Camm, and M. Malik, "Optimal lead configuration in the detection and subtraction of QRS and T wave templates in atrial fibrillation," in *Computers in Cardiology 1998. Vol. 25 (Cat. No.98CH36292)*, pp. 629–632, IEEE, 1998.

[161] Z. Ihara, V. Jacquemet, J. M. Vesin, and A. Van Oosterom, "Adaptation of the standard 12-lead EGG system focusing on atrial electrical activity," in *Computers in Cardiology*, vol. 32, pp. 203–205, IEEE, 2005.

[162] J. Igual, R. Llinares, M. Guillem, and J. Millet, "Optimal Localization of Leads in Atrial Fibrillation Episodes," in *2006 IEEE International Conference on Acoustics Speed and Signal Processing Proceedings*, vol. 2, pp. 1192–1195, IEEE, 2006.

[163] Z. Ihara, A. van Oosterom, V. Jacquemet, and R. Hoekema, "Adaptation of the standard 12-lead electrocardiogram system dedicated to the analysis of atrial fibrillation," *Journal of Electrocardiology*, vol. 40, pp. 1–68, 1 2007.

[164] A. Petrenas, V. Marozas, G. Jaruševičius, and L. Sörnmo, "A modified Lewis ECG lead system for ambulatory monitoring of atrial arrhythmias," in *Journal of Electrocardiology*, vol. 48, pp. 157–163, Churchill Livingstone, 3 2015.

[165] R. Alcaraz and J. J. Rieta, "Adaptive singular value cancelation of ventricular activity in single-lead atrial fibrillation electrocardiograms," *Physiological Measurement*, vol. 29, no. 12, pp. 1351–1369, 2008.

[166] T. Lewis, *Clinical Electrocardiography*. New York: Shaw & Sons, 1913.

[167] A. Haeberlin, T. Niederhauser, T. Marisa, J. Goette, M. Jacoment, D. Mattle, L. Roten, J. Fuhrer, H. Tanner, and R. Vogel, "The optimal lead insertion depth for esophageal ECG recordings with respect to atrial signal quality," in *Journal of Electrocardiology*, vol. 46, pp. 158–165, Churchill Livingstone, 3 2013.

[168] S. Ito, H. Tada, S. Naito, K. Kurosaki, M. Ueda, H. Hoshizaki, I. Miyamori, S. Oshima, K. Taniguchi, and A. Nogami, "Development and validation of an ECG algorithm for identifying the optimal ablation site for idiopathic ventricular outflow tract tachycardia.," *Journal of cardiovascular electrophysiology*, vol. 14, pp. 1280–6, 12 2003.

[169] H. Hachiya, K. Aonuma, Y. Yamauchi, M. Igawa, A. Nogami, and Y. Iesaka, "How to diagnose, locate, and ablate coronary cusp ventricular tachycardia," *Journal of Cardiovascular Electrophysiology*, vol. 13, pp. 551–556, 6 2002.

[170] T. Sadanaga, F. Sadanaga, H. Yao, and M. Fujishima, "An evaluation of ECG leads used to assess QT prolongation," *Cardiology*, vol. 105, no. 3, pp. 149–154, 2006.

[171] T. Feldman, R. W. Childers, and K. G. Chua, "Optimal ECG monitoring during percutaneous transluminal coronary angioplasty of the left anterior descending artery," *Catheterization and Cardiovascular Diagnosis*, vol. 13, pp. 271–274, 7 1987.

[172] P. J. Zimetbaum, S. Krishnan, A. Gold, J. P. Carrozza, and M. E. Josephson, "Usefulness of ST-segment elevation in Lead III exceeding that of lead II for identifying the location of the totally occluded coronary artery in inferior wall myocardial infarction," *American Journal of Cardiology*, vol. 81, pp. 918–919, 4 1998.

[173] R. M. Fuchs, S. C. Achuff, L. Grunwald, F. C. Yin, and L. S. Griffith, "Electrocardiographic localization of coronary artery narrowings: studies during myocardial ischemia and infarction in patients with one-vessel disease.," *Circulation*, vol. 66, no. 6, pp. 1168–1176, 2011.

[174] B. M. Horáček, M. Mirmoghisi, J. W. Warren, G. S. Wagner, and J. J. Wang, "Detection of myocardial ischemia by vessel-specific leads derived from the 12-lead electrocardiogram and its subsets," *Journal of Electrocardiology*, vol. 41, pp. 508–517, 11 2008.

[175] World Health Organisation, "Nomenclature and criteria for diagnosis of ischemic heart disease. Report of the Joint International Society and Federation of Cardiology/World Health Organization task force on standardization of clinical nomenclature.," *Circulation*, vol. 59, pp. 607–9, 3 1979.

[176] K. Thygesen, J. S. Alpert, and H. D. White, "Universal Definition of Myocardial Infarction," *European Heart Journal*, 2007.

[177] Minnesota Department of Health, "Minnesota Chest Pain / Acute Coronary Syndrome Tool-Kit; Patient with Chest Pain Or Potential Acute Coronary Syndrome STEMI, Non-STEMI and Chest Pain," tech. rep., Minnesota Department of Health, 2018.

[178] J. Mair, J. Smidt, P. Lechleitner, F. Dienstl, and B. Puschendorf, "A decision tree for the early diagnosis of acute myocardial infarction in nontraumatic chest pain patients at hospital admission," *Chest*, vol. 108, pp. 1502–1509, 12 1995.

[179] E. W. Grijseels, J. W. Deckers, and A. W. Hoes, "Implementation of a prehospital decision rule in general practice.pdf," *European Heart Journal*, vol. 16, no. 3, pp. 325–332, 1995.

[180] O. Pahlm, D. Case, G. Howard, J. Pope, and W. K. Haisty, "Decision rules for the ECG diagnosis of inferior myocardial infarction," *Computers and Biomedical Research*, vol. 23, pp. 332–345, 8 1990.

[181] W. E. Cayley, "Diagnosing the cause of chest pain.," *American family physician*, vol. 72, no. 10, pp. 2012–21, 2005.

[182] J. Christenson, G. Innes, D. McKnight, C. R. Thompson, H. Wong, E. Yu, B. Boychuk, E. Grafstein, F. Rosenberg, K. Gin, A. Anis, and J. Singer, "A clinical prediction rule for early discharge of patients with chest pain," *Annals of Emergency Medicine*, vol. 47, pp. 1–10, 1 2006.

[183] E. P. Hess, G. A. Wells, A. Jaffe, and I. G. Stiell, "A study to derive a clinical decision rule for triage of emergency department patients with chest pain: Design and methodology," *BMC Emergency Medicine*, vol. 8, 2008.

[184] S. W. Glickman, F. S. Shofer, M. C. Wu, M. J. Scholer, A. Ndubuizu, E. D. Peterson, C. B. Granger, C. B. Cairns, and L. T. Glickman, "Development and validation of a prioritization rule for obtaining an immediate 12-lead electrocardiogram in the emergency department to identify ST-elevation myocardial infarction," *American Heart Journal*, vol. 163, pp. 372–382, 3 2012.

[185] T. Reichlin, C. Schindler, B. Drexler, R. Twerenbold, M. Reiter, C. Zellweger, B. Moehring, R. Ziller, R. Hoeller, M. Rubini Gimenez, P. Haaf, M. Potocki, K. Wildi, C. Balmelli, M. Freese, C. Stelzig, H. Freidank, S. Osswald, and C. Mueller, "One-hour rule-out and rule-in of acute myocardial infarction using high-sensitivity cardiac troponin T," *Archives of Internal Medicine*, vol. 172, pp. 1211–1218, 9 2012.

[186] Medisave, "Omron HCG-801 HeartScan ECG Monitor," 2019.

[187] Medisave, "Welch Allyn CP150 Interpretive ECG," 2019.

[188] Philips, "PageWriter TC70 Cardiograph," 2019.

[189] J. Presedo, J. Vila, S. Barro, F. Palacios, R. Ruiz, A. Taddei, and M. Emdin, "Fuzzy modelling of the expert's knowledge in ECG-based ischaemia detection," *Fuzzy Sets and Systems*, vol. 77, pp. 63–75, 1 1996.

[190] P. Bozzola, G. Bortolan, C. Combi, F. Pinciroli, and C. BroHet, "A hybrid neuro-fuzzy system for ECG classification of myocardial infarction," in *Computers in Cardiology 1996*, pp. 241–244, IEEE, 2002.

[191] G. Li, C. Derwael, R. Fesler, and C. Brohet, "Computer interpretation of the 12-lead electrocardiogram, the Frank-lead vectorcardiogram and the reconstructed vectorcardiogram," in *Computers in Cardiology 1994*, pp. 321–324, IEEE Comput. Soc. Press, 2002.

[192] R. Correa, P. D. Arini, M. E. Valentinuzzi, and E. Laciar, "Novel set of vectorcardiographic parameters for the identification of ischemic patients," *Medical Engineering and Physics*, vol. 35, pp. 16–22, 1 2013.

[193] R. Correa, P. D. Arini, L. S. Correa, M. Valentinuzzi, and E. Laciar, "Novel technique for ST-T interval characterization in patients with acute myocardial ischemia," *Computers in Biology and Medicine*, vol. 50, pp. 49–55, 7 2014.

[194] A. Dhawan, B. Wenzel, S. George, I. Gussak, B. Bojovic, and D. Panescu, "Detection of Acute Myocardial Infarction from serial ECG using multilayer support vector machine," in *Proceedings of the Annual International Conference of the IEEE Engineering in Medicine and Biology Society, EMBS*, pp. 2704–2707, IEEE, 8 2012.

[195] C. Wang, X. Dong, S. Ou, W. Wang, J. Hu, and F. Yang, "A new method for early detection of myocardial ischemia: cardiodynamicsgram (CDG)," *Science China Information Sciences*, vol. 59, no. 1, pp. 1–11, 2016.

[196] R. Bousseljot, D. Kreiseler, and A. Schnabel, "Nutzung der EKG-Signaldatenbank CARDIODAT der PTB über das Internet," *Biomedizinische Technik*, vol. 40, pp. 317–318, 7 1995.

[197] J. L. Garvey, J. Zegre-Hemsey, R. Gregg, and J. R. Studnek, "Electrocardiographic diagnosis of ST segment elevation myocardial infarction: An evaluation of three automated interpretation algorithms," *Journal of Electrocardiology*, vol. 49, no. 5, pp. 728–732, 2016.

[198] E. Pueyo, L. Sörnmo, and P. Laguna, "QRS slopes for detection and characterization of myocardial ischemia," *IEEE Transactions on Biomedical Engineering*, vol. 55, pp. 468–477, 2 2008.

[199] T. Lahiri, U. Kumar, H. Mishra, S. Sarkar, and A. D. Roy, "Analysis of ECG signal by chaos principle to help automatic diagnosis of myocardial infarction," *Journal of Scientific and Industrial Research*, vol. 68, no. 10, pp. 866–870, 2009.

[200] Diana A. Orrego ; Miguel A. Becerra ; Edilson Delgado-Trejos, "Dimensionality reduction based on fuzzy rough sets oriented to ischemia detection," in *Annual International Conference of the IEEE Engineering in Medicine and Biology Society*, (San Diego, CA, USA), IEEE, 2012.

[201] J. Henriques, T. Rocha, S. Paredes, R. Cabiddu, D. Mendes, R. Couceiro, and P. d. Carvalho, "ECG Analysis Tool for Heart Failure Management and Cardiovascular Risk Assessment," in *HIMS'15- International Conference on Health Informatics and Medical Systems 2015*, 2015.

[202] R. Correa, P. Arini, L. Correa, M. Valentinuzzi, and E. Laciar, "Identification of Patients with Myocardial Infarction," *Methods of Information in Medicine*, vol. 55, pp. 242–249, 1 2016.

[203] C. Kan and H. Yang, "Dynamic spatiotemporal warping for the detection and location of myocardial infarctions," in *IEEE International Conference on Automation Science and Engineering*, pp. 1046–1051, IEEE, 8 2012.

[204] A. Muhammad, I. A. Malagore, and F. A. Afsar, "Automatic detection and localization of myocardial infarction using back propagation neural networks," in *2010 4th International Conference on Bioinformatics and Biomedical Engineering, iCBBE 2010*, pp. 1–4, IEEE, 6 2010.

[205] J. E. Norman, J. J. Bailey, A. S. Berson, W. K. Haisty, D. Levy, P. M. Macfarlane, and P. M. Rautaharju, "NHLBI workshop on the utilization of ECG databases: Preservation and use of existing ECG databases and development of future resources," *Journal of Electrocardiology*, vol. 31, pp. 83–89, 4 1998.

[206] "PhysioNet/Computing in Cardiology Challenges."

[207] F. Jager, A. Taddei, G. B. Moody, M. Emdin, G. Antolič, R. Dorn, A. Smrdel, C. Marchesi, and R. G. Mark, "Long-term ST database: A reference for the development and evaluation of automated ischaemia detectors and for the study of the dynamics of myocardial ischaemia," *Medical and Biological Engineering and Computing*, vol. 41, no. 2, pp. 172–182, 2003.

[208] F. Dawoud, G. S. Wagner, G. Moody, and B. M. Horáček, "Using inverse electrocardiography to image myocardial infarction-reflecting on the 2007 PhysioNet/Computers in Cardiology Challenge," *Journal of Electrocardiology*, vol. 41, pp. 630–635, 11 2008.

[209] St.-Petersburg Institute of Cardiological Technics, "12-lead Arrhythmia Database," 2015.

[210] J. P. Martinez, O. Pahlm, M. Ringborn, S. Warren, P. Laguna, and L. Sornmo, "The STAFF III Database: ECGs Recorded During Acutely Induced Myocardial Ischemia," in *2017 Computing in Cardiology Conference (CinC)*, vol. 44, 2018.

[211] U. Pahlm, O. Pahlm, and G. S. Wagner, "The 24-lead ECG display for enhanced recognition of STEMI-equivalent patterns in the 12-lead ECG," *Journal of Electrocardiology*, vol. 47, pp. 425–429, 7 2014.

[212] R. Lynch, "ECG lead misplacement: A brief review of limb lead misplacement," *African Journal of Emergency Medicine*, vol. 4, pp. 130–139, 9 2014.

[213] T. Ashida, K. Nagao, S. Tani, T. Yagi, H. Takahashi, E. Tachibana, S. Furuya, N. Matsumoto, and A. Hirayama, "Novel Usefulness of Synthesized 18-Lead Electrocardiography in the Diagnosis of ST-Elevation Myocardial Infarction: A Pilot Study — Circulation," *Circulation*, vol. 134, 2018.

[214] S. Wada, N. Ito, H. Fukunaga, Y. Tsuda, H. Takahashi, K. Hatori, N. Saito, H. Sasaki, T. Murase, K. Nagao, and S. Sasaguri, "Clinical Significance of Synthesized 18lead Electrocardiography for ST Elevation Myocardial Infarction," *Circulation*, vol. 136, 2017.

[215] T. Li, K. Shinozaki, M. Brave, T. Yagi, and L. B. Becker, "Agreement between actual and synthesized right-sided and posterior electrocardiographic leads in identifying ischemia," *American Journal of Emergency Medicine*, vol. 38, pp. 1346–1351, 7 2020.

[216] J. Petch, S. Di, and W. Nelson, "Opening the black box: the promise and limitations of explainable machine learning in cardiology," *Canadian Journal of Cardiology*, 9 2021.

[217] D. Lee, H. Kwon, H. Lee, C. Seo, and K. Park, "Optimal lead position in patch-type monitoring sensors for reconstructing 12-lead ECG signals with universal transformation coefficient," *Sensors (Switzerland)*, vol. 20, p. 963, 2 2020.

[218] B. J. Schijvenaars, J. A. Kors, G. van Herpen, F. Kornreich, and J. H. van Bemmel, "Interpolation of body surface potential maps," *Journal of Electrocardiology*, vol. 28, pp. 104–109, 1 1995.

[219] A. S. Rababah Msc, R. R. Bond, K. R. Msc, D. Guldenring, J. McLaughlin, and D. D. Finlay, "Novel hybrid method for interpolating missing information in body surface potential maps," *Journal of Electrocardiology*, vol. 57, pp. S51–S55, 11 2019.

[220] B. J. Drew, M. M. Pelter, D. E. Brodnick, A. V. Yadav, D. Dempel, and M. G. Adams, "Comparison of a new reduced lead set ECG with the standard ECG for diagnosing cardiac arrhythmias and myocardial ischemia," *Journal of Electrocardiology*, vol. 35, pp. 13–21, 10 2002.

[221] T. Kusayama, H. Furusho, M. Kinoshita, S. Kaneko, K. Usuda, and M. Takamura, "Characteristics of synthesized right-sided chest electrocardiograms in patients with acute pulmonary embolism," *Journal of Cardiology*, vol. 73, pp. 313–317, 4 2019.

[222] J. Lee, K. Oh, B. Kim, and S. K. Yoo, "Synthesis of Electrocardiogram V-Lead Signals from Limb-Lead Measurement Using R-Peak Aligned Generative Adversarial Network," *IEEE Journal of Biomedical and Health Informatics*, vol. 24, pp. 1265–1275, 5 2020.

[223] Z. Xu, R. Zhou, Y. Cao, B. Yong, X. Wang, and Q. Zhou, "Reconstruction of 12-Lead Electrocardiogram Based on GVM," in *Proceedings - 2018 6th International Conference on Advanced Cloud and Big Data, CBD 2018*, pp. 275–280, Institute of Electrical and Electronics Engineers Inc., 11 2018.

[224] H. J. Lee, D. S. Lee, H. B. Kwon, D. Y. Kim, and K. S. Park, "Reconstruction of 12-lead ECG using a single-patch device," *Methods of Information in Medicine*, vol. 56, pp. 319–327, 1 2017.

[225] J. Sohn, S. Yang, J. Lee, Y. Ku, and H. C. Kim, "Reconstruction of 12-lead electrocardiogram from a three-lead patch-type device using a LSTM network," *Sensors (Switzerland)*, vol. 20, pp. 1–13, 6 2020.

[226] A. Grande-Fidalgo, J. Calpe, M. Redón, C. Millán-Navarro, and E. Soria-Olivas, "Lead reconstruction using artificial neural networks for ambulatory ECG acquisition," *Sensors*, vol. 21, p. 5542, 8 2021.

[227] B. Y. R. Friedrich, M. Peterson, and A. Koster, "The Rise of Generation C," Tech. Rep. 62, 2011.

[228] Q. Z. Sheng, X. Qiao, A. V. Vasilakos, C. Szabo, S. Bourne, and X. Xu, "Web services composition: A decade's overview," *Information Sciences*, vol. 280, pp. 218–238, 10 2014.

[229] B. P. Rimal and I. Lumb, "The Rise of Cloud Computing in the Era of Emerging Networked Society," pp. 3–25, Springer, Cham, 2017.

[230] T. Hulsen, S. S. Jamuar, A. R. Moody, J. H. Karnes, O. Varga, S. Hedensted, R. Spreafico, D. A. Hafler, and E. F. McKinney, "From big data to precision medicine," 2019.

[231] B. Lundell and F. Van Der Linden, "Open source software as open innovation: Experiences from the medical domain," in *Managing Open Innovation Technologies*, vol. 9783642316, pp. 3–16, Springer, Berlin, Heidelberg, 6 2013.

[232] P. Hamilton, "Open source ECG analysis," in *Computers in Cardiology*, vol. 29, pp. 101–104, 2002.

[233] J. C. Hsieh and M. W. Hsu, "A cloud computing based 12-lead ECG telemedicine service," *BMC Medical Informatics and Decision Making*, vol. 12, pp. 1–12, 7 2012.

[234] C. Venkatesan, P. Karthigaikumar, and S. Satheeskumaran, "Mobile cloud computing for ECG telemonitoring and real-time coronary heart disease risk detection," *Biomedical Signal Processing and Control*, vol. 44, pp. 138–145, 7 2018.

[235] M. Shu, N. Wei, J. Xu, and M. Yang, "An intelligent ECG interactive processing system based on Android and cloud computing platform," in *2017 IEEE/CIC International Conference on Communications in China, ICCC Workshops 2017*, vol. 2018-Janua, pp. 1–4, Institute of Electrical and Electronics Engineers Inc., 5 2018.

[236] A. A. Mutlag, M. K. A. Ghani, M. A. Mohammed, A. Lakhan, O. Mohd, K. H. Abdulkareem, and B. Garcia-Zapirain, "Multi-agent systems in fog–cloud computing for critical healthcare task management model (CHTM) used for ECG monitoring," *Sensors*, vol. 21, p. 6923, 10 2021.

[237] O. Cheikhrouhou, R. Mahmud, R. Zouari, M. Ibrahim, A. Zaguia, and T. N. Gia, "One-Dimensional CNN Approach for ECG Arrhythmia Analysis in Fog-Cloud Environments," *IEEE Access*, vol. 9, pp. 103513–103523, 2021.

[238] Z. Zhang, H. Li, Z. Gong, R. Jin, and T. S. Chung, "A Compatible ECG Diagnosis Cloud Computing Framework and Prototype Application," in *PervasiveHealth: Pervasive Computing Technologies for Healthcare*, pp. 135–139, 2020.

[239] R. Bose and L. A. Saxon, "The Democratization of Diagnosis: Bringing the Power of Medical Diagnosis to the Masses," 2 2019.

[240] S. N. Kasthurirathne, "Designing and developing an open source medical informatics module," *XRDS: Crossroads, The ACM Magazine for Students*, vol. 19, pp. 20–23, 12 2012.

[241] S. Van Poucke, Z. Zhang, M. Schmitz, M. Vukicevic, M. V. Laenen, L. A. Celi, and C. De Deyne, "Scalable predictive analysis in critically ill patients using a visual open data analysis platform," *PLoS ONE*, vol. 11, p. e0145791, 1 2016.

[242] M. A. Ghaderi, G. Gupta, and L. S. Tamil, "A flexible software platform for disease management," *ProQuest Dissertations and Theses*, p. 164, 2016.

[243] J. W. Sanders, J. R. Fletcher, S. J. Frank, H. L. Liu, J. M. Johnson, Z. Zhou, H. S. M. Chen, A. M. Venkatesan, R. J. Kudchadker, M. D. Pagel, and J. Ma, "Deep learning application engine (DLAE): Development and integration of deep learning algorithms in medical imaging," *SoftwareX*, vol. 10, p. 100347, 7 2019.

Chapter 3

Datasets and Electrocardiogram Pre-processing

3.1 Datasets

This section will focus on the datasets used throughout this thesis. Three datasets were used, containing ECGs from patients recorded in a clinical setting. All three have been published and have been cited multiple times from various studies, making them well suited for the work carried out in this work.

3.1.1 Horáček et al.

3.1.1.1 Data

The data included were recorded at the Faculty of Medicine of Dalhousie University in Canada, and was described previously [1]. The recording process and subsequent pre-processing is described as follows: A population of 91 patients were involved, all of which had single-vessel coronary artery disease. Subsequently, the patients underwent PTCA in one of three coronary arteries. The lesion was in the LAD artery for 32 patients; in the LCX for 23 patients; and in the RCA for 36 patients. The criteria applied to diagnose coronary artery disease was 60% reduction in artery diameter in any of the three aforementioned arteries, no recent MI diagnosis using a 12-lead ECG, and normal ejection fraction of $\geq 45\%$. The median age in the study

population was 57 years old (±10, one standard deviation from the mean). The recordings were taken from 64 males and 27 females.

Two recordings were acquired per patient. One recording was taken during supine resting conditions, referred to as baseline. Another was taken during the inflation of a balloon catheter in one of the three coronary arteries. During this time, the artery was completely obstructed, meaning no blood could flow. A 120 lead ECG recording was taken for each patient. Three of these leads were distal limb leads (lead I, II, III) and 117 unipolar thoracic chest leads arranged in accordance with the Dalhousie Torso (Figure 3.1). The electrode system was comprised of several silicon strips with multiple electrodes attached to each. These were placed along the chest parallel to each other. Using Laplacian interpolation based on a three dimensional Dalhousie model, the 120 leads were expanded to 352 leads.

The ECG signals were amplified and filtered using a bandpass filter of 0.025–125 Hz. They were recorded with respect to the WCT. The sampling frequency was 500 Hz. The sampling resolution was 12-bits, giving an amplitude resolution of 2.5 μV. The recordings were averaged from a 15 s window to produce a single representative complex: one for the baseline, and one for the peak ischaemic state. The peak ischaemic state is defined as peak balloon inflation (PBI) and subsequent total occlusion of the artery. Fiducial points of the ECG were annotated by two cardiologists. These were P-onset, P-offset, QRS-onset, QRS-offset (J-point), T-onset, and T-offset.

Depending on the difference in the ST segment amplitudes between baseline and PBI, the patients were further split based on responders and non-responders. A responder was said to have a noticeable difference in ST-segment between baseline and PBI. There were 44 responders, with 88 recordings. There were 45 non-responders, with 90 recordings. Two recordings in total per patient, one for baseline and one for PBI. Three patients were excluded due to the presence of balloon inflations in more than one coronary artery. Table 3.1 shows a summary of the resulting dataset to be used throughout this project.

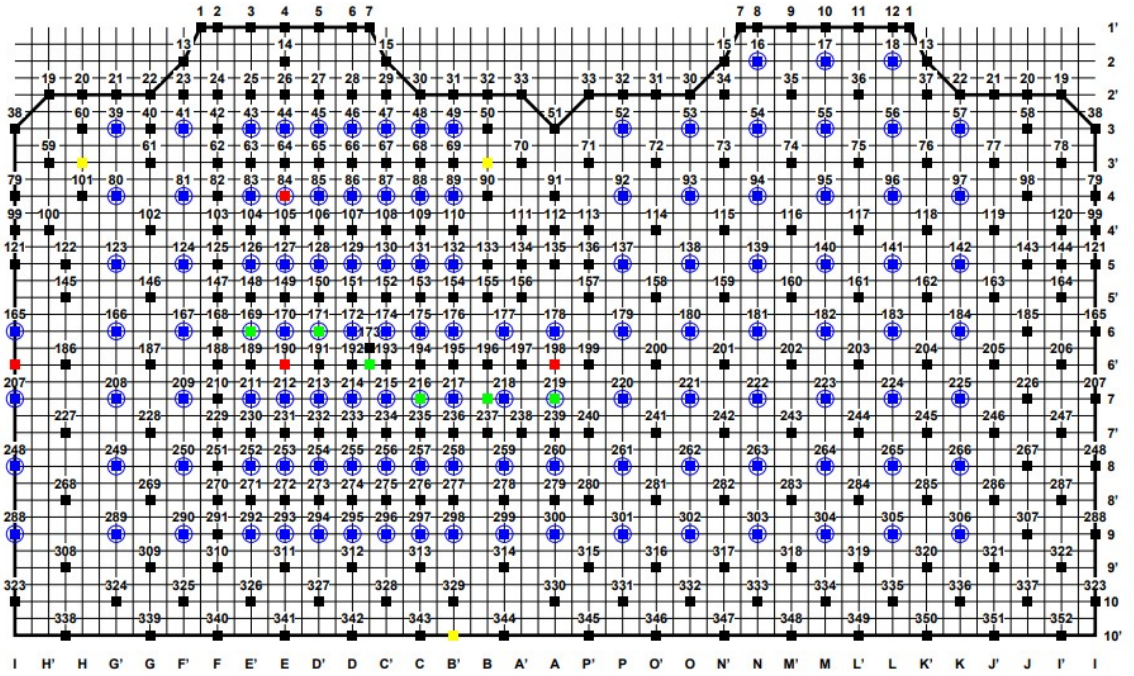

Figure 3.1: Dalhousie torso BSPM showing the 117 thoracic unipolar chest lead locations (blue circle), and interpolated lead locations (black square) [2]. The left half representing the anterior torso, and the right half representing the posterior torso.

3.1.2 Kornreich et al.

3.1.2.1 Data

This dataset was recorded for the Unit for Cardiovascular Research and Engineering in Free University Brussels, Belgium. It was described previously [3, 4]. A total of 746 subjects were involved. Of those, 232 subjects had no cardiac abnormalities or history of cardiac defects, so are deemed normal. Myocardial infarction was present in 277 subjects, confirmed with changes in blood enzyme levels. LVH was present

Table 3.1: Summary of the Horacek et al. dataset

Characteristic	Value
Patients	88
Recordings	176
Baseline recordings	88
PBI recordings	88
LAD recordings	62
LCX recordings	44
RCA recordings	70

Table 3.2: Summary of the Kornreich et al. dataset

Characteristic	Value
Patients	734
Recordings	734
Normal recordings	226
MI recordings	271
LVH recordings	237

in a further 237 subjects. All subjects were over 30 years old. The mean age was 43 years. 72% of the subject population were male. The mean age for subjects presenting with MI was 56. Those subjects with LBBB, RBBB, Wolf Parkinson White syndrome, or left-sided valvular disease were excluded.

One recording was taken per subject. The recordings were acquired in the supine position during rest. A BSPM with 117 unipolar thoracic chest leads was used to record the ECG. Three distal limb leads were also included, bringing the total measured leads to 120. The unipolar chest leads were recorded with respect to the WCT. The sampling frequency was 500 Hz. Leads determined to be invalid were interpolated from nearby leads. A single representative complex was calculated by coherent averaging in each lead of each patient. Laplacian interpolation was used to expand the 120 leads to 352 leads as per the Dalhouse torso [2]. From the original recordings, 12 were excluded due to missing data and excess noise. This left 734 total recordings of one beat in length and 352 leads. Of these, 226 were without disease (normal), 271 with MI, and 237 with LVH. The breakdown is summarised in Table 3.2

3.1.3 STAFF III

3.1.3.1 Data

This dataset was acquired in the Charleston Area Medical Center, USA. It was described previously [5, 6, 7]. A total of 104 patients were involved in the collection. Each patient underwent elective PTCA where a balloon was inflated in one or more coronary arteries. The patients were subjected to a prolonged balloon inflation to simulate AMI. None of the patients involved had acute myocardial abnormalities or chest pain, however, 35 patients with prior MI have been annotated. The mean

Table 3.3: Summary of the STAFF III dataset

Characteristic	Value
Patients	104
Recordings	467
Baseline recordings	352
Inflation recordings	115
LAD inflations	42
LCX inflations	25
RCA inflations	48

inflation time was 4 min 23 seconds, but ranged between 1 min 30 s to 9 min 54 s. A total of 152 occlusions were performed. Of these, 58 were in the LAD, 59 in the RCA and 32 in the LCX. A further three were performed in the LM artery. The study population had a mean age of 60 $\pm$ 11 years. Men make up the majority, 66%, of the patients involved.

A total of 467 recordings were acquired from the patients. Each patient had at least one five-minute recording taken at rest in a separate room to the procedure. Each patient also has at least one recording, taken during the PTCA procedure. The inflation onset and offset times were annotated. A further recording was acquired at rest in a separate room after the procedure. All recordings contain the standard leads of the 12-lead ECG (I–III, V1–V6). These were sampled at 1000 Hz with an amplitude resolution 0.625 μV. No digital filtering was used post-capture. Any recording with excess noise or invalid data were excluded prior. Of the 467 recordings remaining, 352 were taken without an inflation. These were 179 before the PTCA procedure and 173 afterwards. A total of 115 recordings contained balloon inflations. Of these, 42 recordings with LAD inflations, 48 with RCA inflations, and 25 with LCX inflations. A summary of this is shown in Table 3.3.

3.1.3.2 Pre-processing

Recordings from the STAFF III dataset (Section 3.1.3) were filtered to ISO standard 80601-2-86 [8], using a zero-phase second-order IIR bandpass filter with cutoff frequencies of 0.05–150 Hz. Recordings with missing annotations, ventricular tachycardia and invalid values were excluded (n=63). Data were separated to give relevant annotations for AMI detection. Recordings taken during rest were labelled as con-

trols (n=352), whereas those recorded during coronary artery occlusion were treated as AMI (n=115). Those who have experienced a prior MI have also been included (n=167).

3.2 Median Beat Extraction

The STAFF III data described in Section 3.1.3 contained recordings of several minutes in length. For this data to be useful when compared with the other datasets used, it was necessary to derive a single beat complex for each lead, representative of the entire recording. The primary challenge in accomplishing this task was the annotation of beat complexes from the 12-lead ECG. Three methods were considered to extract a single complex from the 12-lead. The first used the VCG, Spatial Velocity Gradient (SVG) and cubic spline interpolation to get one complex. The second used wavelet decomposition to detect the beats before producing a median beat. The third used a third party plugin, the BioSigKit, to annotate the different fiducial points of the ECG before producing a median beat. In this section, the methods employed in each of these potential solutions are shown, with some discussion as to the limitations of each.

3.2.1 VCG/Cubic Spline Method

Dataset three, described in section 4.3.1, contained ECG recordings multiple minutes in duration. Extracting a random beat in a recording that is several minutes in duration is not representative of the entire recording. Instead, a single median beat was derived for each lead of each recording.

The eight independent channels of the 12-lead ECG were extracted (I, II, V1–V6) from each recording of dataset three. Cubic-spline interpolation was used to correct baseline wander [9]. A three-lead Frank VCG was derived using the the Güldenring matrix method [10]. A single-lead SVG was calculated from the Frank VCG. The QRS complex was annotated based off the SVG [11]. The J-point was defined as the QRS offset. A ten second strip was extracted from each recording, at least 60 seconds from the beginning. A single beat was generated for each lead of the 12-lead ECG from the median amplitudes of the ten second excerpt. For baseline ECGs

median beats were calculated from data extracted from 60 seconds after the start of the record. For recordings containing balloon inflations in a coronary artery, median beats were calculated from data extracted from 60 seconds after the onset of balloon inflation. Once median beats were composed, further analysis was conducted to extract relevant amplitudes and morphology features for each lead for each subject. The details of this method are summarised below, but explained in greater detail in the subsequent sections:

1. Derive the VCG from the 12-lead recordings

2. Derive the SVG from the VCG

3. Annotate the QRS onset and offset using the SVG

4. Remove baseline wander using cubic spline interpolation

5. Produce a single median-beat for each lead of each recording

3.2.1.1 Vectorcardiogram derivation

The eight independent channels of the 12-lead ECG were extracted ($\mathbf{12}\boldsymbol{L}$). These are leads I, II, V1–V6, indicated in an $8 \times n$ matrix as follows, where n is the number of samples in the recording:

$$\mathbf{12}\boldsymbol{L} = \begin{bmatrix} I \\ II \\ V1 \\ \vdots \\ V6 \end{bmatrix}$$

A Frank VCG was derived from the independent channels using the Güldenring

matrix, $\boldsymbol{A_{VCG}}$, [10]:

$$\boldsymbol{A_{VCG}} = \begin{bmatrix} 0.5169 & -0.2406 & -0.0715 \\ -0.0722 & 0.6344 & -0.1962 \\ -0.0753 & 0.1707 & -0.4987 \\ 0.0162 & -0.0833 & -0.0319 \\ 0.0384 & 0.1182 & -0.2362 \\ 0.0545 & 0.0237 & -0.0507 \\ 0.1384 & -0.1649 & -0.2007 \\ 0.4606 & 0.2100 & 0.4122 \end{bmatrix}$$

The 3-lead Frank VCG, described as a $m \times 3$ matrix $\boldsymbol{VCG} = [\boldsymbol{x}, \boldsymbol{y}, \boldsymbol{z}]$. It is calculated by the multiplication of the eight independent channels of the 12-lead ECG ($\mathbf{12}\boldsymbol{L}$) by the Güldenring matrix ($\boldsymbol{A_{VCG}}$) as shown in (3.1):

$$\boldsymbol{VCG} = \mathbf{12}\boldsymbol{L} \cdot \boldsymbol{A_{VCG}} \tag{3.1}$$

3.2.1.2 Spatial velocity gradient

The SVG was derived from the VCG to aide QRS annotation. An SVG signal emphasises the QRS complex, while attenuating lower frequencies, such as baseline wander. The SVG is a single-lead vector with length m ($\boldsymbol{v_{SVG}}$), derived using the equation from Mori et al. [11]:

$$\boldsymbol{v_{SVG}} = \sqrt{\left(\frac{dx}{dt}\right)^2 + \left(\frac{dy}{dt}\right)^2 + \left(\frac{dz}{dt}\right)^2} \tag{3.2}$$

where x, y, and z are the respective columns of the derived Frank VCG ($\boldsymbol{VCG}$).

3.2.1.3 Vector magnitude

To facilitate the annotation of the T-waves from the 12-lead ECG data, the vector magnitude (VM) was calculated from the VCG data. The vector magnitude, unlike the SVG, provides prominent P and T waves to assist with the later annotation.

This was calculated using the following formula:

$$VM_{12L} = (VCG_X + VCG_Y + VCG_Z)^2 \tag{3.3}$$

where VCG_X, VCG_Y, and VCG_Z are the three channels of data from the VCG, derived using the Güldenring matrix VCG described previously.

3.2.1.4 QRS annotation

The QRS complexes for each 12-lead ECG recording were calculated using the derived SVG data from the VCG. A potential QRS complex was defined as having an amplitude of greater than or equal to one-sixth of the mean SVG signal across the recording.

$$QRS_{potential}(\boldsymbol{v_{SVG}}) \stackrel{?}{=} \begin{cases} \text{True} & \text{if } \boldsymbol{v_{SVG}} \geq \frac{\overline{\boldsymbol{v_{SVG}}}}{6} \\ \text{False} & \text{otherwise} \end{cases} \tag{3.4}$$

where $QRS_{potential}$ are all potential QRS complexes, v_{SVG} is the VCG derived from the recording, and $\overline{\boldsymbol{v_{SVG}}}$ is the mean VCG signal. Note, '$\stackrel{?}{=}$' denotes that we proceed on the assumption that Equation 3.4 is correct to test this method. Potential QRS complexes with a duration of less than 200 μs were excluded as noise spikes. Additionally, all complexes with a period of less than 300 ms were excluded. This allows for a maximum detectable heart rate of 200 beats per minute. This can be seen in Equation 3.5:

$$\forall QRS_{potential} \in \boldsymbol{v_{SVG}},\ QRS = \begin{cases} \text{True} & \text{if } T(QRS_{potential}) < 200ms \\ \text{False} & \text{otherwise} \end{cases} \tag{3.5}$$

where QRS are the confirmed locations of a QRS complex as per our algorithm, $QRS_{potential}$ are the potential QRS complexes, and $T(QRS_{potential})$ is the time period between two consecutive potential QRS complexes. For each potential QRS complex, the peak amplitude of the SVG was correlated with the 12-lead ECG data to determine the location of the R wave.

To determine the position of the Q and S waves, the predetermined QRS complex locations were used. The S waves were located based on the beginning of each QRS

complex. The criteria used were that previously published by Macfarlane [12]. The beginning of a QRS complex was defined as the first point where the signal drops below 3 mV/s, before the R peak. The Q waves followed the same criteria, but in reverse. The Q wave was defined as the first point where the signal decreases below 3 mV/s, after the R peak. This was carried out for each detected QRS complex.

3.2.1.5 Cubic-spline based baseline correction

The 12-lead ECG still has significant baseline wander as a result of respiration, even after filtering. The use of a 0.05–150 Hz diagnostic filter is not sufficient to remove this without compromising the ST-segment, which is essential for MI diagnosis. The cubic spline interpolation method was used to create a spline curve connected to the isoelectric PQ segment [13]. The amplitude of each sample of the spline is then subtracted from each sample of the 12-lead ECG to produce an interpolated signal tending around 0 V.

3.2.1.6 T wave annotation

Using the SVG signal, the T wave peaks were annotated where the signal drops below 1.5 mV/s following a QRS complex. This is following the criteria previously published by Marfarlane [12]. The T wave ends were annotated using the Philips QT algorithm, described previously by Zhou et al. [14]. The vector magnitude signal was used for this process, where a straight ancillary line is drawn from the T wave peak to a point following the perceived end of the T wave. This was chosen as the isoelectric line (0 V). The point at which the difference between the y axis value of the ancillary line and the vector magnitude signal is the largest was chosen as the T wave offset/end.

3.2.1.7 Beat extraction

It was necessary to produce a single beat complex for each recording, since this is common among datasets previously published, especially with those used as part of this thesis, described in Sections 3.1.1 and 3.1.2. A ten second strip was extracted from each recording, at least 60 seconds from the beginning of the record. Those recordings containing balloon inflations, as described in Section 3.1.3, had ten second

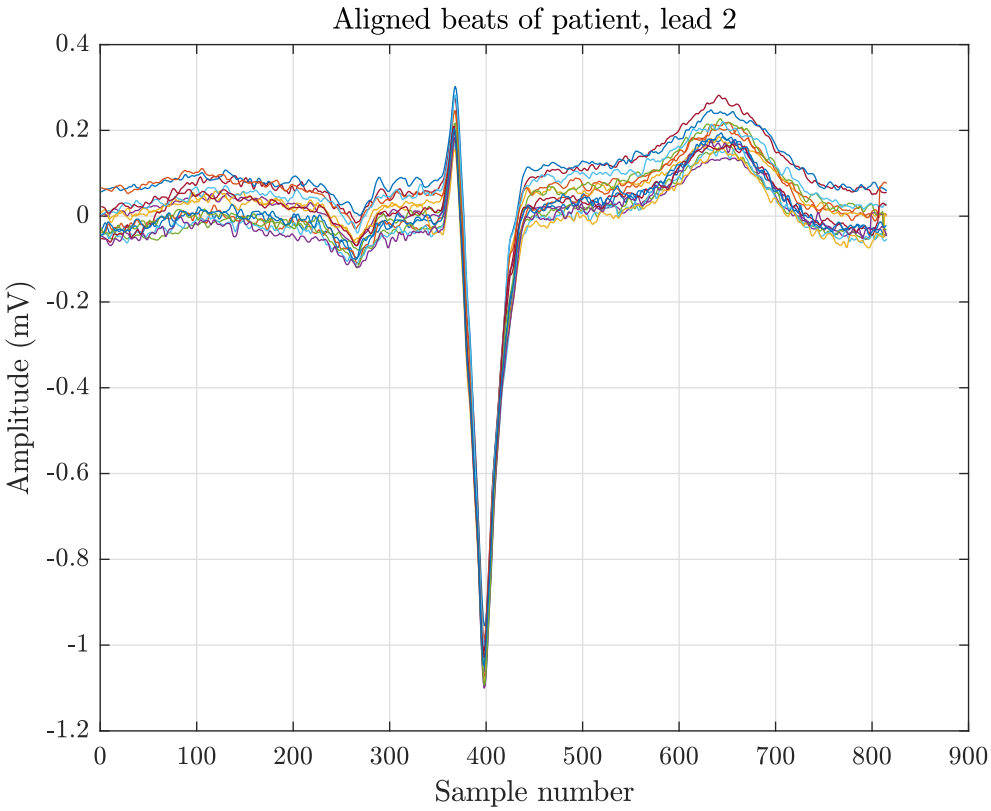

Figure 3.2: Aligned beats from the chosen ten second window of one record. Beats were aligned from the R waves in the precordial chest lead V2

strips extracted 60 seconds from the onset of balloon inflation.

The R wave with the largest peak was chosen as the datum point during the beat alignment. A fixed time of 200 ms before the R wave and 600 ms after the R wave of each beat was used as a beat-wise window. Each complete beat occurring within the ten second strip were extracted into the beat-wise windows. The extracted beats were aligned based on their respective R wave peaks. An example of this can be seen in Figure 3.2:

The median amplitude of each sample in the window was calculated based on all aligned beats. This produced one median complex. The process was repeated for each lead to produce one median complex for every lead in the recording. In this case, the eight independent channels of the 12-lead ECG.

3.2.2 Wavelet Decomposition Method

Wavelets were considered as an alternative method of annotating the QRS complexes of the 12-lead ECG. Wavelet-based methods of detecting beats and abnormalities

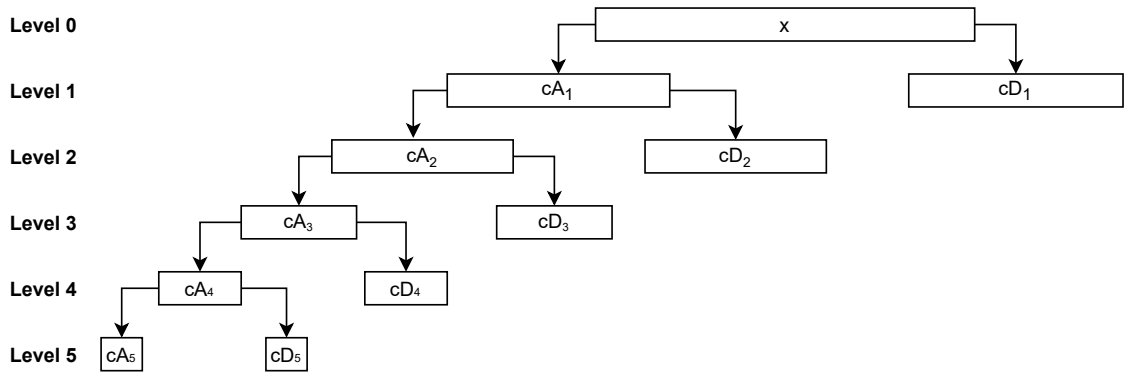

Figure 3.3: A breakdown of wavelet decomposition coefficients from an original signal (x), into average coefficients (cD_n), and detail coefficients (cD_n)

within ECG recordings is common [15, 16, 17]. This method uses banks of high pass and low pass filters to extract information from a designated frequency band. There are many wavelet topologies to choose from, but the Daubechies wavelet has been shown effective in extracting features from the ECG [18, 19, 20]. For this method, a five-level Daubechies-4 wavelet decomposition (db4) was chosen. This method uses five levels of decomposition to create a series of coefficients, called decomposition vectors. Each level has two sets of coefficients: average coefficients (cA_n), and detail coefficients (cD_n). The average coefficients are low-pass filtered, whereas the detail coefficients are high-pass filtered. Figure 3.3 shows this breakdown of coefficients:

The independent channels of the 12-lead ECG were extracted. These leads were then decomposed using the method above. The coefficients were then reconstructed into the separate detail (D_n) and average (A_n) signal branches. This ensures all reconstructed branches are of equal length. The R wave peak was determined as any prominent peak above one third of the mean signal across the reconstructed detail signals in level five (D_5). If an R wave was detected, a window encompassing all samples in a 300 ms period after the detection was extracted. The R wave was then said to be the most prominent peak of the absolute magnitude of the window. Without this window, Q waves would be mistaken for R waves. An example of this process is shown in Figure 3.4.

An example of a reconstructed signal compared with the input signal is shown in Figure 3.5. A total of 15 beats were detected in the window shown. The second graph shows the level five detail layer. This was deemed to be the most apt for R wave detection due to both the prominence of the signal during the QRS complex and

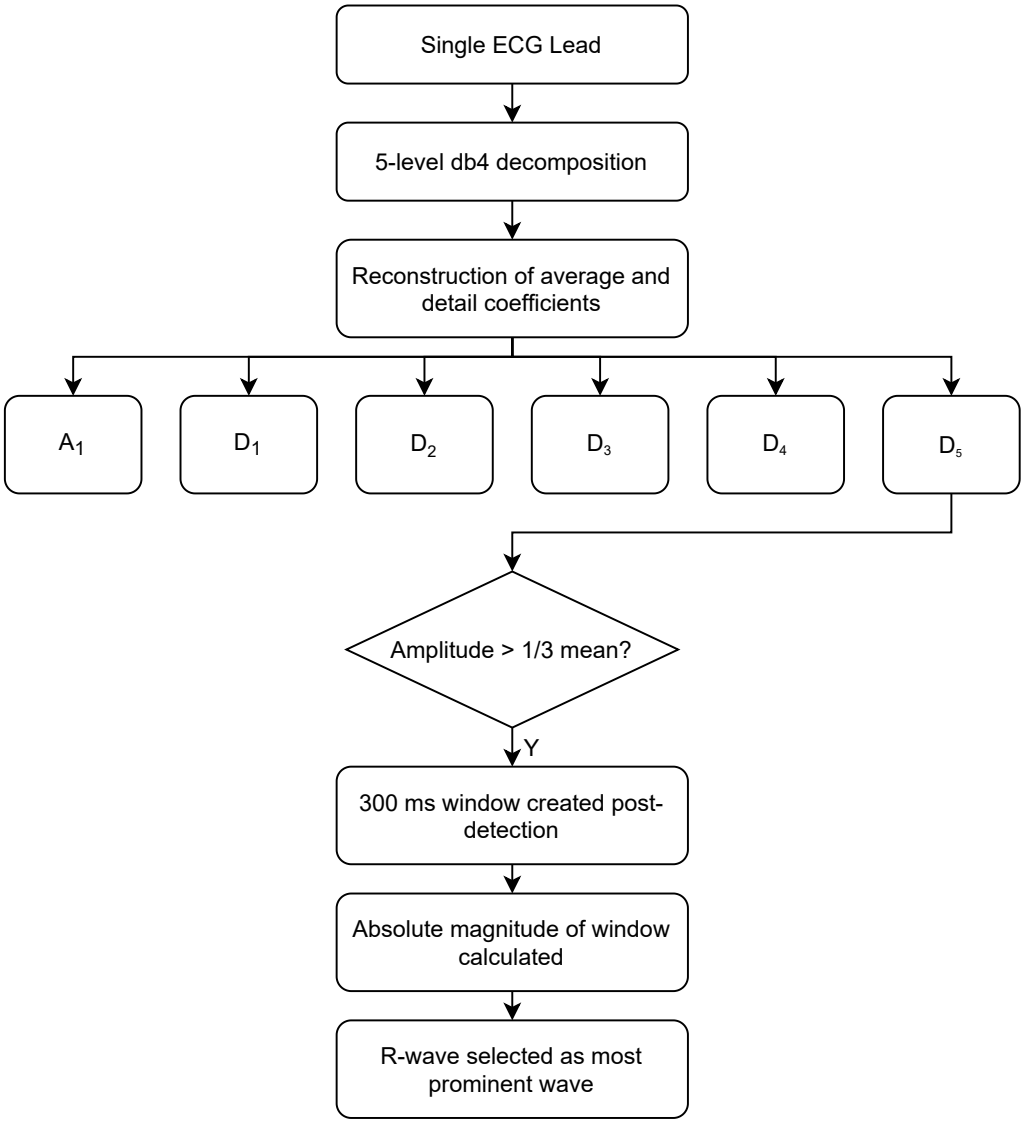

Figure 3.4: A summary of methods used to detect R waves using wavelet decomposition

the lack of noise present. All signals are the same length due to the reconstruction of the different levels. Without this, the lower levels (i.e level 5) would be shorter than the original signal. This would be problematic when extracting the R wave locations from detail coefficients.

To create a single beat complex representative of the recording, a window of 15 beats was created. Each beat from the window were extracted so that the R wave was in the centre. The median amplitude of each sample in the aligned beats was calculated. This produced a single median complex. This process was repeated for each lead. The median beats for a single recording is shown in Figure 3.6.

Ultimately, this method was not chosen to annotate the data described in Section

3.1.3 due to the complexities associated with baseline wander, noise, and feature extraction from the decomposed signals. Baseline wander was not compensated for when using this method. This meant that some median beats had a significant DC offset of up to 0.5 mV. Additionally, a reliable method was not established to signify the start and end of a beat. This resulted in the T wave end of some beats being cut off.

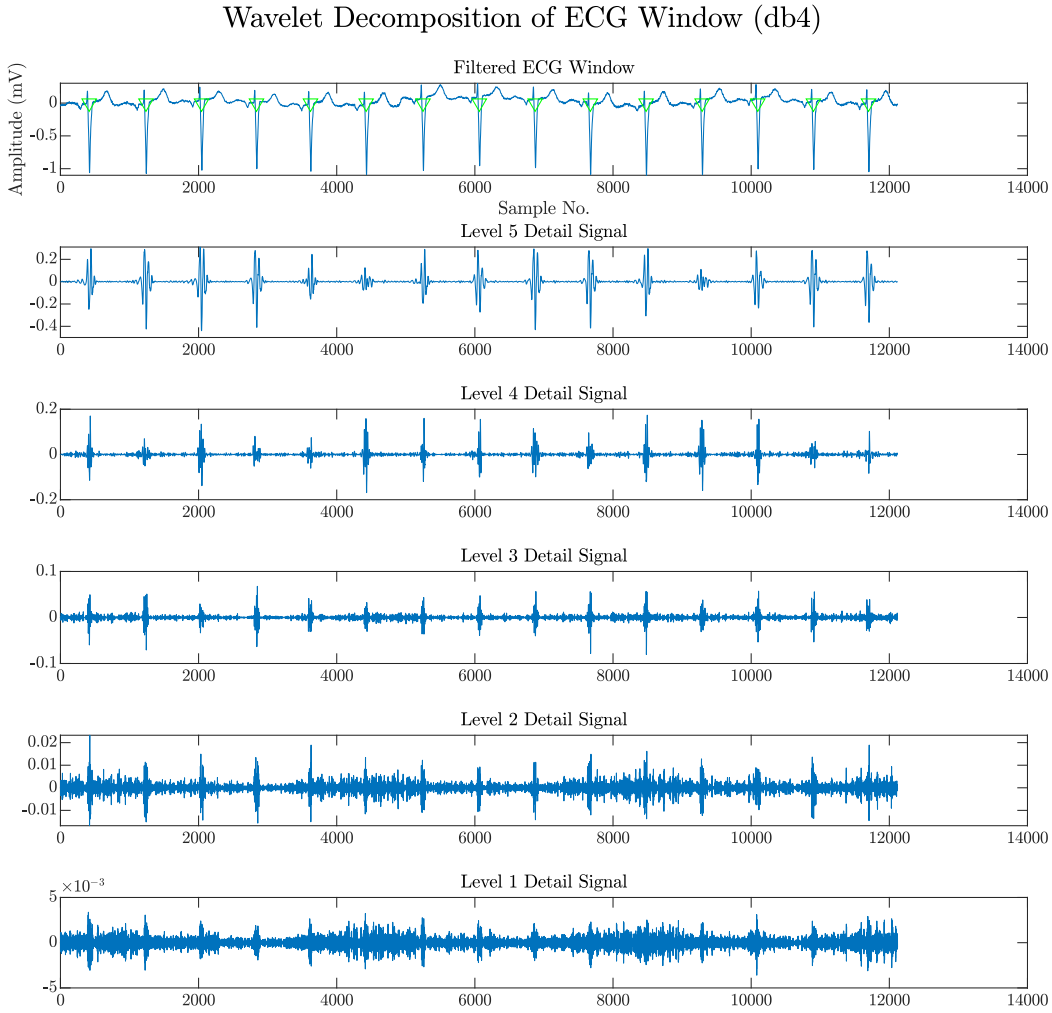

Figure 3.5: Reconstructed detail signal of an ECG lead (V2), following a five-level Daubechies-4 wavelet decomposition. R-wave annotations are annotated as green triangles over the input signal (top)

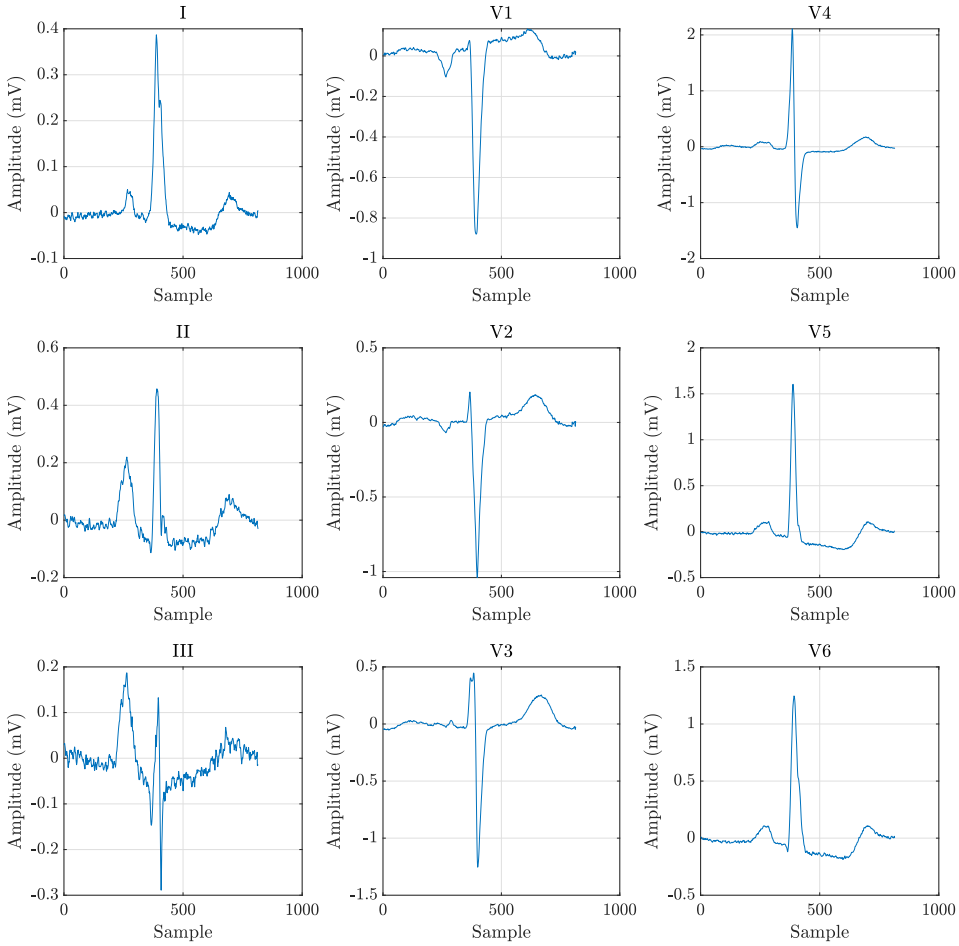

Figure 3.6: The median beats calculated for a single recording using wavelet decomposition and beat alignment using a window of 15 detected R waves

3.3 Conclusion

This chapter introduced the datasets and pre-processing steps used throughout this work. Three ECG datasets were used: Horáček et al., Kornreich et al., and the STAFF III dataset. The BSPM datasets were chosen due to the number of leads across the torso, suited to the derivation of novel leads. Additionally, the prescence of conditions that affect the ST-segment, such as ischaemic-type changes, made them suitable for ST-sensitive lead selection. The STAFF III dataset was chosen due to its reliability as a test set against ischaemic-type ECG changes associated with MI. This dataset can be used to verify novel and derived lead systems.

Two pre-processing methods were investigated to extract a single median beat complex from the STAFF III dataset: VCG/cubic spline interpolation, and wavelet decomposition. The former was chosen due to its reliability and past use within the faculty.

References

[1] B. M. Horacek, J. W. Warren, C. J. Penney, R. S. MacLeod, L. M. Title, M. J. Gardner, and C. L. Feldman, "Optimal electrocardiographic leads for detecting acute myocardial ischemia," *Journal of Electrocardiology*, vol. 34, pp. 97–111, 12 2001.

[2] B. M. Horacek, "Numerical model of an inhomogeneous human torso," *Advanced Cardiology*, vol. 10, no. 51, 1974.

[3] F. Kornreich, T. J. Montague, and P. M. Rautaharju, "Body surface potential mapping of ST segment changes in acute myocardial infarction: Implications for ECG enrollment criteria for thrombolytic therapy," *Circulation*, vol. 87, no. 3, pp. 773–782, 1993.

[4] B. J. Schijvenaars, J. A. Kors, G. van Herpen, F. Kornreich, and J. van Bemmel, "Interpolation of body surface potential maps," *Journal of Electrocardiology*, vol. 28, pp. 104–109, 1 1995.

[5] J. Pettersson, E. Carro, L. Edenbrandt, C. Maynard, O. Pahlm, M. Ringborn, L. Sörnmo, S. G. Warren, and G. S. Wagner, "Spatial, individual, and temporal variation of the high-frequency QRS amplitudes in the 12 standard electrocardiographic leads," *American Heart Journal*, vol. 139, pp. 352–358, 2 2000.

[6] J. P. Martínez, O. Pahlm, M. Ringborn, S. Warren, P. Laguna, and L. Sörnmo, "The STAFF III Database: ECGs recorded during acutely induced myocardial ischemia," in *Computing in Cardiology*, vol. 44, pp. 1–4, 2017.

[7] A. L. Goldberger, L. A. Amaral, L. Glass, J. M. Hausdorff, P. C. Ivanov, R. G. Mark, J. E. Mietus, G. B. Moody, C. K. Peng, and H. E. Stanley, "PhysioBank, PhysioToolkit, and PhysioNet: components of a new research resource for complex physiologic signals.," *Circulation*, vol. 101, no. 23, 2000.

[8] ISO, "80601-2-86 Medical electrical equipment. Part 2-86: Particular requirements for the basic safety and essential performance of electrocardiographs, including diagnostic equipment, monitoring equipment, ambulatory equipment, electrodes," 2018.

[9] L. Sornmo, "Time-varying filtering for removal of baseline wander in exercise ECGs," in *Computers in Cardiology*, pp. 145–148, Publ by IEEE, 1992.

[10] D. Guldenring, D. D. Finlay, D. G. Strauss, L. Galeotti, C. D. Nugent, M. P. Donnelly, and R. R. Bond, "Transformation of the Mason-Likar 12-lead electrocardiogram to the Frank vectorcardiogram," in *Proceedings of the Annual International Conference of the IEEE Engineering in Medicine and Biology Society, EMBS*, pp. 677–680, 2012.

[11] H. Mori, H. Masaki, T. Niki, T. Nagao, S. Matsumo, T. Nii, and T. Oda, "Qrs Waves of the Spatial Velocity Electrocardiogram in Atrial Septal Defect," *Japanese Heart Journal*, vol. 13, no. 5, pp. 407–417, 1972.

[12] P. W. Macfarlane, "ECG waveform identification by digital computer," *Cardiovascular Research*, vol. 5, pp. 141–146, 1 1971.

[13] J. N. Froning, M. D. Olson, and V. F. Froelicher, "Problems and limitations of ECG baseline estimation and removal using a cubic spline technique during exercise ECG testing: Recommendations for proper implementation," *Journal of Electrocardiology*, vol. 21, pp. S149–S157, 1 1988.

[14] S. H. Zhou, E. D. Helfenbein, J. M. Lindauer, R. E. Gregg, and D. Q. Feild, "Philips QT interval measurement algorithms for diagnostic, ambulatory, and patient monitoring ECG applications," *Annals of Noninvasive Electrocardiology*, vol. 14, no. SUPPL. 1, pp. S3–S8, 2009.

[15] J. P. Martínez, R. Almeida, S. Olmos, A. P. Rocha, and P. Laguna, "A Wavelet-Based ECG Delineator Evaluation on Standard Databases," *IEEE Transactions on Biomedical Engineering*, vol. 51, pp. 570–581, 4 2004.

[16] V. X. Afonso, W. J. Tompkins, T. Q. Nguyen, and S. Luo, "ECG beat detection using filter banks," *IEEE Transactions on Biomedical Engineering*, vol. 46, no. 2, pp. 192–202, 1999.

[17] C. A. Ledezma and M. Altuve, "Optimal data fusion for the improvement of QRS complex detection in multi-channel ECG recordings," *Medical and Biological Engineering and Computing*, vol. 57, no. 8, pp. 1673–1681, 2019.

[18] V. Seena and J. Yomas, "A review on feature extraction and denoising of ECG signal using wavelet transform," in *Proceedings of the IEEE International Caracas Conference on Devices, Circuits and Systems, ICCDCS*, Institute of Electrical and Electronics Engineers Inc., 10 2014.

[19] V. Kalidas and L. Tamil, "Real-time QRS detector using stationary wavelet transform for automated ECG analysis," in *Proceedings - 2017 IEEE 17th International Conference on Bioinformatics and Bioengineering, BIBE 2017*, vol. 2018-Janua, pp. 457–461, Institute of Electrical and Electronics Engineers Inc., 7 2017.

[20] K. Mourad and B. R. Fethi, "Efficient automatic detection of QRS complexes in ECG signal based on reverse biorthogonal wavelet decomposition and nonlinear filtering," *Measurement: Journal of the International Measurement Confederation*, vol. 94, pp. 663–670, 12 2016.

Chapter 4

Additional Derived Leads to Improve the Detection of Ischaemic Heart Disease

---

4.1 Abstract

Additional chest leads, particularly those on the right-side and posterior torso, have the potential to increase the spatial resolution of the 12-lead ECG. These leads are unconventional and typically not recorded in the clinical setting. This chapter investigates the derivation of these leads and report on their performance in the detection of ECG changes associated with acute MI.

ECG recordings (n = 1440) were used from three centres. Centre one (n = 176) and two (n = 734) contained BSPM recordings using 117 thoracic unipolar leads, expanded to the 352-node Dalhousie torso using linear interpolation. Ten-fold cross validation was used to generate coefficients for the derivation of posterior (V7–V12) and right-sided (V3R–V6R) chest leads. The eight independent channels of the 12-lead ECG were used as predictors for linear regression. CC and RMSE were calculated to verify the derivation performance on the test set. Centre three recordings (n = 467) contained 12-lead ECG recordings taken at rest (n = 352) and during elective percutaneous coronary intervention (n=115). Posterior and right sided leads were derived using generated coefficients. Derived leads were added

to the 12-lead ECG to form 18 and 22-lead configurations respectively. Previously published STEMI criteria were used to classify ischaemic-type ECG changes for each configuration.

A matrix of derivation coefficients were produced. The correlation coefficient and root mean square error between measured and derived leads varied between 0.83–0.92/30.9–63.1 μV for posterior and 0.92–0.98/34.7–39.0 μV for right-sided chest leads respectively. Compared to previously published derivation coefficients, CC was significantly greater in leads V7–V12. F1 scores for the 12/18/22 lead configurations were 69.1/69.4/69.5% respectively. Sensitivity improved from 58.3–64.4% between 12 and 22-lead configurations. No statistically significant improvements were noted as leads were added.

4.2 Introduction

The inclusion of additional chest leads, complementary to the 12-lead ECG, may increase the sensitivity of AMI detection due to an increased spatial resolution across the torso [1]. Additionally, this provides clinicians a more complete view of the heart, including the potential to locate which artery the infarct resides in [2].

It is known that clinicians sometimes may elect to move an electrode in the conventional 12-lead ECG configuration to explore body surface territories, not captured by the 12-lead ECG. This process involves moving one of the chest lead electrodes to the region of interest. This is done on an ad-hoc basis and does not follow any convention for electrode placement. Conventions do also exist for the simultaneous recording of additional chest leads which are not part of the 12-lead ECG configuration. The posterior (V7–V12) and right-sided chest leads (V3R–V6R), in particular, extend the 12-lead ECG chest leads to facilitate a nearly 360 degree spatial resolution across the heart's longitudinal axis. Some of these leads already exist in the 18-lead ECG configuration, namely V7–V9 and V3R–V5R. Furthermore, the current published criteria for the detection of STEMI make reference to these additional leads and propose criteria relating to voltage thresholds that reflect the indicative ECG changes in these territories. The use of additional leads is especially recommended on the clinical suspicion of MI in vessels of the heart where the 12-lead

ECG has reduced resolution. Regardless, there is very limited routine use of lead systems in clinical practice that extend the 12-lead ECG. These additional leads are often inconvenient in a clinical setting due to their position on the posterior torso. Furthermore, to allow true simultaneous recording of these leads, new hardware is required with a greater number of recording channels. It is however possible to derive the posterior and right-sided chest leads from the 12-lead ECG [3].

Previous studies into the synthesis of chest leads from the 12-lead ECG have shown comparable results to those with those leads physically recorded [4, 5]. Many focus on deriving the 18-lead ECG, due to its capability to detect infarcts in locations not easily visible in the 12-lead ECG. For example, synthesised posterior leads such as V7–V9 has been shown to improve the detection sensitivity of MI, especially infarcts in the posterior of the heart [6, 7], while retaining the ability to distinguish it from other diseases such as Takotsubo syndrome and bundle branch blocks [8, 9]. Synthesised right sided chest leads have a similar effect. They expand the spatial resolution of the ECG to the right chest, improving its capability to detect infarcts in the right coronary artery [4]. While the ST-segment is the most common predictor or acute MI [10]. The derived ECG can also confirm clinical suspicions of MI from anterior leads by exhibiting the opposite response. For example, ST-depression in leads V5–V6 may show ST-elevation in V3R and V4R [7]. Additionally, T-wave changes such as inversion in the posterior lead V7 have been shown to have a high feature importance in detecting ischaemia [8]. The derivation of additional leads has the capability to decrease the time to coronary intervention, called door-to-balloon time, due to the reduced need to physically record the extended lead set [11, 1].

The aim of the work in this chapter is to assess the capability of derived posterior and right-sided chest leads in the detection of AMI using the current diagnostic criteria. This chapter will report on the development of a set of coefficients for the accurate derivation of posterior and right sided leads. Additionally, it will evaluate the derivation performance of these leads by comparing the shape of derived waveforms to actually recorded waveforms. This chapter will also evaluate the performance of the derived leads in the detection of ECG changes associated with acute coronary artery occlusion.

4.3 Methods

4.3.1 Data

Three datasets were used during this chapter, described previously in Chapter 3, with a total of 1440 recordings. These have been broken down as follows:

1. Horáček et al, 176 recordings [12]
2. Kornreich et al, 734 recordings [13, 14]
3. STAFF III, 530 recordings [15, 16, 17]

The first and second datasets, Horáček and Kornreich, were used to generate and evaluate coefficients capable of deriving the right sided and posterior leads from the 12-lead ECG. Data were split at random into ten folds for cross-validation. The training data (n = 819) were used to develop transformation coefficients to allow the derivation of the posterior and right sided leads. The remaining test data (n = 91) were used to compare how well derived posterior and right sided leads matched with actual recorded leads for the same subjects. In the first dataset, rest and PBI recordings were kept together during training and test partition.

The third dataset, STAFF III, was used to evaluate the performance of the derived posterior and right-sided chest leads in the detection of ischaemic-type ECG changes associated with myocardial infarction. These data have been previously described [15, 16, 17]. This dataset was chosen as it allows analysis of the effects of AMI on the ECG within the first five minutes of artery occlusion [18]. Data were separated to give relevant annotations for AMI detection. Recordings taken during rest were labelled as controls (n=352), whereas those recorded during coronary artery occlusion were treated as AMI (n=115). Those who have experienced a prior MI have also been included (n = 167).

4.3.2 Coefficient Generation for Lead Derivation

Eight of the independent channels of the 12-lead ECG were extracted from each recording (I–II, V1–V6). The leads to be derived were also extracted. The leads to be derived consisted of the commonly recognised posterior leads (V7–V12) and

right-sided precordial leads (V3R–V6R). The approximate locations of these leads are shown in Figure 4.1.

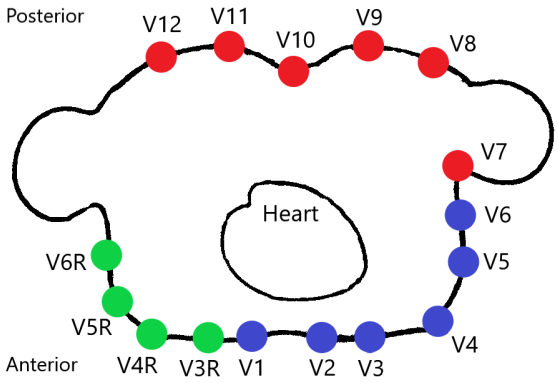

Figure 4.1: Cross section (plan view) of the thorax, adapted from a computed tomography (CT) scan, with approximate locations of precordial leads (blue), posterior leads (red) and right-sided leads (green)

Recorded leads and the leads to be derived were used in the coefficient generation. All recordings in the training dataset (n = 819) were pooled prior to calculation by concatenating each recording. Linear regression was then used to derive the transform coefficients as follows:

$$\beta = \left[\left(RL_{train}^{T} \cdot RL_{train} \right)^{-1} RL_{train}^{T} \right] \cdot DL_{train} \tag{4.1}$$

where β is the resulting 8x10 matrix of coefficients that relates recorded and derived leads. RL_{train} represents an m_{train}x8 matrix of recorded leads (I–II, V1–V6) taken from the training dataset. DL_{train} represents an m_{train}x10 example of derived leads (V7–V12, V3R–V6R) also taken from the training dataset. In all of the experiments, both RL_{train} and DL_{train} were made up of pooled data from the corresponding respective leads from all subjects in the training set. m_{train} indicates the total number of ECG samples in the training set (n = 259,059)

4.3.3 Lead Derivation

The derived leads (V7–V12; V3R–V6R) were generated using the calculated coefficients on the test dataset. The leads were derived using (4.2).

$$\hat{DL}_{test} = RL_{test} \cdot \beta \tag{4.2}$$

where $\hat{DL}_{test}$ was an m_{test}x10 matrix containing the estimate of the derived leads (V7–V12, V3R–V6R). RL_{test} was an m_{test}x8 matrix of recorded leads (I–II, V1–V6) taken from the test dataset. β was the 8x10 matrix of derivation coefficients as defined in (4.1). m_{test} indicates the total number of ECG samples in the test dataset (n = 28,944).

4.3.4 Verification of Derived Leads

The derivation performance was benchmarked by comparing the derived lead with that physically recorded from the BSPM. Samples from the test dataset were used. The Pearson CC and RMSE were calculated by comparing the leads previously extracted from the BSPM data (x) with the derived equivalents (y). CC is calculated as follows:

$$\rho_{(x,y)} = \frac{1}{M-1}\sum_{m=1}^{M}\left(\frac{\overline{y_m - \mu_y}}{\sigma_y}\right)\left(\frac{x_m - \mu_x}{\sigma_x}\right) \tag{4.3}$$

where $\rho_{(x,y)}$ is the CC. x and y represent the recorded leads (RL_{test}) and derived leads ($\hat{DL}_{test}$) respectively. M indicates the number of samples, μ is the mean, σ is the standard deviation and m is the sample number. The RMSE between recorded and derived lead was calculated using Equation (4.4):

$$RMSE_{(x,y)} = \sqrt{\frac{1}{M}\sum_{m=1}^{M}(x_m - y_m)^2} \tag{4.4}$$

4.3.5 Cross Validation of Lead Derivation

Recordings from datasets (i) and (ii) were split using 10-fold cross-validation. The steps outlined in Sections 4.3.2–4.3.4 were repeated for each fold. Ten sets of coefficients were produced from the training data. Ten sets of performance metrics, RMSE and CC, were produced from the test data; one set for each fold. The median of each performance metric was selected for each lead, across all folds. The final coefficients were calculated using all the samples from datasets (i) and (ii).

4.3.6 Median Beat Extraction

Data were processed to yield a median beat for each recording. Median beats were calculated over a period of approximately ten seconds. All beats detected within the ten second window were considered. For baseline (rest) ECGs median beats were calculated from data extracted from 60 seconds after the start of the record. For recordings containing balloon inflations in a coronary artery, median beats were calculated from data extracted from 60 seconds after the onset of balloon inflation. Once median beats were composed, further analysis was conducted to extract relevant amplitudes and morphology features for each lead for each subject. These features were extracted using an in-house automated algorithm and were checked for accuracy by a human observer.

4.3.7 Disease Classification

To verify the performance of derived leads in the detection of ECG changes typical of myocardial ischaemia, existing diagnostic criteria were used based on previously published material [10]. This published criteria focuses on that applicable to the conventional 12-lead ECG, but also extends to include thresholds suitable for use in supplementary leads V7–V9 and V3R–V4R. Criteria are not published for leads V10–V12 and V5R–V6R. For the purposes of this chapter, the same criteria proposed for V7–V9 and V3R–V4R for these further additional leads were used.

To reflect clinical use, the derived leads were separated into groups of 12-lead, 18-lead, and 22-lead. The 18-lead ECG contains the standard 12-lead ECG, with V7–V9 and V3R–V5R. The 22-lead ECG contains the standard 12-lead ECG with all derived leads: V7–V12, V3R–V6R. Table 4.1 summarises the diagnostic criteria applied to each lead configuration.

Following the published criteria by Thygesen et al. [10], an automated algorithm was developed to consider ST-elevation, ST-depression, and T-wave changes during the classification process. The ST-depression criteria requires greater than or equal to 50 μV depression in two or more contiguous leads. T-wave inversion of greater than 100 μV in two contiguous leads and a prominent R-wave or R/S ratio of greater than one was also considered.

Table 4.1: STEMI detection criteria for each combination of ECG leads

12-Lead	**18-Lead**	**22-Lead**
ST-elevation $\geq$ 100 μV at the J-point in two contiguous leads, except from V2–V3 where the following applies: $\geq$ 200 μV in men $\geq$ 40 years; $\geq$ 250 μV in men $<$ 40 years; or $\geq$ 150 μV in women	All 12-lead criteria, or ST-elevation $\geq$ 50 μV at the J-point in two contiguous leads of V7–V9, or $\geq$ 50 μV in leads V3R–V5R, except from males $<$ 30 years where $\geq$ 100 μV applies	All 18-lead criteria, or ST-elevation $\geq$ 50 μV at the J-point in two contiguous leads of V10–V12, or $\geq$ 50 μV in V6R, except from males $<$ 30 years where $\geq$ 100 μV applies

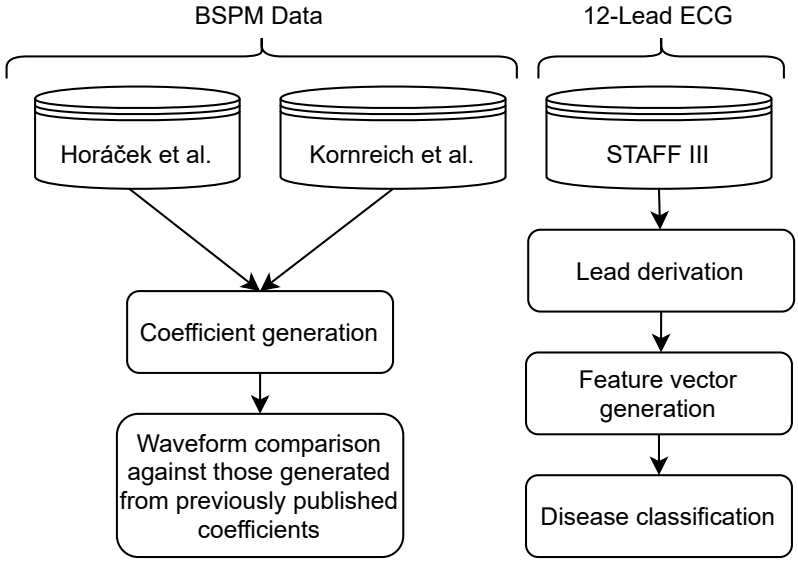

Figure 4.2: Summary of datasets and methods used

4.3.8 Summary of Methods

BSPM datasets were used in the generation of coefficients to derive the posterior and right-sided leads. The performance of the generated coefficients was compared with the performance of coefficients previously published. Twelve-lead ECG data from the STAFF III dataset were used to derive posterior and right sided leads from the generated coefficients. The 12-lead ECG and derived leads were then used to classify changes associated with MI. A summary is shown in Figure 4.2.

Table 4.2: Coefficients (β), median Correlation Coefficients (CC), and median Root Mean Square Error (RMSE) for the derivation of posterior and right-sided chest leads from the eight independent channels of the 12-lead ECG (I–II, V1–V6)

		Derived Leads									
		$V7$	$V8$	$V9$	$V10$	$V11$	$V12$	$V3R$	$V4R$	$V5R$	$V6R$
Recorded Leads	I	0.0705	0.0218	-0.1207	-0.2569	-0.3424	-0.3843	-0.1810	-0.3234	-0.3828	-0.4038
	II	-0.0628	-0.0836	-0.0769	-0.0811	-0.0825	-0.0715	0.1366	0.1728	0.1640	0.1466
	$V1$	-0.1258	-0.1535	-0.1777	-0.1699	-0.1070	-0.0419	0.8286	0.5130	0.3205	0.1814
	$V2$	-0.0386	-0.0449	-0.0250	-0.0188	-0.0219	-0.0356	-0.1901	-0.1419	-0.0922	-0.0638
	$V3$	0.0653	0.0650	0.0446	0.0479	0.0443	0.0579	0.1475	0.0986	0.0433	0.0262
	$V4$	-0.0068	0.0145	0.0059	-0.0159	-0.0247	-0.0365	-0.0697	-0.0338	-0.0001	0.0094
	$V5$	-0.2234	-0.2949	-0.2782	-0.2002	-0.1060	-0.0545	0.0243	0.0192	-0.0041	-0.0349
	$V6$	0.7304	0.6722	0.5469	0.3102	0.1274	0.0543	-0.0457	-0.0604	-0.0473	-0.0155
	CC	0.92	0.89	0.85	0.83	0.89	0.92	0.98	0.96	0.95	0.92
	$RMSE$	$57.8\mu V$	$63.1\mu V$	$56.9\mu V$	$44.9\mu V$	$35.4\mu V$	$30.9\mu V$	$36.1\mu V$	$39.0\mu V$	$34.7\mu V$	$35.3\mu V$

4.4 Results

4.4.1 Generated Coefficients

The coefficients were arranged in an 8x10 matrix as shown in Table 4.2. The rows represent the recorded leads (I–II, V1–V6) with columns representing the derived leads (V7–V12, V3R–V6R). Both CC and RMSE were calculated for each derived lead. The median values are displayed in Table 4.2.

4.4.2 Verification of Derivation Coefficients

4.4.2.1 Derived leads vs recorded leads.

Figures 3(a) and 3(b) show the CC and RMSE values for each derived chest lead respectively. The error-bar plot indicates the median value (circle) with the 25^{th} and 75^{th} interquartile ranges (whiskers). For derived posterior leads (V7–V12), the largest median CC was observed in V7 as 0.92. Median CC decreases towards V10 to the minimum value of 0.83. Median CC increases in V11 and V12. For derived right-sided chest leads (V3R–V6R), median CC decreases from the maximum of 0.98 in V3R to the minimum 0.92 in V6R. The interquartile range of CC for posterior leads varies between 0.04 in V7 to 0.13 in V10. For right-sided chest leads, the interquartile range is reduced between 0.01 in V3R to 0.07 in V6R.

For derived posterior leads, the maximum error was observed in V8 as 63 μV.

This decreased towards V12, which exhibited the minimum error value of 31 μV. For right-sided chest leads, no obvious pattern was observed for RMSE, with errors between 35 μV (V5R) to 39 μV (V4R). The interquartile range of RMSE for posterior leads varies from 18 μV in V12 to 37 μV in V8. For right-sided chest leads, the interquartile range is more uniform between 18 μV in V3R to 20 μV in V5R.

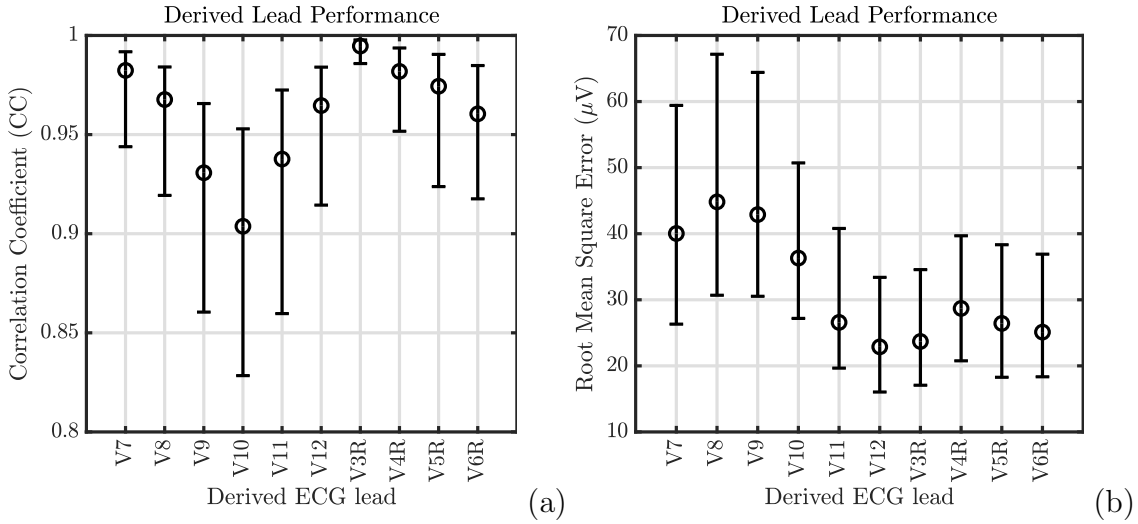

Figure 4.3: Derivation performance between recorded and derived right-sided and posterior chest leads as correlation coefficients 3(a) and root mean square error 3(b)

4.4.2.2 Comparison with previously published coefficients

Coefficients previously published from [19] were used to test the performance of the generated coefficients in the derivation of right sided and posterior leads against a known benchmark. The previously published coefficients transform the 12-lead ECG to posterior leads V7–V12 using coefficients calculated from a multiple regression model. Figure 4.4 shows a box plot comparing the coefficients introduced in this chapter with those previously published. Median (centre), interquartile ranges (box edges) and extremes (whisker) are displayed for both sets of coefficients. A Wilcoxon signed-rank test was used to indicate statistical difference between results for each lead of each subject in the test dataset. Significant improvements in CC ($p<0.05$) between previously published coefficients and the coefficients introduced in this chapter were noted in all tested leads (V7–V12).

Compared to leads derived from previously published coefficients, the median CC values were higher for all leads using coefficients introduced in this chapter.

The largest difference in median CC between previously published coefficients and those in this chapter was 0.038 in V10. The smallest difference in median CC was 0.013 in V7. The largest interquartile range difference between previously published and introduced coefficients was 0.070 (V9). The minimum difference was 0.010 in V7.

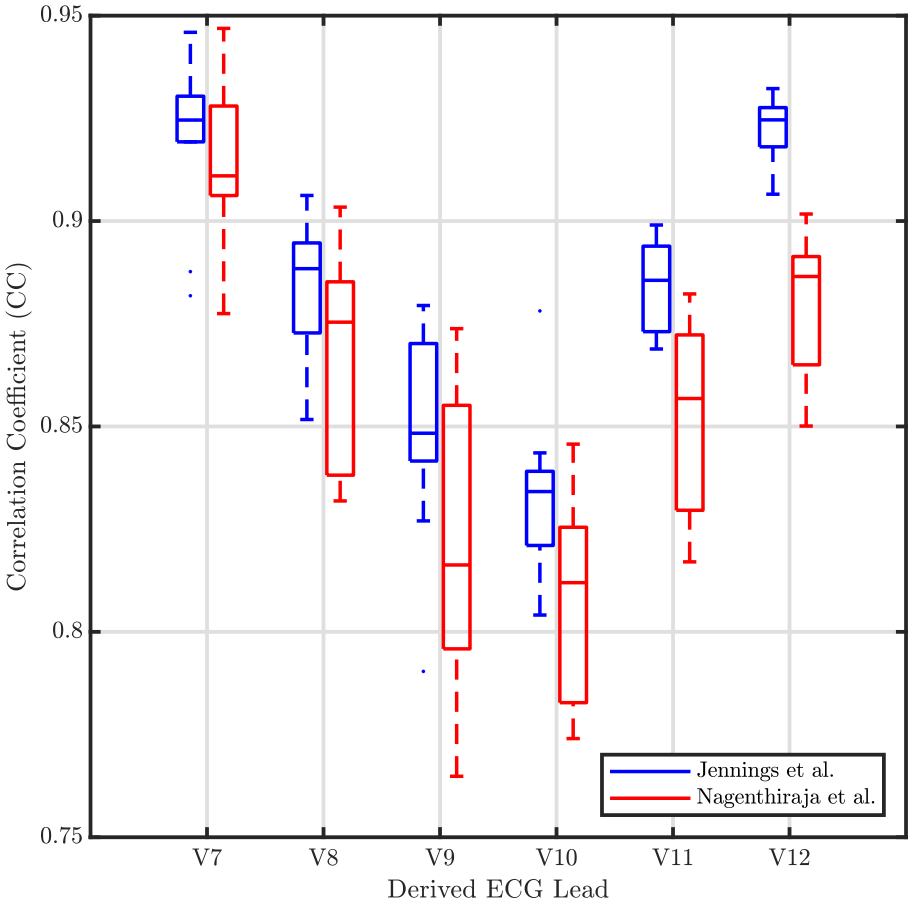

Figure 4.4: Box plot of correlation coefficients comparing previously published coefficients [19] with the those introduced in this chapter

4.4.3 Disease classification

The performance results for classification of myocardial infarction on dataset three (STAFF III) are found in Tables 4.3 and 4.4. When applying the standard diagnostic criteria [10] to the recordings used in this work, comparable results were achieved to those published in related studies [20, 21]. This provides reassurance the diagnostic algorithm is functioning as expected. The highest sensitivity (SE), Negative Predictive Value (NPV), and F1 score, was observed in the 22-lead configuration. The

Table 4.3: Classification performance of each lead derived lead configuration (rows) toward ischaemic-type ECG changes using the current AHA diagnostic criteria for AMI [10]. The highest values for each column have been marked in bold text.

Lead Configuration	SE (%)	SP (%)	PPV (%)	NPV (%)	F1 (%)
12-Lead	58.3	**96.6**	**84.8**	87.6	69.1
18-Lead	63.5	93.8	76.8	88.7	69.4
22-Lead	**64.4**	93.2	75.5	**88.9**	**69.5**

Table 4.4: Sensitivity of STEMI detection by vessel-specific occlusions in one of three coronary arteries: LAD, LCX, and RCA. The highest values for each column have been marked in bold text.

Lead Configuration	All	LAD	LCX	RCA
12-Lead	58.3	73.8	28.0	60.4
18-Lead	63.5	73.8	**36.0**	**68.8**
22-Lead	**64.4**	**76.2**	**36.0**	**68.8**

highest specificity (SP) and Positive Predictive Value (PPV) was observed in the standard 12-lead configuration. The 18-lead configuration had no extreme values.

As the number of leads increased from 12 to 22, the sensitivity increases from 58.3% to 64.4%. The opposite is true for specificity, where a decrease from 96.6% to 93.2% was observed. PPV decreases from 84.8% in the 12-lead to 75.5% in the 18-lead configuration. NPV increases from 87.6% to 88.9% as more leads are added. The F1 score follows the same pattern, with an increased score from 69.1% to 69.5%.

Table 4.4 shows the sensitivity for each lead configuration when occlusions were performed in specific coronary arteries. These include occlusions in the LAD, LCX and RCA. For comparison, the sensitivity from occlusions happening across the entire dataset were included (All).

Across all vessel-specific occlusions, sensitivity increases as the number of leads increases. The highest sensitivity observed was 76.2% in those detected by the 22-lead configuration during LAD occlusions. The lowest sensitivity was 28.0% noted from the 12-lead configuration during LCX occlusions. The largest difference in sensitivity between lead configurations was observed in RCA occlusions, with an 8.4% increase between 12-lead and 18/22-lead configurations.

A McNemar test was performed to ascertain the statistical significance between the 12-lead and the 18/22-lead diagnostic performances. There was no significance

($p > 0.05$) observed between the diagnostic performance of the 12 and 18/22-lead configurations.

4.5 Discussion

In the derivation of posterior leads (V7–V12), CC is inversely proportional to distance from the recorded chest leads (V1–V6). This may be due to the increasing distance between the electrode positions of recorded and derived lead electrode positions on the torso. CC for derived leads increases in V11–V12. The electrode locations of these leads are almost opposite the recorded leads V2–V4 across the thorax, potentially making them pseudo-inverse. This may have increased the accuracy of the derived coefficients. For derived right-sided chest leads (V3R–V6R), CC is similarly inversely proportional to distance from the recorded leads. The high CC value for V3R may be explained by the close proximity to the electrode location of V1.

RMSE does not follow the same pattern as CC. RMSE is proportional to the recorded lead amplitude. Lower potentials present in leads more distal from the heart may have made RMSE appear lower compared to leads more proximal to the heart. For example, V7 is proximal to the heart, however it has the largest CC value of the derived posterior leads, but one of the largest RMSE. In contrast, CC is amplitude independent, and used to measure how strong a relationship is between the recorded and derived leads. To compare the similarity of derived leads to their recorded counterparts, both CC and RMSE must be compared together.

In the classification of ischaemic-type ECG changes associated with myocardial infarction, the 12-lead ECG results were comparable to those previously published [20, 21]. The 12-lead ECG is generally highly specific, but insensitive to these changes. The addition of more leads in the form of the 18 or 22-lead configurations improved the sensitivity. An increased spatial resolution across the torso from the additional leads may allow for infarctions in the posterior of the heart to be detected, where they would have been previously missed by the 12-lead ECG. This is evident in Table 4.4, where the sensitivities of LCX and RCA occlusions were increased by 8.0% and 8.4% between the 12 and 18/22-lead configurations respectively.

Additional derived leads decreased the specificity of STEMI detection. The recommended criteria requires 50 μV of ST-elevation across two contiguous leads in either the posterior or right-sided chest leads. Compared to the 12-lead criteria of 100–200 μV ST-elevation in the chest leads, this is relatively low-amplitude. More false-positives may have resulted from a combination of prior MI and the low amplitude ST-elevation criteria in additional leads.

The median RMSE for each derived lead varies between 30.9 μV (V12) to 63.1 μV (V8). Given the criteria calls for 50 μV of ST-elevation in the derived leads, this may result in many false classifications within leads with larger derivation errors. This is evident when comparing the 12 and 18-lead configurations together. The 18 lead adds V7–V9 and V3R–V5R to the 12-lead ECG. V7–V9 possess the three highest RMSE values among the derived leads. The reduction in specificity may be due to derivation errors causing the ST-segment to exceed the 50 μV STEMI classification criteria. Notwithstanding variations in other performance metrics, the F1 score increases linearly as the number of derived leads increases.

There were recordings involving participants with prior MI in the dataset (n=167). When recordings involving patients with prior MI are excluded, both the specificity of STEMI detection in the 12-lead and 18/22-lead configurations increase to 94.40% and 91.8% respectively. In a clinical setting, the history of prior MI would be investigated by the clinician to inform their diagnosis. This was not considered in this chapter, as only the ST-segment and T-wave criteria were employed.

When splitting recordings with inflations into their respective vessels, the maximum sensitivity values increased to 76.2% in the 22-lead configuration for LAD occlusions. The 12-lead configuration was less sensitive than the 22-lead ECG across all coronary arteries, with a maximum sensitivity of 73.8% during LAD occlusion. MI detection in the LCX artery was poor in comparison to others, with 28% in the 12-lead configuration. However, MI detection saw the greatest improvement between 12 and 18/22-lead configurations during LCX occlusion, with an 8% increase in sensitivity. The 18-lead adds V7–V9 across the left torso. This may have improved the resolution of the ECG to detect occlusions in the LCX compared with the precordial chest leads V5 and V6. RCA occlusions were detected with higher sensitivity in the 18/22-lead configurations, increasing by 8.4% compared to the 12-lead ECG.

Similarly to the LCX occlusions, the sensitivity may have been improved by the addition of V3R–V5R in the 18-lead ECG. This may increase the resolution of MI detection towards the right side of the heart, where RCA occlusions may occur.

To compare with those coefficients previously published, described in Section 4.4.2.2, the 18-lead ECG was also derived for each subject of dataset (iii). The MI classification performances were 64.0% (SE), 96.0% (SP) and 70.9% (F1). The sensitivity and F1 score was higher using these coefficients, however the specificity was lower. Additionally, these results were not statistically significant compared with the 12-lead ECG classification.

4.6 Limitations

Deriving leads instead of recording them adds error into the derived leads. As such, the 18 and 22-lead configurations that contain derived leads may not be representative of a recorded signal. This may affect ST-segment amplitudes, particularly those with electrode locations further from recorded leads such as leads V6R and V12.

In the pre-processing step, discussed in Section 4.3.6, median beats were produced for each lead of the 12-lead ECG. This may have introduced both amplitude and phase errors during the conversion due to misalignment of R-waves, differences in beat length and noise. Additionally, the J-point annotations, although manually reviewed, may not be entirely accurate. This may introduce erroneous J-point amplitudes to the STEMI classifier, resulting in a false positive or false negative.

ST-elevation criteria for the detection of ischaemic-type ECG changes in derived leads were not available for leads V10–V12 and V5R–V6R. Instead, the criteria were assumed by extending the criteria for their neighbouring leads respectively. This is not currently clinically accepted, potentially affecting the validity of the 22-lead ECG observations. Additionally, Q-wave criteria were not employed during this chapter. Abnormal Q-waves in posterior leads can be a predictor of MI [22]. This may has reduced the overall performance of the derived leads.

4.7 Conclusion

In this chapter, coefficients were introduced toward the derivation of posterior and right-sided chest leads from the 12-lead ECG with an improvement in derivation accuracy compared to previously published coefficients. Additionally, it has been shown that derived posterior and right sided chest leads are capable of detecting ischaemic-type ECG changes associated with myocardial infarction. The addition of derived leads was shown to increase the sensitivity and F1 score of STEMI detection, however, these results were not statistically significant.

References

[1] S. Wada, N. Ito, H. Fukunaga, Y. Tsuda, H. Takahashi, K. Hatori, N. Saito, H. Sasaki, T. Murase, K. Nagao, and S. Sasaguri, "Clinical Significance of Synthesized 18lead Electrocardiography for ST Elevation Myocardial Infarction," *Circulation*, vol. 136, 2017.

[2] T. Ashida, S. Tani, K. Nagao, T. Yagi, N. Matsumoto, and A. Hirayama, "Usefulness of synthesized 18-lead electrocardiography in the diagnosis of STEMI-TOC and title pages," *American Journal of Emergency Medicine*, vol. 35, no. 3, pp. 448–457, 2017.

[3] D. Wei, "Derived electrocardiograms on the posterior leads from the 12-lead system: Method and evaluation," in *Annual International Conference of the IEEE Engineering in Medicine and Biology - Proceedings*, vol. 1, pp. 74–77, 2003.

[4] A. Tamura, K. Torigoe, Y. Goto, S. Naono, K. Shinozaki, H. Zaizen, and N. Takahashi, "Reliability of ST-segment shifts in the synthesized V3R-V5R leads after coronary balloon inflations during percutaneous coronary intervention," *American Journal of Cardiology*, vol. 114, pp. 1187–1191, 10 2014.

[5] T. Li, K. Shinozaki, M. Brave, T. Yagi, and L. B. Becker, "Agreement between actual and synthesized right-sided and posterior electrocardiographic leads in identifying ischemia," *American Journal of Emergency Medicine*, vol. 38, pp. 1346–1351, 7 2020.

[6] K. Shimojo, K. Takagi, Y. Morita, Y. Kanzaki, H. Nagai, N. Watanabe, N. Yoshioka, R. Yamauchi, S. Komeyama, H. Sugiyama, T. Imaoka, G. Sakamoto, T. Ohi, H. Goto, H. Tsuboi, and I. Morishima, "Prevalence and prognosis of isolated posterior ST-segment elevation acute myocardial infarction using synthesized-V7–9 lead," *Cardiovascular Intervention and Therapeutics*, pp. 1–11, 9 2021.

[7] H. Shemirani and E. Nayeri-Torshizi, "Electrocardiographic characteristics of posterior myocardial infarction in comparison to angiographic findings," *ARYA Atherosclerosis*, vol. 11, no. 1, pp. 30–35, 2015.

[8] M. Shimizu, S. Cho, K. Hara, M. Ohmori, T. Kaneda, R. Tateishi, Y. Yamakami, H. Shimada, T. Manno, A. Isshiki, S. Kimura, H. Fujii, M. Suzuki, M. Nishizaki, and T. Sasano, "Diagnostic performance of 18-leads electrocardiography to distinguish takotsubo syndrome and acute anterior myocardial infarction," *European Heart Journal*, vol. 41, 11 2020.

[9] D. Schreck, M. Viscito, and C. Brotea, "The derived N-Lead electrocardiogram," *Annals of Emergency Medicine*, vol. 44, pp. S73–S74, 10 2004.

[10] K. Thygesen, J. S. Alpert, A. S. Jaffe, B. R. Chaitman, J. J. Bax, D. A. Morrow, and H. D. White, "Fourth universal definition of myocardial infarction (2018)," *European Heart Journal*, vol. 24, pp. 107–138, 8 2019.

[11] N. Eppe, R. Levy, M. Vandoorslaert, B. Kerzmann, J. de Castro, T. Sottiaux, and J. Adam, "Synthesized 18-lead electrocardiogram as routine myocardial ischemia detection in an emergency department: a preliminary evaluation in Europe," *Critical Care*, vol. 19, p. P161, 3 2015.

[12] B. M. Horacek, J. W. Warren, C. J. Penney, R. S. MacLeod, L. M. Title, M. J. Gardner, and C. L. Feldman, "Optimal electrocardiographic leads for detecting acute myocardial ischemia," *Journal of Electrocardiology*, vol. 34, pp. 97–111, 12 2001.

[13] F. Kornreich, T. J. Montague, and P. M. Rautaharju, "Body surface potential mapping of ST segment changes in acute myocardial infarction: Implications for ECG enrollment criteria for thrombolytic therapy," *Circulation*, vol. 87, no. 3, pp. 773–782, 1993.

[14] B. J. Schijvenaars, J. A. Kors, G. van Herpen, F. Kornreich, and J. van Bemmel, "Interpolation of body surface potential maps," *Journal of Electrocardiology*, vol. 28, pp. 104–109, 1 1995.

[15] J. Pettersson, E. Carro, L. Edenbrandt, C. Maynard, O. Pahlm, M. Ringborn, L. Sörnmo, S. G. Warren, and G. S. Wagner, "Spatial, individual, and temporal variation of the high-frequency QRS amplitudes in the 12 standard electrocardiographic leads," *American Heart Journal*, vol. 139, pp. 352–358, 2 2000.

[16] J. P. Martínez, O. Pahlm, M. Ringborn, S. Warren, P. Laguna, and L. Sörnmo, "The STAFF III Database: ECGs recorded during acutely induced myocardial ischemia," in *Computing in Cardiology*, vol. 44, pp. 1–4, 2017.

[17] A. L. Goldberger, L. A. Amaral, L. Glass, J. M. Hausdorff, P. C. Ivanov, R. G. Mark, J. E. Mietus, G. B. Moody, C. K. Peng, and H. E. Stanley, "PhysioBank, PhysioToolkit, and PhysioNet: components of a new research resource for complex physiologic signals.," *Circulation*, vol. 101, no. 23, 2000.

[18] S. G. Warren and G. S. Wagner, "The STAFF studies of the first 5 minutes of percutaneous coronary angioplasty balloon occlusion in man," in *Journal of Electrocardiology*, vol. 47, pp. 402–407, Churchill Livingstone Inc., 7 2014.

[19] Nagenthiraja K, Andersen M P, and Struijk J, *Linear model for deriving the posterior ECG leads V7-V12 in healthy subjects - Project Library, Aalborg University.* PhD thesis, Aalborg Universitet, Aalborg, 2008.

[20] J. J. Wang, O. Pahlm, J. W. Warren, J. L. Sapp, and B. M. Horáček, "Criteria for ECG detection of acute myocardial ischemia: Sensitivity versus specificity," *Journal of Electrocardiology*, vol. 51, no. 6, pp. S12–S17, 2018.

[21] U. Pahlm, O. Pahlm, and G. S. Wagner, "The 24-lead ECG display for enhanced recognition of STEMI-equivalent patterns in the 12-lead ECG," *Journal of Electrocardiology*, vol. 47, pp. 425–429, 7 2014.

[22] Y. Igarashi, T. Chikamori, S. Hida, K. Hirose, T. Saito, and A. Yamashina, "Usefulness of posterior leads derived from the 18-lead electrocardiogram in the diagnosis of posterior myocardial infarction," *European Heart Journal*, vol. 38, 8 2017.

Chapter 5

Utilising Short-spaced Leads in the Detection of Ischaemic-type ECG Changes

---

5.1 Abstract

The 12-lead ECG is the most prevalent tool in clinical use to detect acute cardiac syndromes. In particular, myocardial infarction and related ischaemic disorders. This lead system is inconvenient for ambulatory use, especially when detecting paroxysmal conditions. A patch-based lead system is more convenient for these use-cases. There is a lack of such lead systems that are specific to ST-segment monitoring, so one must be derived. In particular, the use of a SSL patch with lead spacing of 100 mm or less would be sufficiently comfortable while allowing the wearer to undertake ambulatory tasks. In this chapter, a SSL patch-based lead system suitable for ST-segment monitoring will be introduced and evaluated.

This chapter is broken into three parts. Part one focuses on the selection of a patch-based SSL system from BSPM data showing ischaemic-type ECG changes. Part two focuses on the derivation of the SSL system from the 12-lead ECG via linear interpolation, while producing transform coefficients. The final section uses both machine learning techniques and ST-segment based criteria to classify ST-segment changes associated with AMI in the absence of specific diagnostic criteria

for SSLs.

The SSL selected was below 100 mm in distance between electrodes. It is located between an electrode between Dalhousie nodes 173 and 254). A spatially orthogonal lead was also introduced between Dalhousie nodes 212 and 234. The derivation coefficients between 12-lead ECG and the SSL patch ST-lead and spatially orthogonal lead had a CC or 0.969 and 0.987 respectively. The RMSE was 18.6 μV for the ST-lead and 15.5 μV for the orthogonal lead. In the classification of ischaemic-type ECG changes in the SSL patch, the ST lead had the highest F1 score of 80.4% using a Naive Bayes classifier. The sensitivity and specificity were 86.7% and 80.4% respectively.

In this chapter, SSL patch suited to the classification of ischaemic-type ST-segment changes associated with AMI has been introduced. Transform coefficients were generated to derive this lead system from the 12-lead ECG. Additionally, it was shown a SSL patch to be capable of classifying myocardial ischaemic-type ECG changes.

The code for this chapter is freely available on GitHub. [1].

5.2 Introduction

Current diagnostic criteria recommends that decision thresholds are met in at least two contiguous leads in the diagnosis of MI [2]. This makes the 12-lead ECG highly specific to ischaemic-type changes. However, the 12-lead ECG is inconvenient for ambulatory use, or when recording from body positions other than supine. Additionally, a 12-lead recording is usually between three to ten seconds in duration. This may not detect certain paroxysmal conditions such as atrial fibrillation or unstable angina [3]. Additionally, the placement of electrodes across the torso is inconvenient compared to other systems designed for longer term monitoring that use fewer electrodes. A patch-based lead system is more convenient compared to the 12-lead ECG, with the capability for ambulatory monitoring. The development of new patch-based SSL ECG systems to detect cardiac defects has increased dramatically, with a lack of academic literature investigating their performance [4]. Novel techniques of ambulatory monitoring are capable of storing and transmitting ECG

data for diagnostic purposes [5]. Furthermore, a patch-based lead system has been shown to be effective in the detection of cardiac arrhythmia [6, 7], including those that display intermittent ECG changes, such as ventricular tachycardia [8]. Existing patch-based lead systems such as the Zio XT and BradyDx CAM have shown comparable performance to the standard ambulatory Holter monitors [9], but with a longer recording period than 24 hours [10]. However, there are a lack of patch-based ECG systems sensitive to ST-segment changes [11]. Many focus on the reproduction of the 12-lead ECG for further analysis [12, 13], or focus on the diagnosis of other cardiac abnormalities, such as AF [14].

Deviation from 12-lead ECG configurations has been shown to reduce the diagnostic accuracy of algorithms relying on current ST amplitude criteria [15, 12]. The Zio® XT is an example of an existing SSL patch-based ECG monitor designed to challenge existing diagnostic methods, particularly with longer recording duration and automated arrhythmia detection [16]. Further studies have discussed novel VSLs to detect STEMI [17].

Machine learning might be an effective method for detecting STEMI when trained using ECG data, particularly when applied to pre-hospital admission [18]. Machine learning has allowed more diverse methods of classifying cardiac abnormalities than the 12-lead ECG [19]. Patch-based lead systems have been introduced for cardiac arrhythmia monitoring, however, there has been less emphasis on the development and reporting of systems designed for ischaemic heart disease [20]. Such devices are prone to placement errors, however, machine learning can detect misplacement [21]. There are currently no agreed criteria for the diagnosis of ischaemia using patch-based devices; potentially due to the lack of clinical uptake in patch-based monitoring devices. This means criteria for the diagnosis of ECG changes associated with MI must be assumed from existing lead systems, such as the 12-lead ECG.

The first aim is to investigate a new SSL as a means to detect ST-Elevation (STE) constrained to 100 mm between electrodes suitable for patch-based continuous monitoring. Secondly, the introduction and evaluation of coefficients for the derivation of the ST-sensitive SSL patch. Thirdly, assessing the performance of the SSL-based system using both machine learning and traditional ST-based methods

in the classification of STEMI.

5.3 Method

5.3.1 Short Spaced Lead Selection

The proposed method uses BSPMs to investigate lead placement in the detection of STE for SSLs.

5.3.1.1 Data

The data are previously described in Section 3.1.1 [22, 23] and include recordings (n = 88) from 44 subjects undergoing elective PTCA. Electrocardiograms during PBI (n = 44) were assumed to represent changes compatible with those observed in patients suffering ischaemic episodes, while those with no balloon inflation (n = 44) were assumed to represent normal baseline recordings.

5.3.1.2 Algorithm

The difference between non-ischaemic (baseline) and ischaemic (peak-balloon inflation) recordings formed the basis of selecting the SSL. Bipolar leads with the largest difference between these two scenarios can be sensitive to ECG changes associated with MI. In particular, amplitude changes in the ST-segment were used to select the SSL.

MATLAB 2021b was used to calculate all possible lead combinations (n = 123904) from all possible pairs of the 352 nodes. The signal amplitude was extracted from 40 ms after the J-point (J + 40 ms) to give a representative measure of ST-segment value. The difference at J + 40 ms between baseline and PBI was calculated. This process was repeated for all leads created previously. Each lead was sorted in descending order of absolute ST-segment change (ΔST). This process was repeated for each subject (n = 44), where the sort-index given to a lead for the previous subject is added to the sort-index of the next subject. The lowest sort-index value denotes the lead with the highest ΔST across all subjects. A generic 3D torso (Dalhousie torso) described in a previous study [22] was used to calculate

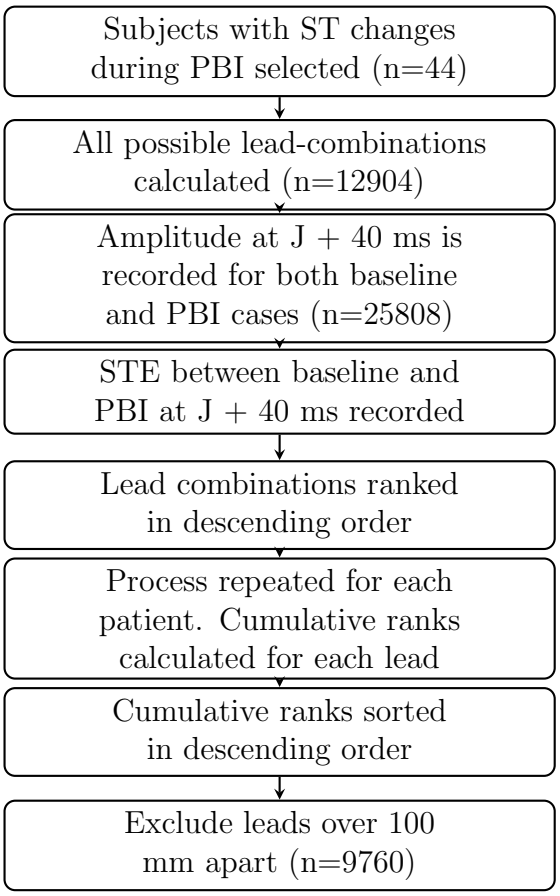

Figure 5.1: Sorting algorithm

the distance between electrodes for each lead. Leads with electrode spacing greater than 100 mm apart were excluded. The SSL was selected as the lead with the lowest cumulative sort-index from remaining leads (n = 9760). Figure 5.1 shows this process.

5.3.2 Short Spaced Lead Derivation

5.3.2.1 Data

The dataset used in this section has been described previously in Section 3.1.2 [24, 25]. The data were comprised of recordings (n = 734) from patients experiencing MI (n = 271), LVH (n = 237), and healthy controls (n = 226). The data were recorded using a BSPM of 117 unipolar thoracic leads, recorded with respect to the WCT. Distal limb leads were also recorded. Each recording was a single beat in length, sampled at 500 Hz. These were expanded to the 352-node Dalhousie torso [26, 27] using Laplacian interpolation. The data were split at random to 80%

training (n = 588) and 20% test (n = 146).

5.3.2.2 Coefficient Derivation

The eight independent channels of the 12-lead ECG were extracted from each recording (I–II, V1–V6). The two bipolar leads of the SSL patch were also extracted: an ST-sensitive lead (SSL_{ST}) and a spatially orthogonal lead (SSL_{orth}). The positions of these leads were decided based on Section 5.3.1.2. Specifically, the SSL_{ST} electrodes are at nodes 173 and 254 while SSL_{orth} is located between nodes 234 and 212 on the Dalhousie torso.

Both recorded leads (12-lead) and leads to be derived (SSL patch) were used in generating the coefficients. All training set recordings (n = 588) were concatenated prior to computation. Linear regression was used to calculate transform coefficients as shown in Equation 5.1:

$$\beta = \left[\left(RL_{train}^{T} \cdot RL_{train} \right)^{-1} RL_{train}^{T} \right] \cdot DL_{train} \tag{5.1}$$

where β represented an 8x2 matrix of transform coefficients. RL_{train} and DL_{train} were matrices of m_{train}x8 and m_{train}x2 respectively. They represented recorded leads (I–II, V1–V6) and leads to be derived from the training dataset (n = 588). m_{train} was the total number of samples in the training dataset (n = 171,726).

5.3.3 Lead Derivation

Using the coefficients derived in section 5.3.2.2, the leads to be derived can be calculated from the test dataset (n = 146). These were calculated using Equation 5.2:

$$\hat{DL}_{test} = RL_{test} \cdot \beta \tag{5.2}$$

where $\hat{DL}_{test}$ was an m_{test}x2 matrix containing an estimate of the derived leads: SSL_{ST}, and SSL_{orth}. RL_{test} was an m_{test}x8 matrix of recorded leads (I–II, V1–V6) taken from the test dataset (n = 147). β was the 8x2 matrix of derivation coefficients as defined in Equation (4.1). m_{test} indicates the total number of ECG samples in the test set (n=42,802)

5.3.3.1 Derivation Performance

Recorded leads from the test dataset were used to benchmark how accurately the leads were derived. Pearson CC and RMSE were calculated by comparing the recorded leads (x), previously extracted from the BSPM data, with the derived equivalents (y). CC was calculated as shown in Equation 5.3:

$$\rho_{(x,y)} = \frac{1}{M-1} \sum_{m=1}^{M} \left(\frac{\overline{y_m - \mu_y}}{\sigma_y} \right) \left(\frac{x_m - \mu_x}{\sigma_x} \right) \tag{5.3}$$

where $\rho_{(x,y)}$ is the CC. x and y represent the recorded leads (RL_{test}) and derived leads ($\hat{DL}_{test}$) respectively. M indicates the number of samples, μ is the mean, σ is the standard deviation and m is the sample number. Similarly, the RMSE between recorded and derived leads was calculated using Equation (5.4):

$$RMSE_{(x,y)} = \sqrt{\frac{1}{M} \sum_{m=1}^{M} (x_m - y_m)^2} \tag{5.4}$$

5.3.4 Ischaemia Classification - Machine Learning

Two methods of classifying ECG changes associated with MI were used. The first was a machine learning approach, using subjects (n = 44) from the Horacek et al. dataset [28] described in Section 3.1.1.

5.3.4.1 Feature Extraction

The amplitudes at the J-point for each generated lead of the patch-based lead system. This comprised the feature set. The SSL_{ST} and SSL_{orth} identified in Section 5.3.1.2 formed the basis of the patch. To increase spatial resolution, all possible bipolar leads within 100 mm of the patch were added. A total of six bipolar SSLs were used: ST-sensitive (SSL_{ST}), spatially orthogonal (SSL_{orth}) and four complementary leads (SSL_{3-6}).

The amplitude at the J-point was extracted as the feature for each SSL based on its importance in standard STEMI criteria [2]. This resulted in six features for each recording, one for each SSL. Recordings at rest were annotated as healthy (false), whereas PBI were annotated as STEMI (true).

5.3.4.2 STEMI Detection

Given that no criteria exist for the new leads, a machine-learning based approach was employed to assess the performance of the extracted J-points at distinguishing between ECGs recorded at rest and those indicative of MI. The standard STEMI detection criteria were also used, as applied to the standard 12-lead ECG that were extracted for the same patient. 12-lead ECG channels were extracted from each recording at both rest and PBI. Currently accepted STEMI criteria were employed based on J-point amplitudes, age and sex [2]. The criteria used did not include new Q-wave, ST-slope or T-wave changes.

Three classifiers were used to detect STEMI. The C4.5 (J48) decision tree [29], MLP and Naive Bayes [30] classifiers. These were performed using the WEKA 3.8.4 software. Three different combinations of SSLs were used for each classifier. The first involved all SSLs (n=6). The second omitted the four complementary SSLs, leaving only the SSL_{ST} and SSL_{orth} leads. The third involved only SSL_{ST}. Ten-fold cross validation was used in generating the respective models.

5.3.5 Ischaemia Classification - ST-Amplitudes

The second method of detecting ischaemia in the patch system was based on the amplitude of the ST-segment. The STAFF III dataset was used for this method, previously described in Section 3.1.3. It comprised of recordings (n = 467) at baseline (n = 352) and PBI in the LAD (n = 42), LCX (n = 25), and RCA (n = 48). This dataset was chosen since it was not involved in the selection of the patch, or the generation of derivation coefficients. It is an independent test set.

5.3.5.1 Feature Extraction and Classification

The eight independent channels of the 12-lead ECG were extracted. The leads of the patch system were derived from the 12-lead ECG using the coefficients and methods described in Section 5.3.2.2. The amplitude of SSL_{ST} and SSL_{orth} at the J-point were extracted as features for MI classification. The diagnostic criteria for patch leads were an ST-elevation or depression of greater than a variable threshold. This threshold was in 50 μV increments from 50–300 μV.

$$f(x, y, z) = \begin{cases} \text{True} & \text{if } |x| > z \wedge |y| > z \\ \text{False} & \text{otherwise} \end{cases} \tag{5.5}$$

where x and y are the amplitudes of SSL_{ST} and SSL_{orth} at the J-point. Either of these values must exceed the variable threshold, z, to class as potential MI. A recording with an inflation present in any coronary artery was assumed to be indicative of MI.

5.4 Results

5.4.1 Short Spaced Lead Selection

5.4.1.1 Position of selected lead

The selected SSL which reflected the highest ST-segment change within the physical 100 mm constraint was identified as being on the anterior torso between a region in the left precordium and a more inferior abdominal region. Specifically, according to the node numbering on the Dalhousie torso, the SSL was positioned between an electrode superior to V3 (Dalhousie torso node 173) and an electrode left of the sagittal axis between the epigastric and umbilical abdominal regions (Dalhousie torso node 254). Figure 5.2 illustrates the position of the SSL with respect to the the six precordial leads of the 12-lead ECG. The BSPM shows the median observed signal amplitude during PBI at J + 40 ms for subjects undergoing LAD occlusion PTCA (n=14).

5.4.1.2 ST segment changes on selected lead

The two leads comprising the patch-based lead system, SSL_{ST} and SSL_{orth}, are plotted in Figure 5.3. The recording shown was taken from a subject undergoing PBI in the LAD coronary artery. SSL_{ST} shows an ST-segment difference between baseline and PBI of 275 μV. SSL_{orth} does not show the same difference at the ST-segment, with little difference between the two scenarios.

Figure 5.4 shows the absolute change in ST-elevation (ΔST) across all subjects as median, 25th and 75th percentiles. The SSL has a median ΔST of 125 μV with

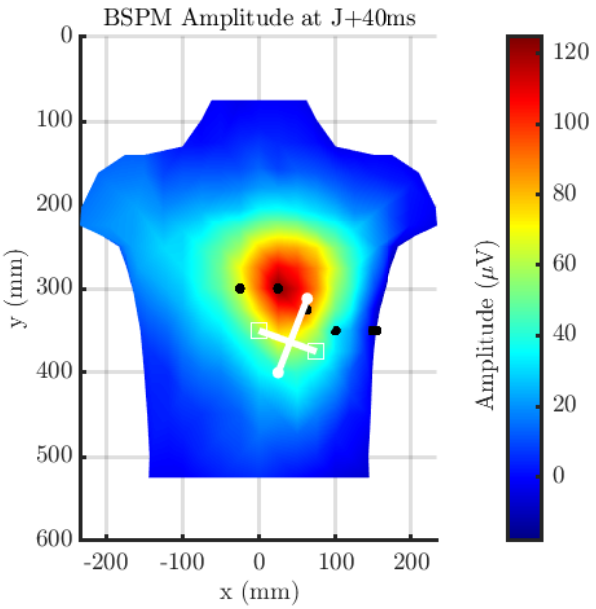

Figure 5.2: Location of short spaced leads SSL_{ST} (white circles) and SSL_{orth} (white squares). Torso-wide median amplitude 40 ms after the J-point in patients with LAD occlusion. Precordial chest leads (V1–V6) plotted as black circles.

a maximum value of 277 μV. This performs comparatively with the precordial lead V2. VSLs from a previous study [28] are used in comparison with the SSL and 12-lead ECG for a critical analysis. The median ΔST for VSLs are as follows: LAD = 156 μV, LCX = 162 μV, RCA = 187 μV.

5.4.1.3 LAD occlusion

To further analyse the SSL performance, it is necessary to look at specific vessel occlusions. In this example, only subjects with LAD occlusion are considered with the same method as described in Section 5.3.1.2 (n=14). The observed median ΔST of 134 μV in the SSL, comparable with the precordial leads V2 and V3 both showing 137 μV ΔST. This is 36% lower than the relevant VSL. The maximum SSL ΔST recorded across all subjects was during LAD occlusion at 277 μV. Figure 5.5 shows the performance of each lead at J + 40ms across LAD PTCA subjects.

5.4.1.4 LCX occlusion

In subjects undergoing PTCA in the LCX coronary artery (n=15), a ΔST median of 65 μV was observed in the SSL. The SSL performs comparatively to V3, with a median of 58 μV. Figure 5.6 illustrates the SSL characteristics. This is the lowest

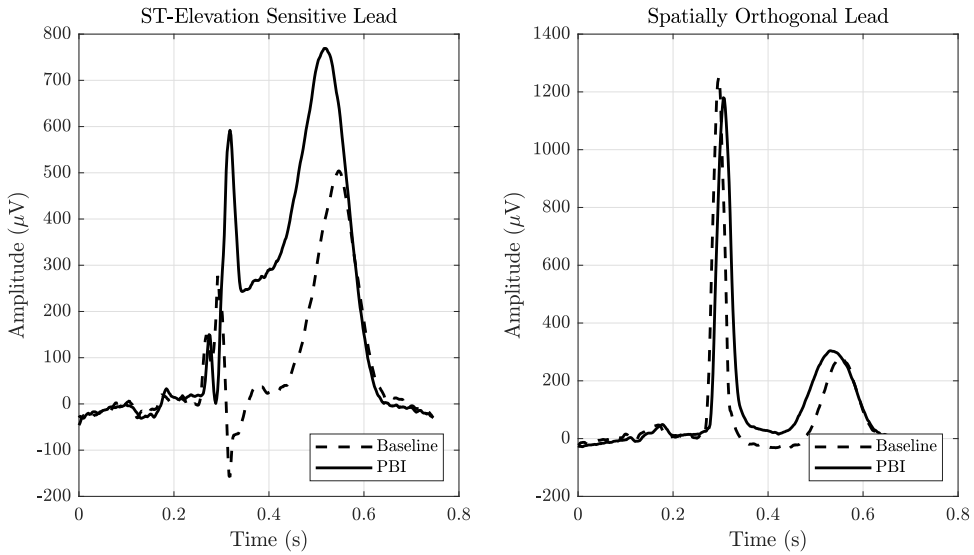

Figure 5.3: SSL_{ST} and SSL_{orth} before inflation (baseline) and during inflation PBI in the LAD coronary artery.

ΔST value observed across the three coronary arteries at 63% below the VSL. The maximum ΔST in the SSL was 166 μV.

5.4.1.5 RCA occlusion

ΔST observed in RCA PTCA subjects (n=15) possess the highest overall values. The SSL shows a median ΔST of 166 μV, 28% below the relevant VSL. The SSL exhibits similar ST-segment changes to aVF which has a median ΔST of 151 μV across subjects. Figure 5.7 shows the SSL performance. The maximum ΔST in the SSL was 257 μV.

5.4.2 Short Spaced Lead Derivation

The coefficients calculated in section 5.3.2.2 (β) are shown in Table 5.1. They are arranged in an 8x2 matrix where the rows represent the recorded leads (I–II, V1–V6), and the columns represent the leads to be derived of the SSL patch (SSL_{ST}, SSL_{orth}). CC and RMSE for each lead are included at the bottom: For the ST-sensitive SSL, SSL_{ST}, the CC was lowest with 0.97. It had the highest RMSE with 18.6 μV. The spatially orthogonal lead, SSL_{orth}, had a higher CC of 0.9872, and a lower RMSE of 15.5 μV

Figure 5.8 shows the recorded leads (RL_{test}) and the derived leads ($\hat{DL}_{test}$) for

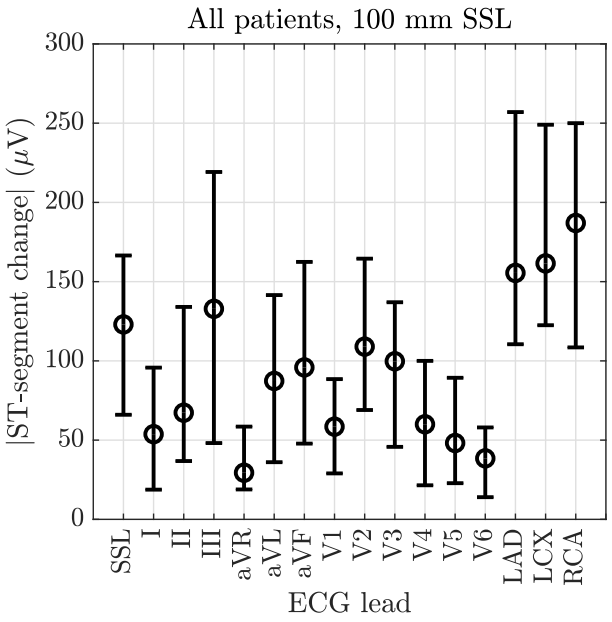

Figure 5.4: ΔST across all leads, all subjects (n=44)

one recording, as performed in section 5.3.3. The recording was taken from a patient with MI. The leads to be derived are shown with a dashed line, and derived leads are shown as a solid line.

5.4.3 Ischaemia Classification

5.4.3.1 Machine Learning

The sensitivity (Se), specificity (Sp) and F1 score (F1) were calculated for each SSL combination and classifier. Table 5.2 shows the results. The results are also visualised in Figure 5.9. The highest overall performance was using only SSL_{ST} with a Naive Bayes algorithm. The sensitivity and specificity were 86.7% and 71.1% respectively.

The chosen classifiers generally exhibited greater sensitivity than specificity in their default configurations. It should be noted that these classifiers do not offer the facility to easily adjust thresholds towards either sensitivity or specificity. Further work is required to facilitate this or a ROC based approach. The C4.5 and Naive Bayes classifiers had similar performances across lead combinations. Overall, sensitivity and specificity were higher when only SSL_{ST} was used. The MLP is an exception to this. Performance was considerably reduced when a single SSL was used with MLP. This classifier is a feed-forward classifier that relies on back-propagation.

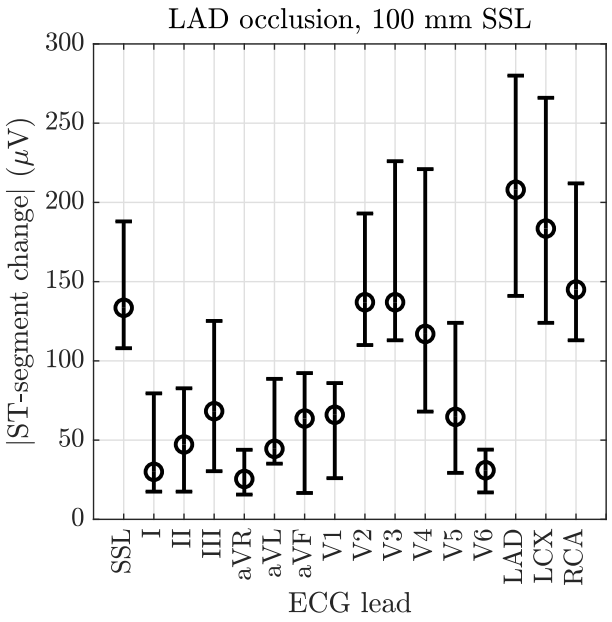

Figure 5.5: ΔST deviation, LAD occlusions only (n=14)

A lack of input features may negatively affect its performance [31].

The 12-lead ECG classifier based on current diagnostic criteria had a sensitivity and specificity of 62% and 93%, respectively. This is comparable to the known 12-lead diagnostic capability [32]. Unlike the SSL-based classifiers, the specificity is higher than sensitivity. The 12-lead ECG has a higher spatial resolution than an SSL patch which may increase specificity to ischaemic-type ECG changes.

Compared to the 12-lead ECG, the SSL_{ST}-based Naive Bayes classifier was more sensitive. The bipolar lead of the SSL is across the highest amplitude gradient on the torso during the ST-segment. This will emphasise J-point changes in this lead during ischaemia. The SSL is unspecific in comparison. There is a lower distance between electrodes compared to the 12-lead ECG. The 12-lead criteria used age, sex and J-point changes, however, the SSLs only used J-point changes.

Electrode placement errors affect the diagnostic capability of lead systems. An SSL patch may be affected more than the 12-lead ECG by misplacement. This may reduce the sensitivity of STEMI detection.

5.4.3.2 Variable ST-Amplitude

Table 5.3 shows the classification performance of derived patch-based lead system. As the elevation or depression ST criteria increase, the sensitivity and PPV decrease.

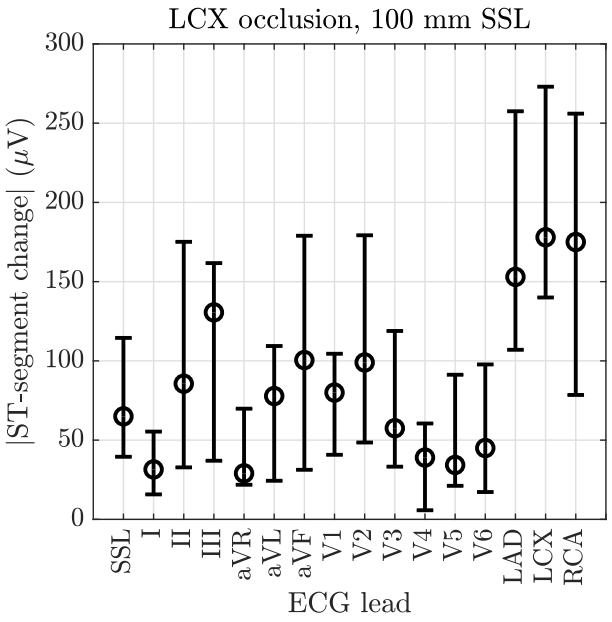

Figure 5.6: ΔST deviation, LCX occlusions only (n=15)

Contrarily, the specificity and NPV decrease. The F1 score varies, with 100 μV of ST deviation obtaining the same score as the 12-lead ECG.

The affect of vessel-specific occlusions on the sensitivity are shown in Table 5.4. The highest sensitivity for each vessel was recorded in the patch lead system with 50 μV elevation or depression. This decreases as the ST threshold increases, with the lowest sensitivity recorded with a threshold of 300 μV.

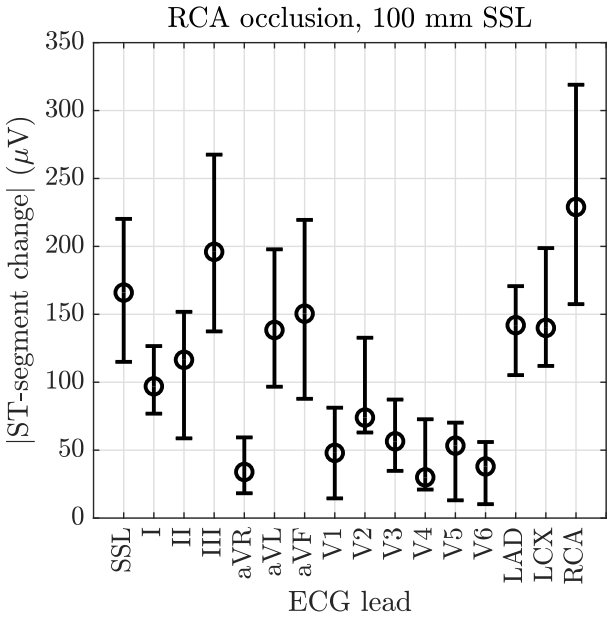

Figure 5.7: ΔST deviation, RCA occlusions only (n=15)

Table 5.1: Derived lead coefficients (β) and their calculated performance as CC and RMSE

		Derived Leads	
		SSL_{ST}	SSL_{orth}
Recorded Leads	I	0.4479	-0.1503
	II	-0.7107	-0.0464
	$V1$	-0.4740	-0.8052
	$V2$	0.4327	-0.0662
	$V3$	0.2623	0.0801
	$V4$	-0.0453	0.6295
	$V5$	0.1277	-0.0769
	$V6$	0.0324	-0.0311
	CC	0.9695	0.9872
	$RMSE$	$18.6\mu V$	$15.5\mu V$

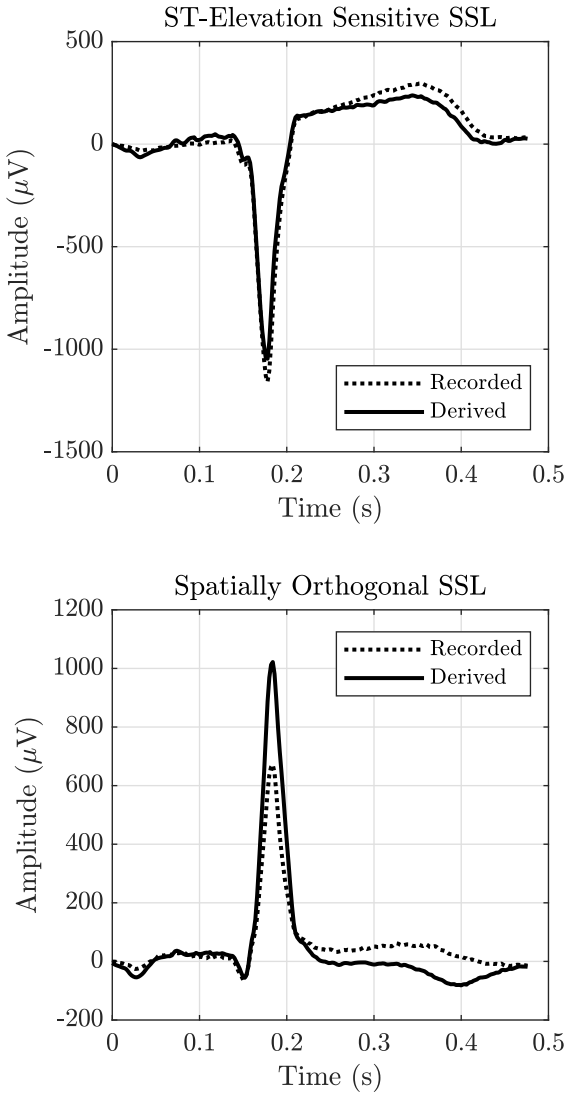

Figure 5.8: Recorded leads (RL_{test}) and derived leads ($\hat{DL}_{test}$) for both the ST-elevation sensitive SSL (SSL_{ST}) and the spatially orthogonal SSL (SSL_{orth}) from a patient with myocardial infarction

Table 5.2: Classifier performance for each combination of SSLs

Classifier		Short Spaced Lead (SSL) Combination		
		SSL_{ST}	SSL_{ST} & SSL_{orth}	All SSLs
C4.5 (J48)	Se (%)	86.7	86.7	80.0
	Sp (%)	68.9	66.7	60
	F1 (%)	79.6	78.8	72.7
MLP	Se (%)	53.3	80.0	75.6
	Sp (%)	46.7	68.9	68.9
	F1 (%)	51.6	75.8	73.1
Naive Bayes	Se (%)	86.7	84.4	82.2
	Sp (%)	71.1	66.7	66.7
	F1 (%)	80.4	77.6	76.3

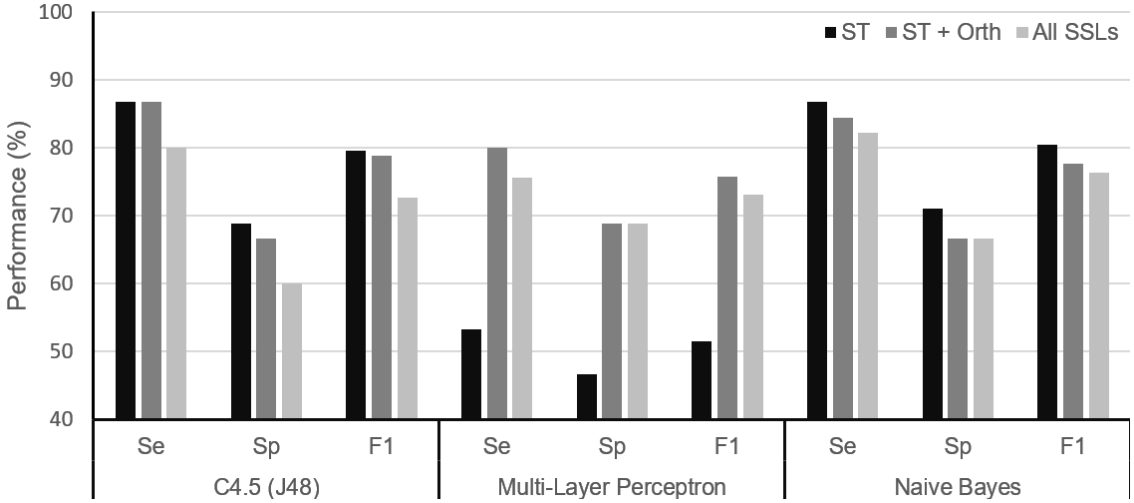

Figure 5.9: Sensitivity (Se), specificity (Sp) and F1 score (F1) for different combinations of short-spaced leads (SSL)

Table 5.3: Classification performance of each lead lead configuration (rows) toward ischaemic-type ECG changes. ST-elevation and depression criteria for the patch are shown in brackets. The highest values for each column have been marked in bold text.

Lead Configuration	SE (%)	SP (%)	PPV (%)	NPV (%)	F1 (%)
12-Lead	62.6	**93.5**	75.8	88.4	**68.6**
Patch (50 μV)	**83.5**	62.8	42.2	**92.0**	56.1
Patch (100 μV)	61.7	94.0	77.2	88.3	**68.6**
Patch (150 μV)	49.6	99.4	96.6	85.8	65.5
Patch (200 μV)	37.4	99.7	97.8	83.0	54.1
Patch (250 μV)	27.0	**100**	**100**	80.7	42.5
Patch (300 μV)	23.5	**100**	**100**	80.0	38.0

Table 5.4: Sensitivity of STEMI detection for the patch-based lead system by vessel-specific occlusions in one of three coronary arteries: LAD, LCX, and RCA. The highest values for each column have been marked in bold text.

Lead Configuration	All	LAD	LCX	RCA
12-Lead	62.6	73.8	28.0	60.4
Patch (50 μV)	**83.5**	**85.7**	**72.0**	**87.5**
Patch (100 μV)	61.7	71.4	40.0	64.6
Patch (150 μV)	49.6	69.1	20.0	47.9
Patch (200 μV)	37.4	50.0	16.0	37.5
Patch (250 μV)	27.0	40.5	4.00	27.1
Patch (300 μV)	23.5	31.0	4.00	27.1

5.5 Discussion

SSL_{ST} shows ST-elevation symptomatic of MI, whereas SSL_{orth} provides increased spatial resolution by showing cardiac activity orthogonally from SSL_{ST}. A high CC value was reported for both SSL_{ST} and SSL_{orth}. This may be due to the proximity of these leads to the precordial chest leads used during derivation. SSL_{ST} had a lower CC, but also a higher RMSE. This is potentially due to the energy present in SSL_{ST} recordings being higher than that of SSL_{orth}. In the detection of STEMI, the ST criteria for the precordial leads of the 12-lead ECG requires between 150-250 μV depending on age and sex. The 18.6 μV of SSL_{ST} is below that range. However, a patient presenting with a marginal STEMI using a 12-lead ECG may not be detected using a patch-lead system. Furthermore, the error may result in more false positives in women, whose ST-elevation criteria are lower than men. The shorter distance between electrodes in patch based systems result in lower amplitude recordings. This may also affect the ability of such a system to detect changes associated with MI.

No specific criteria exist for cardiac abnormality detection using patch-based devices, especially regarding behaviour of the ST-segment. To fully evaluate such a lead system in the detection of disease, a clinical consensus must be reached. Placement errors are an issue for all lead systems, including the 12-lead ECG [33]. A placement error for a patch-based lead system may have a more amplified effect than those of the 12-lead ECG due to the decreased spatial resolution of a patch across the torso. The non-standard locations of this lead system may result in a larger number of placement errors than existing ambulatory systems such as the Holter monitor. In the data collection described previously, a homogeneous torso was used to interpolate the 117-node recordings to the 352-node Dalhousie torso. This may not be representative of all patients, further exacerbating derivation errors. There are limited datasets available to evaluate patch-based lead systems. This emphasises the need to derive them from other, more prominent, datasets such as the 12-lead ECG. The efficacy of such a lead system in the detection of cardiac abnormalities cannot be fully determined since limited data specific to this lead configuration exist. More data is required to evaluate patch-based leads further.

The diagnostic criteria for patch-based ST monitoring explored in this chapter were basic compared with the 12-lead ECG. Consideration was only given for the absolute amplitude, rather than separate criteria for ST-elevation and depression. Additionally, no consideration was given for patient metadata, such as age or sex. By developing these criteria further, the diagnostic performance could be greatly increased.

An SSL patch is more convenient than the 12-lead ECG. An unskilled operator could fit the patch prior to paramedical intervention and recording of the 12-lead ECG. Additionally, such a device could be complementary to the 12-lead ECG to increase performance. One proposed design for such a device is using a four-electrode, two-lead patch such as that described in this chapter. SSL_{orth} can be used for QRS detection while SSL_{ST} is used for ST-segment monitoring. Figure 5.10 shows two SSLs during PBI in the right-coronary artery.

There is no doubt that the performance of the 12-lead ECG will be superior to that with a greatly reduced number of leads. This has been well illustrated in the past when limited lead systems have been considered for derivation of the 12-lead ECG from a reduced number of recording sites. Nevertheless, this work has indicated that there is potential to greatly reduce the recording complexity of the 12 lead ECG towards a patch based system. This may greatly streamline the acquisition process. This work has introduced machine learning techniques and further refinement of these methods could bring the performance of the patch based system closer to that of the 12-lead system. Further work is required to allow us to tune the machine learning techniques so that a better comparison can be made, in terms of the sensitivity and specificity balance, with the 12-lead ECG. A larger dataset of ischaemic-type ECGs will also strengthen this comparison. Specifically, there is a need to further evaluate the proposed patch based leads in more complex MI disease cohorts, e.g. those with multi-vessel disease. In addition, it is envisaged that future work will also investigate the variations in placement that may be encountered in the use of such a patch based system whose application is not based on the well known anatomical landmarks associated with 12-lead precordial lead placement.

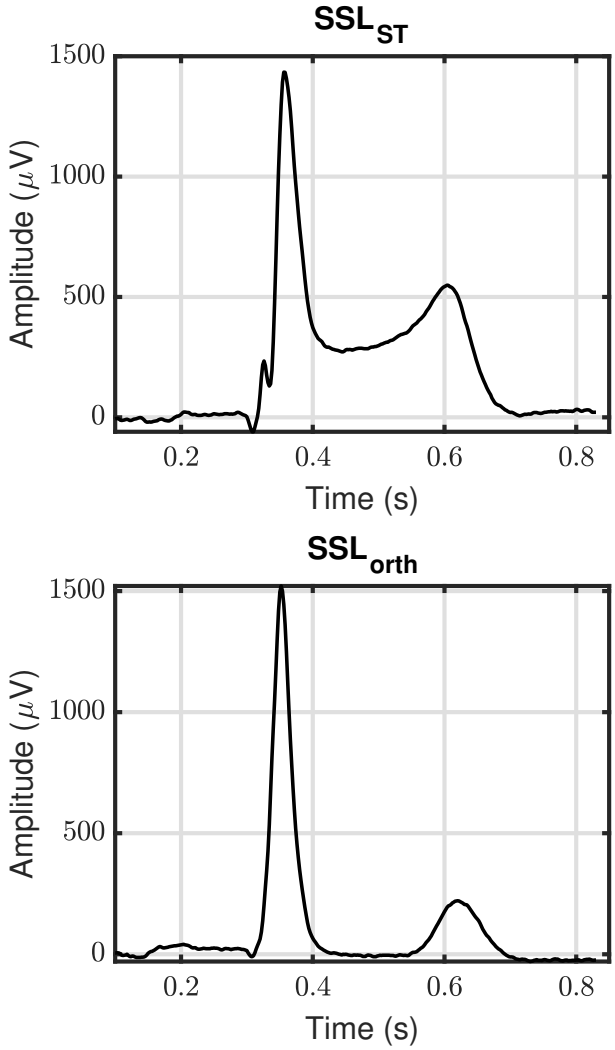

Figure 5.10: SSL_{ST} (top) and SSL_{orth} (bottom) plotted for one recording. PBI in the RCA.

5.6 Conclusion

In this chapter, an SSL-patch based lead system suitable for the detection of ischaemic-type ECG changes associated with AMI has been introduced. This patch based system had two bipolar leads, one ST-sensitive lead and one spatially orthogonal lead. The ST-sensitive lead was between Dalhousie nodes 173 and 254. The spatially orthogonal lead was between Dalhousie node 212 and 234. The SSL shows the highest performance during RCA occlusion which has been verified by the associated body surface potential maps and previously studied vessel specific leads.

Additionally, coefficients towards the derivation of this patch-based SSL system from the 12-lead electrocardiogram using a linear regression method were generated.

The Pearson's correlation coefficient and root mean square error were above 0.97 and below 75 μV for both leads respectively.

Out of nine different combinations of leads and classifiers, a single SSL coupled with a Naive Bayes classifier yielded the highest sensitivity/specificity combination (86.7%/71.1%). 12-lead ECG recordings and current diagnostic criteria were used for comparison purposes (62%/93%). Further research into patch placement, feature extraction and classification methods must be carried out to truly evaluate the lead system.

Although the findings of this chapter support an SSL-based method of detecting ST elevation, a larger dataset is required with more complex coronary artery lesions to verify the results. Patient specific 3D torso models would improve the location accuracy of the chosen lead and account for anatomical variability. Furthermore, the need for at least two contiguous leads for STEMI detection reduces the impact of an SSL for clinical use. Specifically, these studies may investigate the use of SSLs toward detection of MI and their use in patch-based ECG.

References

[1] M. R. Jennings, C. Turner, and D. D. Finlay, "The identification of a patch-based lead system sensitive to ST segment changes associated with myocardial infarction.," 2022.

[2] K. Thygesen, J. S. Alpert, A. S. Jaffe, B. R. Chaitman, J. J. Bax, D. A. Morrow, and H. D. White, "Fourth universal definition of myocardial infarction (2018)," *European Heart Journal*, vol. 24, pp. 107–138, 8 2019.

[3] F. M. Fesmire, R. F. Percy, J. B. Bardoner, D. R. Wharton, and F. B. Calhoun, "Usefulness of automated serial 12-lead ECG monitoring during the initial emergency department evaluation of patients with chest pain," *Annals of Emergency Medicine*, vol. 31, pp. 3–11, 1 1998.

[4] A. Bansal and R. Joshi, "Portable out-of-hospital electrocardiography: A review of current technologies," *Journal of Arrhythmia*, vol. 34, pp. 129–138, 4 2018.

[5] M. K. Hasan, M. Shahjalal, M. Z. Chowdhury, and Y. M. Jang, "Real-time healthcare data transmission for remote patient monitoring in patch-based hybrid OCC/BLE networks," *Sensors (Switzerland)*, vol. 19, p. 1208, 3 2019.

[6] N. J. Wimmer, B. M. Scirica, and P. H. Stone, "The clinical significance of continuous ECG (ambulatory ecg or holter) monitoring of the ST-segment to evaluate ischemia: A review," *Progress in Cardiovascular Diseases*, vol. 56, no. 2, pp. 195–202, 2013.

[7] T. F. Simpson and N. Goldschlager, "Sudden cardiac death preceded by ST segment elevations during ECG patch monitoring," *Journal of Electrocardiology*, vol. 51, pp. 330–331, 3 2018.

[8] Z. Cai, J. Li, X. Zhang, Q. Shen, A. Murray, and C. Liu, "How Accurate are ECG Parameters from Wearable Single-lead ECG System for 24-hours Monitoring," in *Computing in Cardiology*, vol. 2019-Septe, IEEE Computer Society, 9 2019.

[9] R. Rho, M. Vossler, S. Blancher, and J. E. Poole, "Comparison of 2 ambulatory patch ECG monitors: The benefit of the P-wave and signal clarity," *American Heart Journal*, vol. 203, pp. 109–117, 9 2018.

[10] C. P. Karunadas and C. Mathew, "Comparison of arrhythmia detection by conventional Holter and a novel ambulatory ECG system using patch and Android App, over 24 h period," *Indian Pacing and Electrophysiology Journal*, vol. 20, no. 2, pp. 49–53, 2020.

[11] D. Duncker, W. Y. Ding, S. Etheridge, P. A. Noseworthy, C. Veltmann, X. Yao, T. J. Bunch, and D. Gupta, "Smart Wearables for Cardiac Monitoring—Real-World Use beyond Atrial Fibrillation," *Sensors 2021, Vol. 21, Page 2539*, vol. 21, p. 2539, 4 2021.

[12] D. Guldenring, D. D. Finlay, R. R. Bond, A. Kennedy, and J. McLaughlin, "Limitations of the smartphone based single ECG-lead evaluation of STEMI," *Journal of Electrocardiology*, vol. 51, p. e3, 1 2018.

[13] J. B. Muhlestein, V. Le, D. Albert, F. L. Moreno, J. L. Anderson, F. Yanowitz, R. B. Vranian, G. W. Barsness, C. F. Bethea, H. W. Severance, B. Ramo, J. Pierce, A. Barbagelata, and J. B. Muhlestein, "Smartphone ECG for evaluation of STEMI: Results of the ST LEUIS Pilot Study," *Journal of Electrocardiology*, vol. 48, pp. 249–259, 3 2015.

[14] S. S. Lobodzinski, "ECG patch monitors for assessment of cardiac rhythm abnormalities," *Progress in Cardiovascular Diseases*, vol. 56, pp. 224–229, 9 2013.

[15] R. Bond, D. D. Finlay, D. Guldenring, and C. Breen, "Data driven computer simulation to analyse an ECG limb lead system used in connected health environments," *Methods of Information in Medicine*, vol. 55, pp. 258–265, 1 2016.

[16] E. Fung, M. R. Järvelin, R. N. Doshi, J. S. Shinbane, S. K. Carlson, L. P. Grazette, P. M. Chang, R. S. Sangha, H. V. Huikuri, and N. S. Peters, "Electrocardiographic patch devices and contemporary wireless cardiac monitoring," *Frontiers in Physiology*, vol. 6, no. May, p. 149, 2015.

[17] B. M. Horáček, M. Mirmoghisi, J. W. Warren, G. S. Wagner, and J. J. Wang, "Detection of myocardial ischemia by vessel-specific leads derived from the 12-lead electrocardiogram and its subsets," *Journal of Electrocardiology*, vol. 41, pp. 508–517, 11 2008.

[18] S. Al-Zaiti, L. Besomi, Z. Bouzid, Z. Faramand, S. Frisch, C. Martin-Gill, R. Gregg, S. Saba, C. Callaway, and E. Sejdić, "Machine learning-based prediction of acute coronary syndrome using only the pre-hospital 12-lead electrocardiogram," *Nature Communications*, vol. 11, 2020.

[19] M. H. Islam Chowdhuryy, M. Sultana, R. Ghosh, J. U. Ahamed, and M. Mahmood, "AI Assisted Portable ECG for Fast and Patient Specific Diagnosis," in *International Conference on Computer, Communication, Chemical, Material and Electronic Engineering, IC4ME2 2018*, Institute of Electrical and Electronics Engineers Inc., 9 2018.

[20] P. Guzik and M. Malik, "ECG by mobile technologies," *Journal of Electrocardiology*, vol. 49, pp. 894–901, 11 2016.

[21] K. Rjoob, R. Bond, D. Finlay, V. McGilligan, S. J. Leslie, A. Iftikhar, D. Guldenring, A. Rababah, C. Knoery, A. McShane, and A. Peace, "Data driven feature selection and machine learning to detect misplaced V1 and V2 chest electrodes when recording the 12-lead electrocardiogram," *Journal of Electrocardiology*, vol. 57, pp. 39–43, 11 2019.

[22] B. M. Horáček and J. C. Clements, "The inverse problem of electrocardiography: A solution in terms of single- end double-layer sources on the epicardial surface," *Mathematical Biosciences*, vol. 144, pp. 119–154, 9 1997.

[23] F. Dawoud, G. S. Wagner, G. Moody, and B. M. Horáček, "Using inverse electrocardiography to image myocardial infarction-reflecting on the 2007 PhysioNet/Computers in Cardiology Challenge," *Journal of Electrocardiology*, vol. 41, pp. 630–635, 11 2008.

[24] F. Kornreich, T. J. Montague, and P. M. Rautaharju, "Body surface potential mapping of ST segment changes in acute myocardial infarction: Implications for ECG enrollment criteria for thrombolytic therapy," *Circulation*, vol. 87, no. 3, pp. 773–782, 1993.

[25] B. J. Schijvenaars, J. A. Kors, G. van Herpen, F. Kornreich, and J. van Bemmel, "Interpolation of body surface potential maps," *Journal of Electrocardiology*, vol. 28, pp. 104–109, 1 1995.

[26] B. M. Horacek, "Numerical model of an inhomogeneous human torso," *Advanced Cardiology*, vol. 10, no. 51, 1974.

[27] B. Horacek, J. W. Warren, C. J. Penney, R. S. MacLeod, L. M. Title, M. J. Gardner, C. L. Feldman, B. M. Horacek, J. W. Warren, C. J. Penney, R. S. MacLeod, L. M. Title, M. J. Gardner, and C. L. Feldman, "Optimal electrocardiographic leads for detecting acute myocardial ischemia," *Journal of Electrocardiology*, vol. 34, pp. 97–111, 10 2001.

[28] B. M. Horáček, M. Mirmoghisi, J. W. Warren, G. S. Wagner, and J. J. Wang, "Detection of myocardial ischemia by vessel-specific leads derived from the 12-lead electrocardiogram and its subsets," *Journal of electrocardiology*, vol. 41, no. 6, pp. 508–517, 2008.

[29] J. Ross Quinlan, *C4.5: Programs for Machine Learning*. San Mateo, California: Morgan Kaufmann Publishers, 2014.

[30] G. H. John and P. Langley, "Estimating Continuous Distributions in Bayesian Classifiers," in *Proceedings of the Eleventh conference on Uncertainty in artificial intelligence*, pp. 338–345, 1995.

[31] S. ELLIOTT, "Active Control of Nonlinear Systems," in *Signal Processing for Active Control*, pp. 367–409, Elsevier, 1 2001.

[32] A. Perron, T. Lim, U. Pahlm-Webb, G. S. Wagner, and O. Pahlm, "Maximal increase in sensitivity with minimal loss of specificity for diagnosis of acute coronary occlusion achieved by sequentially adding leads from the 24-lead electrocardiogram to the orderly sequenced 12-lead electrocardiogram," *Journal of Electrocardiology*, vol. 40, pp. 463–469, 11 2007.

[33] R. R. Bond, D. D. Finlay, C. D. Nugent, C. Breen, D. Guldenring, and M. J. Daly, "The effects of electrode misplacement on clinicians' interpretation of the standard 12-lead electrocardiogram," *European Journal of Internal Medicine*, vol. 23, pp. 610–615, 10 2012.

Chapter 6

Web-based Architecture Toward the Democratisation of Digital Signal Processing

---

6.1 Abstract

Cloud computing has the ability to offload processing tasks to a remote computing resources. Presently, the majority of biomedical digital signal processing involves a ground-up approach by writing code in a variety of languages. This may reduce the time a researcher or health professional has to process data, while increasing the barrier to entry to those with little or no software development experience. This chapter aims to provide a service capable of handling and processing biomedical data via a code-free interface. Furthermore, this solution should support multiple file formats and processing languages while saving user inputs for repeated use.

A web interface via the Python-based Django framework was developed with the potential to shorten the time taken to create an algorithm, encourage code reuse, and democratise digital signal processing tasks for non-technical users using a code-free user interface. A user can upload data, create an algorithm and download the result. Using discrete functions and multi-lingual scripts (e.g. MATLAB or Python), the user can manipulate data rapidly in a repeatable manner. Multiple data file formats are supported by a decision-based file handler and user authentication-based storage

allocation method.

A web-based system was introduced capable of reducing the barrier to entry for inexperienced programmers. Furthermore, this system is reproducible and scalable for use in a variety of clinical or research fields.

The code for this chapter is freely available on GitHub.. Additionally, this work as been published in Computer Methods and Programs in Biomedicine (CMPB) [1].

6.2 Introduction

Previous chapters have discussed the computation and classification of ECG signals, however, the algorithms developed are not readily available for clinicians or other researchers to use. To run the algorithms introduced previously, knowledge of source control, MATLAB, and data types is required. Additionally, the machine running the code must meet the minimum systems requirements. Accessible code sharing platforms such as server-side processing are potential alternatives for clinicians or researchers who do not have the time or ability.

Server-side processing of biomedical signals is widely prevalent [2, 3] to the extent where specific standards have been formulated to support aspects of this approach [4]. However, the sharing of code and processing techniques is limited by both the skill of the user and the willingness of the developer to format their code comprehensibly. This could be indifference of a developer to format code legibly, or it could be aversion due to time constraints. For example, there are an abundance of DSP algorithms proliferating, but limited initiatives are making these accessible to others. AI techniques garner significant interest in multidisciplinary research, however, the abstraction from the developer to the user causes a lack of uptake in many cases. Additionally, few developers are willing to share their models directly, forcing the user to recreate already existing software. Furthermore, whilst new software tools and techniques have made specialist domains like DSP more accessible the technical barrier to comprehending algorithms based on advanced techniques remains high. Many junior developers find it more difficult to reuse or recreate another published algorithm due to a lack of information surrounding its use or a lack of clarity in the method. This may reduce the eagerness of others to begin research into a novel area

or technique and further publication bias [5]. Additionally, it may discourage junior developers from furthering their understanding of the area since an extensive time investment is required.

Notwithstanding, non-developers could benefit most from the increased availability of well-documented code since they are often experts in the application of software, rather than it's development. One example is that from the medical domain. Specifically, a physician likely has little-to-no experience in software development, but they process large quantities of data on a daily bases. Much of this data is processed using experience and judgement learned through years of training, however, this training is not available to everyone. Additionally, many assignments undertaken by the clinician are, in fact, quite routine and could be automated, allowing them to focus time on other areas. A system that allows the clinician to offload the processing of data has the capability to reduce the decision-time overhead, potentially enabling more patient-centric care. Additionally, medical data science is often undertaken by non medical professionals. Removing the coding barrier may facilitate the discovery of new findings in medical science by increasing its availability.

Clinicians often have access to biomedical data such as the ECG which require extensive filtering between capture and interpretation. Presently, cardiology professionals are required to manually review information and return a diagnosis or opinion. ECG traces may be seconds to hours in length for some ambulatory monitors, requiring considerable time for interpretation. Cloud-based approaches to interpretation of biomedical signals may be a solution to this. Previous research have tackled code-free server-side signal processing and data-visualisation [6, 7, 8, 9, 10], however, such approaches do not allow the user to develop their own algorithm or experiment with different functions. One solution may be an architecture that allows users to create algorithms by connecting multiple combinations of code or functions then expose it to data. Such a system allows the code to be reused; essential to overcome the 'replication crisis' in health informatics [11].

There are many different file formats that can be used containing patient data, although, they are generally not interchangeable [12]. Previous research have proposed middleware format conversion methods capable of adapting data to a universal

format [13, 14].

In the work reported in this chapter, a system capable of abstracting the user from the need to write code or possess a strong understanding of digital signal processing was developed. This has been developed based on the notion of streamlining the algorithm development process and aiding code reuse by allowing the rapid configuration of new algorithms while supporting the repeatability of experiments. In this work, particular attention has been paid to the notion of abstracting the user from the various integration issues such as different programming languages, compatible functions, and data formats to allow them to focus on processing biomedical data. In addition to facilitating biomedical data processing functionality, the work proposed in this chapter also includes provision to facilitate storage of associated data. This data storage functionality has been incorporated to reduce the probability of data silos forming due to the distributed nature of sensitive information [15] by offering a central data store and development area for each user [16]. It is hoped that this may increase the willingness of healthcare providers to share information by removing incurred costs [17], potentially negating many of the data-sharing complications that result in inconsistent care [18].

Furthermore, this work will provide a more beginner-friendly system to those unfamiliar with DSP with the capability to further the democratisation of computational health informatics [19]. This platform aims to be language-agnostic by supporting multiple different programming languages e.g. MATLAB or Python. The suggested framework will offer a platform for peer review where code written by one author can be shared with another. This may reduce the impact by which applications created by non-experts with potentially unethical consequences have on the community [20] since the code can be compared against other 'gold standard' approaches.

6.3 Background

To investigate the context of source code sharing and reuse culture in academia, a sub-review was devised. The purpose of the sub-review was to quantify the proportion of authors who share their source code, program or provide an example

Table 6.1: Sub-review of Code Sharing Prevalence in Literature

Metric	Prevalence
Total Articles	25
Included Articles	13
Excluded Articles	12
Matching 'T' Criteria	3 (23%)
Matching 'F' Criteria	10 (77%)

application e.g. working website. Using Google Scholar, a search was devised using the terms "novel web framework". The top 25 results were used as the basis for the following rules. The inclusion criteria comprised of journal or conference papers with a clear indication a computerised method published in the past ten years (since 2011). Articles that did not fulfill the inclusion criteria were excluded (n = 12). Those matching the inclusion criteria (n = 13) were sorted into two categories: 'T', representing those linking their source code, website, or program in the article; 'F', representing those who did not meet the 'T' criteria. Those matching the 'T' (n = 3) and 'F' (n = 10) criteria comprised 23% and 77% of the included set respectively. These results are shown in Table 6.1.

Of the articles in this sub-review, only 23% shared their code, website or application. To facilitate the democratisation of DSP and code reuse, a higher number of authors must release their source code. This allows other researchers to not only evaluate the performance, but verify their results and collaborate on changes as part of the scientific method.

6.4 Methods

6.4.1 Framework

A framework abstracts common software functions and provides a template which can save development time [21]. Multiple frameworks were evaluated, with the Python-based Django framework being chosen. The Django framework was chosen as the basis of this chapter due to the apparent ease of use in creating web applications, primarily in the provision of an automatic graphical administrator (admin) interface to assist with database management. This allows an administrator to add and remove data without writing code. Additionally, it has a comprehensive docu-

mentation library and active user community to aid debugging. Furthermore, using a popular language such as Python may facilitate the reuse of this system by making it more accessible to those willing to recreate it. In the spirit of reusability, the source code of this project has been made available.

Django abstracts database creation to a number of potential SQL backends. The database schema is derived directly from classes within the source code, with items within the class informing columns and attributes within the database. This ensures consistency between the software and database schema and automated database migrations.

The Django framework is inherently open-source. This allows developers to view and edit aspects of the framework to suit their application [22]. In this chapter, the Django request-handling middleware was not manipulated, however, it is an important feature when considering scaling a project or addressing architectural issues in future [23].

6.4.2 Database Construction

The database structure is central to a cloud computing architecture. The purpose of the database, in this chapter, was to hold data files, code/executable files (scripts), user details and user inputs. Primarily, the database stored what data the user would like to process (File), what scripts to run (Script) and their order (Algorithm), and the result of each script (Execution). This allows the user to see upload data and process it repeatedly using either a novel or existing Algorithm they have created. In Django, database tables are referred to as models. Five database tables (models) were identified as core to this chapter:

Algorithm is the highest-level model in that it contains multiple other models within it. It is a user-created entry with a number of potential scripts to be executed in order. This model is linked to one user allowing them to document the order in which their uploaded data is processed. One field, *scripts*, is linked to a Script via a many to many relationship. This link is made through an intermediary table, Execution, which provides further details. One example of an Algorithm could be a disease classifier. An input file of patient data (XML) would be uploaded by the user. The data could be passed through two hypothetical scripts: first a

MATLAB file 'data_sanitisation.m' and secondly a Python file 'knn_classifier.py' to return a spreadsheet or Comma Separated Variable (CSV) file with the result. In principle, however, an arbitrary number of such processes could be employed within an Algorithm. This architecture allowed multiple combinations of the same Script to be called across various Algorithms without destroying or editing the original Script.

Execution is an object used to describe an instance of one file being processed by one script to produce an output file. Any data file being processed by a MATLAB or Python script will become part of an Execution. This model is hidden from the user. It contains one input file *data_input*, a script to execute the data *script*, and an output file *data_output*. The order in which each script was executed is stored in *order*. The purpose of this model was to separate each processing step of an Algorithm by handling the inputs and outputs of each Script individually. This allowed error handling, logging of output files and subsequently the removal of unused intermediary files.

Script is an executable file model. Its programming language (*language*), supported input file format (*data_input*) and output file format (*data_output*) are core fields. Only an admin can upload a Script to reduce the risk of malicious code injection. A *description* field is included to provide instructions for use and information as to how the Script works. The executable file is held in *uploaded_script* and is stored in a media file folder (/algorithms/). This allowed each executable file to be read-only by a user and so improved the application's security. Additionally, only an admin could edit the contents of the executable file repository. An example of a Script might be a MATLAB low pass filter function that supports a single row CSV file and outputs the same type of file.

File is any file that can be attached to a user. For example, data files uploaded by the user or the result of an Execution. The user can provide a descriptive name (*name*) for the data and specify the data format (*format*). A example File may be a MATLAB data file ('.mat') of ECG data with the *name* 'ecg_data.mat'

FileFormat contains metadata for a File instance. Primarily, this model is used to filter what Scripts are supported via a one to many relationship with the Script entries *data_input* and *data_output*. Also, FileFormat is used to store the

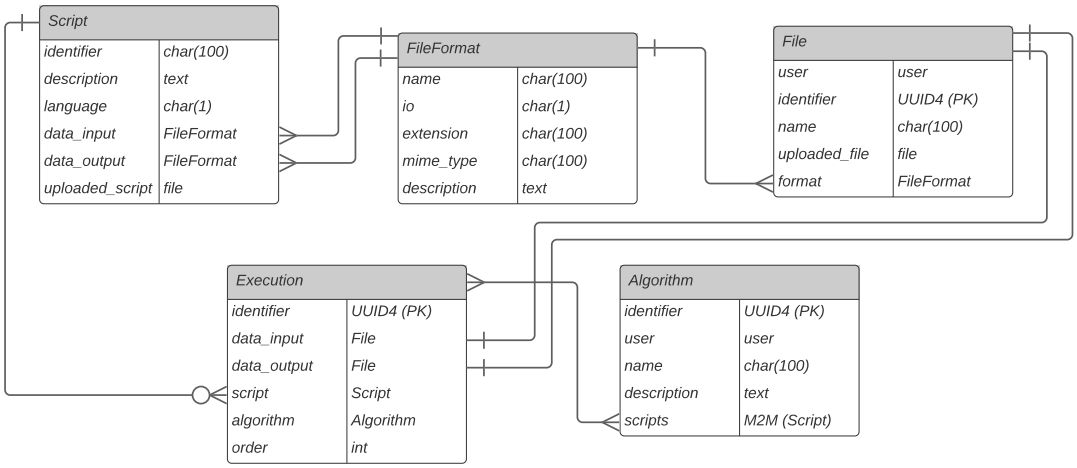

Figure 6.1: Entity relationship diagram (ERD) of the algorithm development database. Each table represents a model in the Django framework. 'Algorithm' is the user-created entry consisting of a list of 'Scripts' which process 'Files' in the order set by 'Execution' providing they are a compatible 'FileFormat'

Multipurpose Internet Mail Extensions (MIME) type for if the user downloads the file (*mime_type*). It is important to note the MIME type does not decide if a File is supported by a Script, that is handled by the administrator-controlled list of supported FileFormats for a given Script. The field *io* shows if the file is in input file, output file or both.

This schema allows users to create a library of data files in various formats, and build algorithms comprised of individual scripts to act upon them in a reproducible manner. This also makes the evolution and comparison of algorithms a more streamlined process.

Figure 6.1 shows an entity relationship diagram (ERD) of each table (model).

6.4.3 Data Upload

Data are handled in two discrete scenarios: upload and execution.

Only authenticated users can upload data. When accessing the file upload page, an empty instance of File is created. In the class-based approach of Django, this creates an empty row in the File table. The user is prompted to upload their file, give it a descriptive name and specify the input format. These were stored in a media directory (/user_data/) and assigned a filename corresponding to the username and a universally unique identifier (UUID) e.g. 'user_a535562 ... .csv'. In this way data

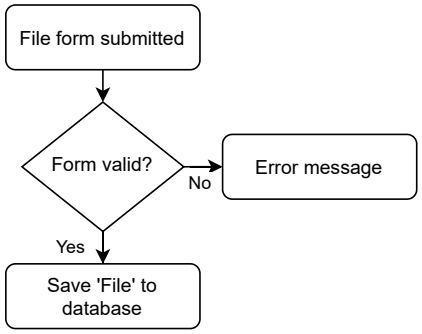

Figure 6.2: Overview of the POST request checking following the user uploading a data file. Note: 'File' is a table (model) representing the data file and user metadata

can be traced to a user by searching file structure or querying the database.

Data are passed to the controller using a POST request. If the form data and file upload were valid, the file would be saved within the system and the model instance of File updated with the user-provided information. The path to the uploaded file and meta information such as FileFormat could be accessed by a database query. Figure 6.2 shows the process to upload user data.

6.4.4 Data Processing

6.4.4.1 Algorithm Creation

Creating an algorithm is handled in a similar way to uploading data. A blank HTML form was created with the following fields: Algorithm name, description, input data and scripts. The name and description are customisable to assist the user in keeping track of previous entries and to ensure a research team have a shared knowledge of the algorithm construction. The input data is derived from a selectable list of user data files. Only files from the current user are shown. The script form fields allow the user to select one or more Scripts in the desired execution order. Once submitted, a POST request is sent to the controller with the user-selected input data, executable scripts and a description from the algorithm creation form. In the model layer, an intermediary table was created to handle the ordering and metadata for each script. The Execution model was used for this. An instance of Execution was created for each chosen Script and the order assigned. This allows for additional Scripts to be added into the Algorithm construction at a later date. The input file chosen by the user is assigned to the first Execution. The input and output files for other

Executions are set to null temporarily.

6.4.4.2 Execution

A complete instance of Execution contains an input data file, executable script and output data file. To complete the first instance of Execution for this Algorithm, the input data file was passed to the Script via a handler file. The handler file is different depending on the language of the Script. For example, a MATLAB file will have a 'handler.m' file and Python may have another file. The role of the handler file is to take the file path of the input data file, run a script at a given file path and return the file identification number. The output file was then assigned to the first Execution to complete it. The next Execution uses the output data file of the previous Execution as its input data file. It executes the script and returns an output file. If the last execution is reached, the output data file is returned to the user as a downloadable file and all previous intermediary files are cleared from the system to reduce storage overhead.

6.4.4.3 MATLAB Engine for Python

The Django framework uses Python, so the native environment can be used to process scripts, however, the same is not true for licensed software such as MATLAB. The MATLAB Engine for Python is an API for Python capable of accessing the MATLAB work space and executing scripts. This allows a licensed copy of MATLAB to be stored on the server with the current session shared with the Python virtual environment. Errors from MATLAB can be passed to Python via the API and raised to the user as a MatlabExecutionError. Figure 6.3 shows a flowchart of how data is executed.

6.4.5 User Interaction

A front-end was developed to facilitate testing. Separate webpages were created to demonstrate the following features: uploading and viewing data files, creating and viewing algorithms, and user registration.

When uploading a file, the user was presented with three input fields as an HTML form: "Name", "Uploaded file", and "Format". The user could view and manage

their stored files via an HTML table including deleting unwanted data files. Each table row was an instance of File attributed to that user

To create an Algorithm, the user entered details into another HTML form. They could select a file from the file management area to process or enter it from the form directly. The following input fields were available: "Algorithm name", "Description", "Data input" and "Scripts". For the purposes of demonstration, up to four scripts were allowed, however an arbitrary number can be used within the model and administrator interface. Each successive script field denotes an instance of Script and allocated the order of each Execution instance. The data file selection is a filtered list of files for only that user. Once the user submits the Algorithm creation form, the data file will be processed in the manner previously described. The user will be requested to download the data output file. The user could also view and edit their created algorithms using the same method as data files. Figure 6.4 shows the suggested user interaction with the system.

To show the user interaction in more detail, Figure 6.5 provides a sequence diagram of user inputs followed by the backend response. Five objects have been described here. First, the web interface, is the frontend developed for testing purposes. This provides renders of forms such as file upload and algorithm creation forms. Second, the web application, is the backend model-view-controller architecture written using the Django framework. It handles user requests, renders and queries to the database. Third, the processing engine or API, describes the system which executes a given file by passing it to the selected script as an argument. The API will then return a result file and status message to indicate a successful execution. Finally, the database, is used to store the tables described in Section 6.4.2 and allows the user input to be preserved in case of an exception e.g. the processing API raises an error.

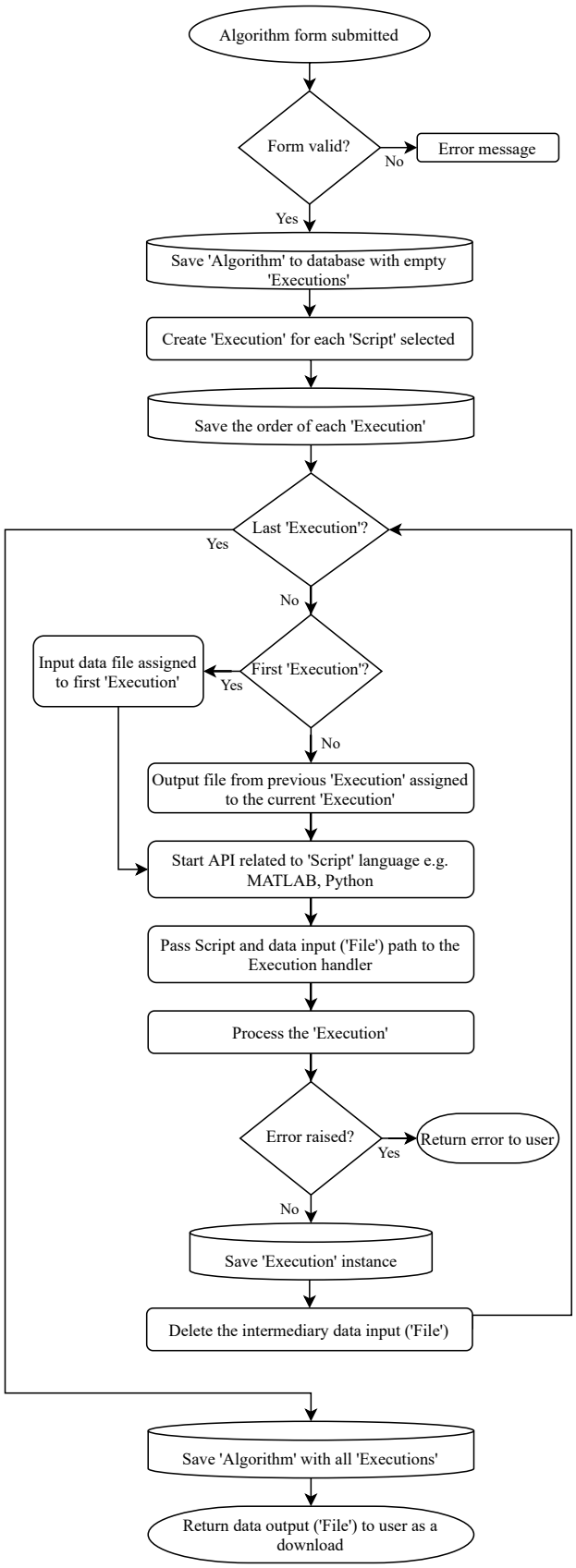

Figure 6.3: Data flow following the submission of an 'Algorithm' form to process a user input file through multiple different scripts ('Execution') and return an output file

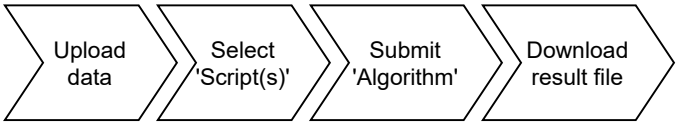

Figure 6.4: User interaction steps required to process data

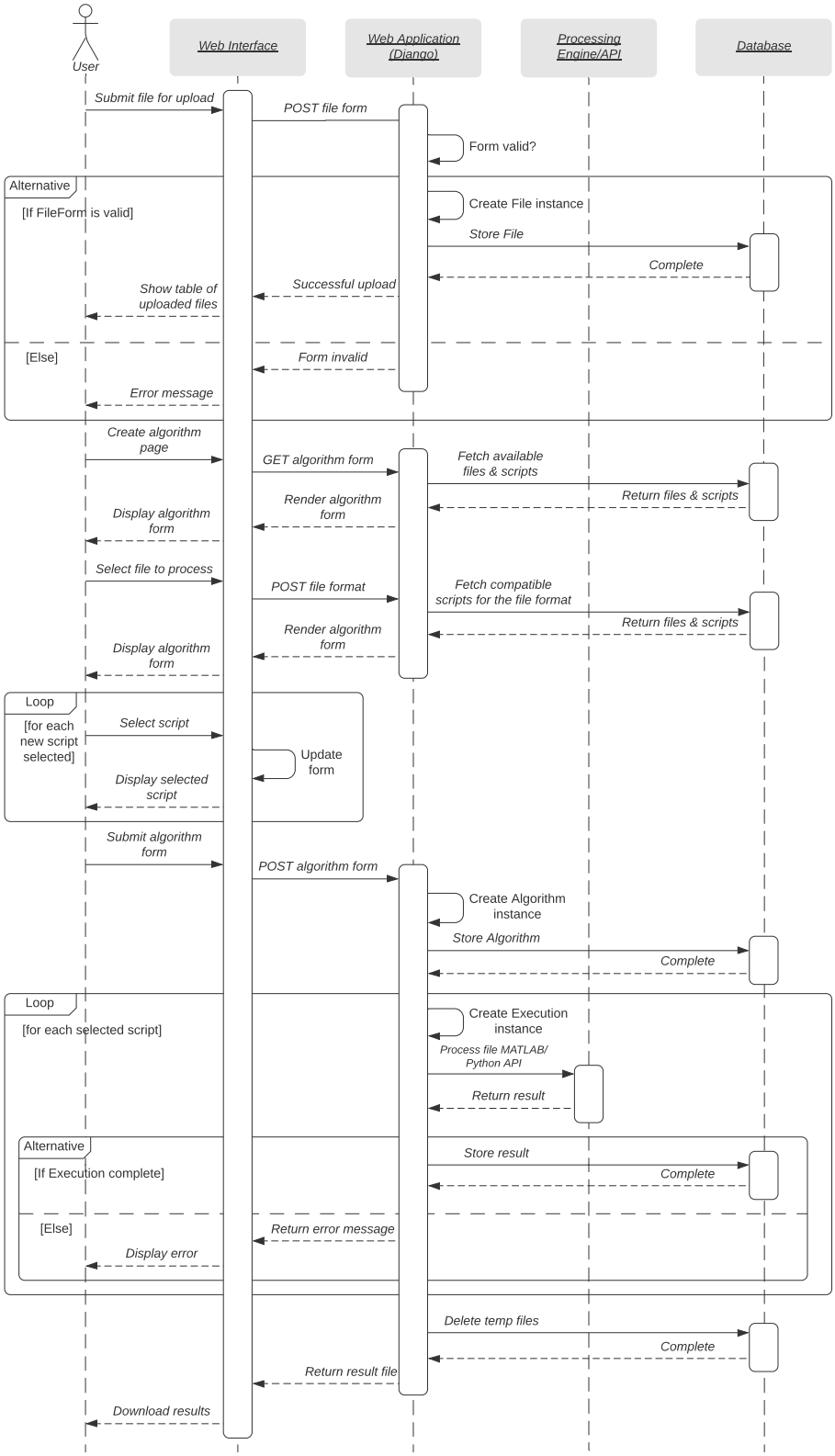

Figure 6.5: Sequence diagram showing interactions between the user and the system when uploading a file, creating an algorithm and running the algorithm. User interface refers to the frontend browser-based platform. The web application is the backend model-view-controller logic. The processing engine is the API which uses a selected script to process a file e.g. MATLAB or Python. The database is the server used for storage and queries.

6.5 Discussion

A web-based approach to algorithm development allows a user to trial many different parameters without writing code. For example, a user can combine different filters and compare which has the most favourable performance for their signal. Additionally, a user could compare classifiers written by different team members. This system is not limited to comparing scripts though, it could be utilised by medical professionals for statistical analysis or used by administrators to sort patient records without prior knowledge of programming.

Code reuse, particularly in open source software, has the capability to reduce development time and increase collaboration [24, 25]. This system allows code to be stored in the form of discrete functions. Users can reuse a function multiple times and in different orders. In particular, a developer can see all previously created Algorithms or Scripts with metadata on the inputs, outputs and function of the program. If a Script has been previously created, there is no need for a developer to recreate it, thus, saving time during the development process. A function-based approach to Scripts abstracts the user from the coding aspect of algorithm design to promote a trial and error method where non-experts can experiment with their data. Additionally, a Script is linked to the user who uploaded it. In teams of developers or clinicians, this allows a potential user of the Script to contact the original author or team they are associated with. When compared with existing systems such as Apache Kafka, this system is complementary. Kafka implements an event-driven approach for data monitoring, however, this system employs a data-driven approach instigated by the user to allow experimentation. This may be beneficial in the design-phase of automation algorithms as a test-bench before using an event-driven architecture such as Kafka.

DSP software is often licensed. For a user to operate the software, they must purchase a licensed copy and activate it. Each user requires a license which some institutions or companies may not be able to afford. This system requires a single server license by running one copy of licensed software in the backend. Functions are called via the handler by using an API, negating the requirement for the user to have licensed software.

Many users may not have an in-depth understanding of file formats or DSP principles. There may be many errors when processing data. Licensed software APIs such as the MATLAB Engine for Python raise errors in the Django framework. This enables the development of an error handler to return exceptions to the user. This is a reactive error handling which happens after the error has occurred. A pro-active approach is to query the backend before submitting the Algorithm. Javascript in the form of an AJAX query was used to filter the supported Scripts available to the FileFormat of the input data file. This would reduce the likelihood of import errors, however, it would not address run-time errors.

Using APIs and file handlers allows the use of multiple programming languages and data types. For example, the output of a MATLAB Execution may be a CSV file. This could be passed to a Python Execution and processed interchangeably. Providing the Script supports a particular data file, it can be executed without knowledge of the previous programming language which processed it. This may introduce an environment where DSP software development teams can write functions in multiple languages without the need for single-language specialists. When recruiting developers, this would increase the number of potential candidates for a role and encourage a deeper understanding of the DSP principles rather than a deep understanding of one programming language.

This application is user agnostic. A wider variety of individuals can interact without specialist knowledge of the software. For example, a medic could process patient records to show risk factors for a specific ailment. Likewise, an embedded systems engineer could design filter coefficients for a medical device to meet a regulatory requirement. Abstraction of these tasks from the user reduces the time invested in the task, allowing them to focus elsewhere. The principle of democratisation in software development is to allow any user to interact and access the core functionality. A user agnostic system by default achieves these principles.

Data files are uploaded by users to the system. Keeping data files in one system can reduce the probability of data silos forming, especially when the data storage is centralised. The user can provide descriptive information to describe their data file, potentially increasing the prospect of data reuse and collaboration.

In this system, only MATLAB and Python scripts have been tested. The archi-

tecture has the potential for many different programming languages and programs to execute arbitrary scripts in various languages such as R, C++ and Java, but with administrative safety measures. Additionally, this system could be used to output typographic information by employing TeX-based compilers. One utilisation instance of typographic processing could be the cleaning of patient record files to output a formatted table or document.

Executable scripts can only be uploaded by admins or super-users. This reduces the risk of malicious code injection by only allowing users to upload data files. Additionally, it ensures that only approved executable files are included in the Script database. In a software development environment, this would be post code-review and could reduce the number of errors experienced by clients.

This architecture is inherently scalable. An object-based approach to processing scripts allows multiple instances of 'Executions', each with their own engine. For example, multiple MATLAB engines or Python environments can be created, each with separate memory. Since the memory space is not shared by these 'Executions', they can be containerised using platforms such as Docker and Kubernetes. These systems allow scaling to occur automatically while processing data in parallel to the main web application thread.

The file management system links all files with a user. This enables efficient clearing of old or disused files by the user or by an administrator. Additionally, data associated with the user can easily be collated or removed to comply with right-to-erasure requests such as GDPR or similar 'right to be forgotten' requests.

Assessing the security and vulnerabilities of a code is an important factor due to the increase in global cyber security threats. The code has been subjected to vulnerability scanning using Bandit, a popular tool used to detect known common issues in Python code. According to the scan the security risk of the code is considered 'medium' due to the MATLAB engine requiring the use of command-line tools.

6.6 Limitations

Remote code execution (RCE) presents a considerable security concern in web-based applications. Malicious code can be injected to such a system and potentially lead to

compromise of the system [26]. The Django framework provides features to improve security such as cross site scripting (XSS) and SQL injection protection [27], however specific protection measures would be required for the deployment environment.

Regular expressions (regex) and user input sanitisation was limited during this chapter in the interest of time. For this application to be deployed and secured, care would be taken to reduce the likelihood of string-based injection attacks by parsing user files for executable scripts [28].

At present, handler functions are used to execute scripts. The handler function is passed an absolute file path to the data and script files. This requires a file to be present for each execution instance. For less complex scripts, much of the processing time would be allocated to reading and writing data files. It would be more efficient to use the Django framework to handle the files as imported variables, however this was beyond the scope of this chapter.

6.7 Future Work

Many DSP functions collate multiple data files during execution. For example, combining ECG waveforms and contextual patient metadata to produce a patient-specific diagnosis. This would require multiple data files for each instance of Execution, necessitating a database architecture change. Following this, a user could select multiple data files of different file formats for one script. This may allow more context to be given to classifiers.

To reduce the risk of damage due to malicious code injection, a sandboxing method could be employed. Sandboxing can isolate server instances to that user or group of users to assist with malware detection [29]. A compromised sandbox instance will damage the virtual machine (VM) it is incased within, however, it is less likely to affect other sandboxes due to their distributed nature.

Automation of file upload and execution could be handled by the development of an API. More specifically, medical devices and embedded systems could use this architecture to offload processing requirements to the cloud. This can reduce the size and cost of hardware required while allowing algorithm and software changes to be handled remotely, reducing the need for product recall and firmware updates.

Medical devices such as Holter monitors could upload ECG data and have near to real-time decisions using this approach. Additionally, all patient data would be accumulated in one location, lessening the data silo effect. Cloud storage systems could be linked such as Microsoft OneDrive or Google Drive to further improve the centralisation of data. However, this would be limited by regulations on patient data sharing with third parties.

Error handling in this chapter is limited, however a separate error handling user interface could allow users to debug data files and code simultaneously. Furthermore, the handler could include a conditional-based flow during the Execution phase whereby a certain output may trigger a response. For example, if a single row of a patient record is missing it could be estimated by another script instead of raising an error.

6.8 Conclusions

This chapter has presented an adaptive cloud computing architecture capable of processing arbitrary input files through ordered executable scripts using multiple processing languages in a repeatable manner. Using the Django framework, a database was introduced to handle and store files as they are processed. This work has the capability to assist algorithm research teams during development by reducing the time taken to incorporate previously developed code. Additionally, this work provided an insight into the potential for automation to process IoT device data, particularly long-term patient monitoring systems.

References

[1] M. R. Jennings, C. Turner, R. R. Bond, A. Kennedy, R. Thantilage, M. T. Kechadi, N. A. Le-Khac, J. McLaughlin, and D. D. Finlay, "Code-free cloud computing service to facilitate rapid biomedical digital signal processing and algorithm development," *Computer Methods and Programs in Biomedicine*, vol. 211, p. 106398, 11 2021.

[2] H. Xia, I. Asif, and X. Zhao, "Cloud-ECG for real time ECG monitoring and analysis," *Computer Methods and Programs in Biomedicine*, vol. 110, pp. 253–259, 6 2013.

[3] S. Pandey, W. Voorsluys, S. Niu, A. Khandoker, and R. Buyya, "An autonomic cloud environment for hosting ECG data analysis services," in *Future Generation Computer Systems*, vol. 28, pp. 147–154, North-Holland, 1 2012.

[4] International Standards Organisation, "ISO/IEEE International Standard for Health informatics – Point-of-care medical device communication – Part 20702: Medical devices communication profile for web services," *ISO/IEEE 11073-20702:2018(E)*, pp. 1–52, 2018.

[5] A. Cockburn, P. Dragicevic, L. Besançon, and C. Gutwin, "Threats of a replication crisis in empirical computer science," in *Communications of the ACM*, vol. 63, pp. 70–79, Association for Computing Machinery, 7 2020.

[6] M. A. Kumar, A. Srinivasan, and N. Bussa, "HTML5 powered web application for telecardiology: A case study using ECGs," in *IEEE EMBS Special Topic Conference on Point-of-Care (POC) Healthcare Technologies: Synergy Towards Better Global Healthcare, PHT 2013*, pp. 156–159, 2013.

[7] X. Wang, Q. Gui, B. Liu, Z. Jin, and Y. Chen, "Enabling smart personalized healthcare: A hybrid mobile-cloud approach for ECG telemonitoring," *IEEE Journal of Biomedical and Health Informatics*, vol. 18, no. 3, pp. 739–745, 2014.

[8] L. Jin and J. Dong, "Intelligent Health Vessel ABC-DE: An Electrocardiogram Cloud Computing Service," *IEEE Transactions on Cloud Computing*, 4 2018.

[9] A. Joshi, D. Scheinost, H. Okuda, D. Belhachemi, I. Murphy, L. H. Staib, and X. Papademetris, "Unified framework for development, deployment and robust testing of neuroimaging algorithms," *Neuroinformatics*, vol. 9, no. 1, pp. 69–84, 2011.

[10] E. S. Martin, D. D. Finlay, C. D. Nugent, R. R. Bond, and C. J. Breen, "An interactive tool for the evaluation of ECG visualisation formats," in *Computing in Cardiology*, (Zaragoza, Spain), pp. 779–782, IEEE, 9 2013.

[11] E. Coiera, E. Ammenwerth, A. Georgiou, and F. Magrabi, "Does health informatics have a replication crisis?," *Journal of the American Medical Informatics Association*, vol. 25, pp. 963–968, 8 2018.

[12] R. R. Bond, D. D. Finlay, C. D. Nugent, and G. Moore, "A review of ECG storage formats," *International Journal of Medical Informatics*, vol. 80, pp. 681–697, 10 2011.

[13] X. Li, V. Vojisavljevic, and Q. Fang, "An XML based middleware for ECG format conversion," in *Proceedings of the 31st Annual International Conference of the IEEE Engineering in Medicine and Biology Society: Engineering the Future of Biomedicine, EMBC 2009*, pp. 1691–1694, IEEE Computer Society, 2009.

[14] R. R. Bond, D. D. Finlay, C. D. Nugent, and G. Moore, "XML-BSPM: An XML format for storing Body Surface Potential Map recordings," *BMC Medical Informatics and Decision Making*, vol. 10, p. 28, 5 2010.

[15] R. Ranchal, P. Bastide, X. Wang, A. Gkoulalas-Divanis, M. Mehra, S. Bakthavachalam, H. Lei, and A. Mohindra, "Disrupting healthcare silos: Addressing data volume, velocity and variety with a cloud-native healthcare data ingestion service," *IEEE Journal of Biomedical and Health Informatics*, vol. 24, pp. 3182–3188, 11 2020.

[16] R. Reda, F. Piccinini, and A. Carbonaro, "Towards consistent data representation in the IoT healthcare landscape," in *ACM International Conference Proceeding Series*, vol. 2018-April, (New York, NY, USA), pp. 5–10, Association for Computing Machinery, 4 2018.

[17] A. R. Miller and C. Tucker, "Health information exchange, system size and information silos," *Journal of Health Economics*, vol. 33, pp. 28–42, 1 2014.

[18] R. Reda, F. Piccinini, and A. Carbonaro, "Semantic modelling of smart healthcare data," in *Advances in Intelligent Systems and Computing*, vol. 869, pp. 399–411, Springer Verlag, 9 2018.

[19] R. Fang, S. Pouyanfar, Y. Yang, S. C. Chen, and S. S. Iyengar, "Computational health informatics in the big data age: A survey," 6 2016.

[20] R. Bond, A. Koene, A. Dix, J. Boger, M. D. Mulvenna, M. Galushka, B. W. Bradley, F. Browne, H. Wang, and A. Wong, "Democratisation of usable machine learning in computer vision," 2 2019.

[21] O. David, J. C. Ascough, W. Lloyd, T. R. Green, K. W. Rojas, G. H. Leavesley, and L. R. Ahuja, "A software engineering perspective on environmental modeling framework design: The Object Modeling System," *Environmental Modelling and Software*, vol. 39, pp. 201–213, 1 2013.

[22] S. Weber, *The Success of Open Source*. No. 1, Harvard University Press, 2009.

[23] D. M. Le, D. Link, A. Shahbazian, and N. Medvidovic, "An Empirical Study of Architectural Decay in Open-Source Software," in *Proceedings - 2018 IEEE 15th International Conference on Software Architecture, ICSA 2018*, pp. 176–185, Institute of Electrical and Electronics Engineers Inc., 7 2018.

[24] S. Haefliger, G. Von Krogh, and S. Spaeth, "Code reuse in open source software," *Management Science*, vol. 54, pp. 180–193, 1 2008.

[25] A. Mockus, "Large-scale code reuse in open source software," in *First International Workshop on Emerging Trends in FLOSS Research and Development, FLOSS'07*, pp. 7–11, IEEE Computer Society, 2007.

[26] M. M. Hassan, U. Mustain, S. Khatun, M. S. A. Karim, N. Nishat, and M. Rahman, "Quantitative Assessment of Remote Code Execution Vulnerability in Web Apps," in *Proceedings of the 5th International Conference on Electrical, Control & Computer Engineering*, vol. 632, (Kuantan, Pahang, Malaysia), pp. 633–642, Springer, 2019.

[27] Django Software Foundation, "Security in Django — Django documentation — Django," 2017.

[28] Y. Zheng and X. Zhang, "Path sensitive static analysis of web applications for remote code execution vulnerability detection," in *Proceedings - International Conference on Software Engineering*, pp. 652–661, 2013.

[29] M. Vasilescu, L. Gheorghe, and N. Tapus, "Practical malware analysis based on sandboxing," in *Proceedings - RoEduNet IEEE International Conference*, IEEE Computer Society, 11 2014.

Chapter 7

Conclusions

The aim of this thesis was to investigate different processing techniques and methods to improve upon MI detection techniques from the ECG. To achieve this, several objective were met, including a) reviewing the current state-of-the-art presented in published literature surrounding the processing of ECG data for MI diagnosis b) identifying suitable datasets to investigate how ischaemia affects the ECG c) exploring how additional derived leads can improve upon the diagnostic performance of the 12-lead ECG d) introducing a short spaced lead system sensitive to ST segment changes associated with MI e) developing a framework to facilitate the rapid creation of biomedical digital signal processing algorithms by non-coders.

Chapter 2 provided a detailed review of the literature surrounding the work in this thesis. An introduction and overview of different ECG lead systems related to the detection of MI was presented. Specific attention was given to reduced lead systems, including ambulatory and patch-based devices. During this process, it was identified that the spatial resolution of the 12-lead ECG could be expanded by using additional leads. A hypothesis formed around the use of derived additional leads for MI classification. This formed the basis of the work for Chapter 4. Additionally, the rise of ambulatory devices for conditions such as AF presented an opportunity to investigate the use of such a device in detecting ECG changes associated with MI. This formed the hypothesis surrounding the work in Chapter 5. It was found that few publications make the code used during the study open for public use. Additionally, the algorithms developed were not readily implemented by clinicians,

potentially due to a lack of coding skills or lack of access to a suitable software platform such as MATLAB. These identified issues justified the work carried out in Chapter 6.

Three datasets containing ischaemic ECG recordings were discussed in Chapter 3. Two of the datasets included BSPM data. The first had BSPMs (n = 176) recordings from subjects at rest (n = 88) and during PBI in one of three coronary arteries. Dataset two contained BSPM recordings (n = 734) from subjects in one of three categories: normal controls (n = 226), those with MI (n = 271), and those with LVH (n = 237). The third dataset contained 12-lead ECG recordings (n = 467) from subjects (n = 104) undergoing elective PTCA in one or more coronary arteries (n = 115). Also discussed in Chapter three were the different pre-processing techniques used to allow the experimental work discussed later in the thesis, including VCG and Discrete Wavelet Transform (DWT) methods to annotate the beats within 12-lead ECG signals.

Chapter 4 introduced coefficients toward the derivation of posterior (V7-V12) and right-sided (V3R-V6R) chest leads from the 12-lead ECG with an improvement in derivation accuracy compared to previously published coefficients. Additionally, it was found that derived posterior and right sided chest leads are capable of detecting ischaemic-type ECG changes associated with MI. The addition of derived leads was shown to increase the sensitivity of STEMI detection from 58.3% in the 12-lead ECG to 64.4% in the 22-lead ECG. F1 score increased from 69.1% in the 12-lead configuration to 69.5% in the 22-lead configuration. However, these results were not statistically significant with a p-value greater than 0.05.

Chapter 5 introduced an SSL-patch based lead system suitable for the detection of ischaemic-type ECG changes associated with AMI. This patch based system had two bipolar leads, one ST-sensitive lead and one spatially orthogonal lead. The ST-sensitive lead was between Dalhousie nodes 173 and 254. The spatially orthogonal lead was between Dalhousie node 212 and 234. The SSL shows the highest sensitivity during RCA occlusion which has been verified by the associated body surface potential maps and previously studied vessel specific leads. Additionally, coefficients towards the derivation of this patch-based SSL system from the 12-lead electrocardiogram using a linear regression method were generated. The Pearson's

CC and RMSE were above 0.96 and below 18.7 μV for both leads respectively. Out of nine different combinations of leads and classifiers, a single SSL coupled with a Naive Bayes classifier yielded the highest sensitivity/specificity combination (86.7%/71.1%). 12-lead ECG recordings and current diagnostic criteria were used for comparison purposes (62%/93%). An additional classification method using varying ST-segment elevation or depression showed the highest F1 score to be 68.6% with an ST-threshold of 100 μV. The F1 score was the same for the 12-lead ECG. Further research into patch placement, feature extraction and classification methods must be carried out to truly evaluate the lead system. Although the findings of this study support an SSL-based method of detecting ST elevation, a larger dataset is required with more complex coronary artery lesions to verify the results. Patient specific 3D torso models would improve the location accuracy of the chosen lead and account for anatomical variability. Furthermore, the need for at least two contiguous leads for STEMI detection reduces the impact of an SSL for clinical use. Specifically, these studies may investigate the use of SSLs toward detection of MI and their use in patch-based ECG.

Chapter 6 presented an adaptive cloud computing architecture capable of processing arbitrary input files through ordered executable scripts using multiple processing languages in a repeatable manner. Using the Python-based Django framework, a database was introduced to handle and store files as they are processed through multiple scripting languages such as MATLAB or Python. Scripts could be uploaded via an administrator interface, and shared between teams of developers. Users could design algorithms from these scripts without the need to write code. The algorithms would then be stored for later use. This work has the capability to assist algorithm research teams during development by reducing the time taken to incorporate previously developed code. Additionally, this study provided an insight into the potential for automation to process IoT device data, particularly long-term patient monitoring systems.

Future work should focus on the clinical testing of the lead systems presented in this thesis. Additional lead systems such as the posterior, right-sided leads, and patch-based leads were derived and compared with existing data, however, this was not tested on real subjects in a clinical setting. To verify the practicality and

efficacy of the patch-based lead system introduced in Chapter five of this thesis, further studies must be carried out by clinicians to verify the position is feasible and convenient for ambulatory monitoring. Additionally, the nuances of physically creating such a device may add more scope for refinement in the position and size of the patch. The framework introduced in Chapter six was tested locally, but not deployed in the two use cases discussed: a software development team, and a team of clinicians needing to experiment with patient data. Future work in this area should focus on deploying this web framework and performing in-situ user tests. Additionally, the security vulnerabilities identified in the chapter should be resolved before committing to a live test.

Appendix A

Glossary of Terms

Atrial Fibrillation Rapid uncoordinated contractions of the atria of the heart resulting in a lack of synchronism between heartbeat and pulse beat. 2, 32, 34–36, 39, 40, 42, 43, 124, 169

Bundle Branch Block An acute episode of coronary heart disease marked by the death or damage of heart muscle due to insufficient blood supply to the heart usually as a result of a coronary artery becoming blocked by a blood clot formed in response to a ruptured or torn fatty arterial deposit. 15, 25, 41, 42, 50, 51

Ejection Fraction The percentage of blood that is pumped out of a filled ventricle as a result of a heartbeat. 37

Electrocardiogram The electrocardiogram (ECG or EKG) is a noninvasive test that is used to reflect underlying heart conditions by measuring the electrical activity of the heart. ix, x, xiii, xiv, 1–4, 8, 12–34, 36–63, 85, 86, 88–96, 99, 101, 104–113, 115–119, 122–125, 127–131, 134, 135, 138, 140–143, 148, 149, 153, 164, 165, 169–171

Left Ventricular Hypertrophy Enlargement or overgrowth of the left ventrical of the heart due to the increased size of the constituent cells. 21, 23, 25, 26, 42, 46, 48, 51, 53, 58, 87, 88, 126, 170

Myocardial Infarction An acute episode of coronary heart disease marked by the death or damage of heart muscle due to insufficient blood supply to the heart usually as a result of a coronary artery becoming blocked by a blood clot formed in response to a ruptured or torn fatty arterial deposit. 1–4, 13–15, 17, 18, 20, 21, 23–31, 33, 36–38, 41, 42, 44–55, 63, 85, 88, 90, 94, 101, 104–107, 111, 117, 118, 123–126, 128–130, 133, 140, 141, 143, 169–171

Non-ST Elevation Myocardial Infarction A form of myocardial infarction where no ST-elevation is present on the electrocardiogram. 31, 42, 46, 49, 50, 54

Percutaneous Coronary Intervention A nonsurgical procedure that relieves narrowing and obstruction of the arteries to the muscle of the heart. 19, 20, 24, 45, 46

Percutaneous Transluminal Coronary Angioplasty The insertion of a balloon-tipped catheter inserted through an artery in the groin or wrist to enlarge a narrowing in a coronary artery. 20, 27, 30, 32, 34, 44, 48, 52, 53, 85, 88, 89, 125, 130–132, 170

Short-Spaced Lead An electrocardiographic bipolar lead with a short spacing, usually below 100 mm, between electrodes. xi, 3, 122–128, 130–134, 137, 141–143, 170, 171

ST-Elevation An increased amplitude of the ST-segment of the electrocardiogram. This is commonly associated as a symptom of myocardial infarction. 124–126

ST-Elevation Myocardial Infarction A myocardial infarction with ST-segment elevation present on two or more contiguous leads. xiii, xiv, 19–21, 23, 24, 28, 30–32, 42, 44–47, 49, 50, 54, 55, 105, 111, 115, 117–119, 124, 125, 128, 129, 134, 139, 140, 143, 170, 171

Sudden Cardiac Death A medical emergency with absent or inadequate contraction of the left ventricle of the heart that immediately causes bodywide circulatory failure. 37, 38

Vectorcardiogram a method of recording the direction and magnitude of the electrical forces of the heart by means of a continuous series of vectors that form a curving line around a centre. ix, 24–27, 43, 48–51, 90–93, 101, 170

Ventricular Fibrillation An abnormal and irregular heart rhythm in which there are rapid uncoordinated fluttering contractions of the lower chambers (ventricles) of the heart. 45

Ventricular Tachycardia An abnormal heart rhythm that is rapid and regular and that originates from an area of the lower chamber (ventricle) of the heart. 29, 35, 38

Wilson Central Terminal The isoelectric (0 V) point for ECG leads, calculated from distal bipolar limb leads. 16, 22, 86, 88, 126

Appendix B

Research Output

Journal Publications

Jennings, M.R., Turner, C., Bond, R.R., Kennedy, A., Thantilage, R., Kechadi, M.T., Le-Khac, N.A., McLaughlin, J. and Finlay, D.D., 2021. Code-free cloud computing service to facilitate rapid biomedical digital signal processing and algorithm development. Computer Methods and Programs in Biomedicine, 211, p.106398.

Jennings, M.R., McCausland, C., Turner, C., Güldenring, D., Brisk, R., Bond, R.R., Biglarbeigi, P., Mclaughlin, J., Finlay, D.D., 2021. Computational approach to deriving posterior and right sided chest leads in the detection of ECG changes associated with acute myocardial ischaemia. IOP Physiological Measurement [Submitted]

Conference Publications

Jennings, M., Guldenring, D., Bond, R., Rababah, A., McLaughlin, J. and Finlay, D.D., 2019, September. ST Changes Observed in Short Spaced Bipolar Leads Suitable for Patch Based Monitoring. In 2019 Computing in Cardiology (CinC) (pp. 1-4). IEEE.

Jennings, M.R., Biglarbeigi, P., Bond, R.R., Brisk, R., Güldenring, D., Kennedy,

A., McLaughlin, J. and Finlay, D.D., 2020, September. Machine Learning Approach to Assess the Performance of Patch Based Leads in the Detection of Ischaemic Electrocardiogram Changes. In 2020 Computing in Cardiology (pp. 1-4). IEEE.

Jennings, M.R., Rababah, A.S., Biglarbeigi, P., Brisk, R., Güldenring, D., Bond, R., McLaughlin, J. and Finlayl, D.D., 2020, September. Coefficients for the Derivation of Posterior and Right Sided Chest Leads From the 12-lead Electrocardiogram. In 2020 Computing in Cardiology (pp. 1-4). IEEE.

Jennings, M., Rababah, A., Gueldenring, D., McLaughlin, J. and Finlay, D., 2021, June. Coefficients for the Derivation of an ST Sensitive Patch Based Lead System from the 12 Lead Electrocardiogram. In Computing in Cardiology 2021.

Other Publications

Guldenring, D., Finlay, D.D., Kennedy, A., Bond, R.R., **Jennings, M.** and McLaughlin, J., 2019, September. The Effects of 40 Hz Low-Pass Filtering on the Magnitude of the Spatial Ventricular Gradient. In 2019 Computing in Cardiology (CinC) (pp. Page-1). IEEE.

McCallan, N., Finlay, D., Biglarbeigi, P., Perpiñan, G., **Jennings, M.**, Ng, K.Y., McLaughlin, J. and Escalona, O., 2019, September. Wearable Technology: Signal Recovery of Electrocardiogram From Short Spaced Leads in the Far-Field Using Discrete Wavelet Transform Based Techniques. In 2019 Computing in Cardiology (CinC) (pp. Page-1). IEEE.

Guldenring, D., Rababah, A., Finlay, D.D., Bond, R.R., Kennedy, A., **Jennings, M.**, Rjoob, K. and McLaughlin, J., 2020, September. Regression or Pseudo-Inverse-Which Method Should be Preferred When Developing Inverse Linear ECG-Lead Transformations?. In 2020 Computing in Cardiology (pp. 1-4). IEEE.

Brisk, R., Bond, R.R., Finlay, D., McLaughlin, J., Jasinska-Piadlo, A., **Jennings,**

M. and McEneaney, D., 2021, April. Neural networks for ischaemia detection: revolution or red herring? A systematic review and meta-analysis. In 45th International Society for Computerized Electrocardiology.

Finlay, D., Bond, R., **Jennings, M.**, McCausland, C., Guldenring, D., Kennedy, A., Biglarbeigi, P., Al-Zaiti, S.S. and McLaughlin, J., 2021. Overview of featurization techniques used in traditional versus emerging deep learning-based algorithms for automated interpretation of the 12-lead ECG. Journal of Electrocardiology.

Rababah, A.S., Bear, L.R., Dogrusoz, Y.S., Good, W., Bergquist, J., Stoks, J., MacLeod, R., Rjoob, K., **Jennings, M.**, Mclaughlin, J. and Finlay, D.D., 2021. The effect of interpolating low amplitude leads on the inverse reconstruction of cardiac electrical activity. Computers in biology and medicine, 136, p.104666.

Appendix C

Twelve-lead electrocardiogram recording from a patient undergoing percutaneous transluminal coronary angioplasty in the left anterior descending coronary artery

---

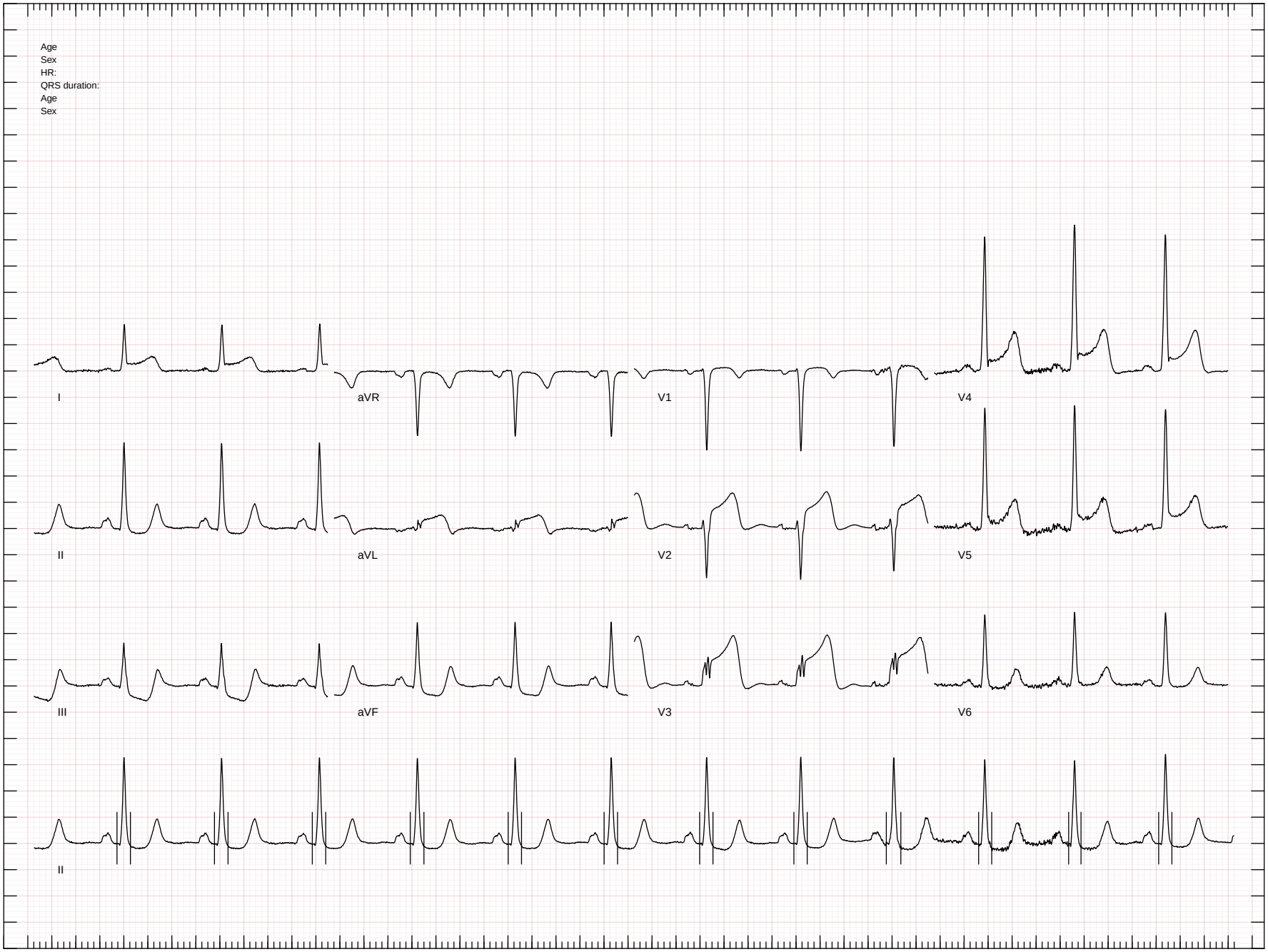
Age
Sex
HR:
QRS duration:
Age
Sex
I
aVR
V1
V4
II
aVL
V2
V5
III
aVF
V3
V6
II